공학박사 학위논문

Design and Synthesis of Conjugated Polymers with Efficient Light Absorption for High Performance Polymer Solar Cells

고성능 고분자 태양전지를 위한 효율적인 빛 흡수를 갖는 공액 고분자의 설계 및 합성

2016년 2월

서울대학교 대학원

재료공학부

이 종 원

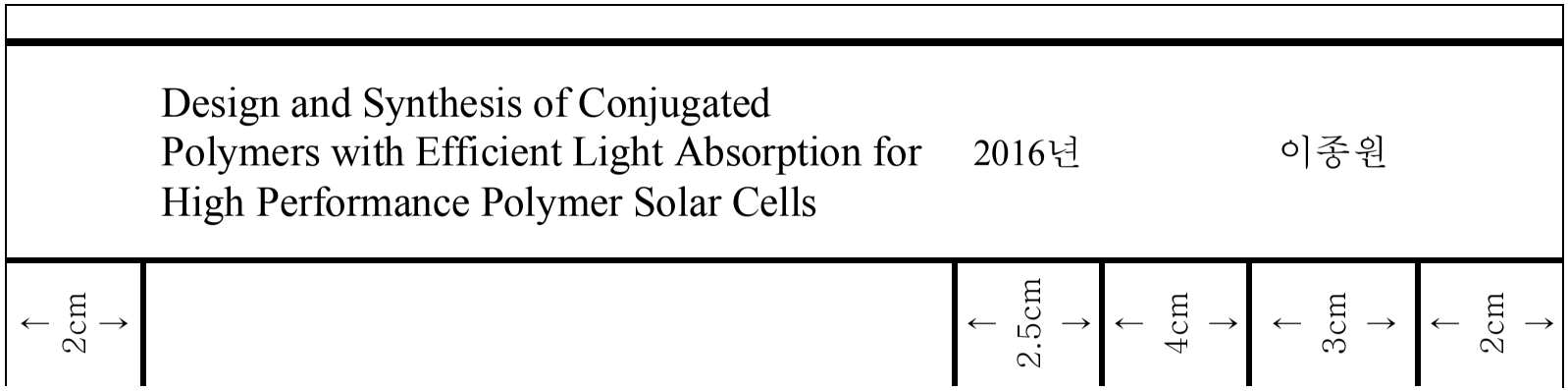
Design and Synthesis of Conjugated
Polymers with Efficient Light Absorption for
High Performance Polymer Solar Cells
2016년
이종원
← 2cm →
← 2.5cm →
← 4cm →
← 3cm →
← 2cm →

Abstract

Design and Synthesis of Conjugated Polymers with Efficient Light Absorption for High Performance Polymer Solar Cells

Jong Won Lee

Department of Materials Science and Engineering

The Graduate School

Seoul National University

Until now regioregular poly(3-hexylthiophene) (P3HT) has been studied as an electron donor material for organic photovoltaics, and bulk heterojunction photovoltaic devices based on P3HT and [6,6]-phenyl C_{61} butyric acid methyl ester ($PC_{61}BM$) have been reported to have power conversion efficiency (PCE) as high as 5%. However for devices utilizing, the main problem of P3HT is its quite large bandgap (1.9–2.0 eV) which limits the light absorption from the solar spectrum.

To overcome the absorption limitation, extensive effort has focused on developing donor–acceptor (D–A) conjugated polymers. One unique feature of these polymers is that their HOMO and LUMO energy levels are governed by the HOMO energy level of the donor and the LUMO energy level of the acceptor, respectively. Therefore, the energy levels of polymers can be tuned by choosing appropriate combination of D and A unit.

Among various semiconducting polymers for polymer solar cells (PSCs),

a copolymer consisting of fluorene and dithienyl benzothiadiazole (PFDTBT) exhibits a high V_{OC} of around 1 V because of its deep HOMO energy level, but it shows relatively low PCE with moderate J_{SC} due to a large bandgap of 1.8 eV, which is the same problem of P3HT. For the purpose of reducing the bandgap of PFDTBT, we introduced a strong electron-donating oxygen atom into fluorene to synthesize benzochromene (BC), which was then polymerized with electron deficient dithienyl benzothiadiazole (DTBT) to afford two low-bandgap polymers, PBCDTBT. The PBCDTBT-based solar cell exhibits a high power conversion efficiency (PCE) of 5.74%, which is much higher than that of the reference fluorene-based polymer (PFDTBT) (2.56%). The higher PCEs of PBCDTBT is mainly attributed to higher J_{SC}, which arises from stronger and broader absorption, higher exciton generation rate, more effective charge separation and higher hole mobility as compared to PFDTBT, although the V_{OC} is sacrificed to some extent.

Then, to enhance the J_{SC} without V_{OC} loss, we introduce ternary blend strategy. Ternary blends incorporating multiple donor absorbers with complementary absorption into active layers provide an opportunity to enhance the PCE of organic solar cells. In addition to complementary absorption between the donors, ternary blends exhibit improved internal morphology by choosing appropriate third component. For this purpose, in this study we design a ternary blend solar cell with two donors composed of diketopyrrolopyrrole-based polymer (PTDPP2T) and small molecule ($(TDPP)_2Ph$), and one acceptor ($PC_{71}BM$). Consequently, the PCE of ternary blend solar cell is increased from 6.60% (PTDPP2T:$PC_{71}BM$) to 7.48% (PTDPP2T:$(TDPP)_2Ph$:$PC_{71}BM$), which is attributed to complementary absorption behavior between PTDPP2T and $(TDPP)_2Ph$. Also, when the small amount of $(TDPP)_2Ph$ (<10 wt%) is added to PTDPP2T:$PC_{71}BM$, a narrower fibril size with face-on orientation in q_z direction on the substrate is obtained, which facilitates charge transport.

Another effective strategy to further enhance J_{SC} of the PSCs is to synthesize random copolymers composed of one electron donating unit and two different electron accepting units, if the absorptions of two electron accepting units are complementary to each other. To this end, we synthesized a new series of conjugated random copolymer composed of bithiophene (electron donating unit) with TDPP and pyridine-capped diketopyrrolopyrrole (PyDPP) (co-electron accepting units). The random copolymers show broad light absorption and face-on orientation on the substrate, which is beneficial to achieving high short circuit current. The V_{OC} of the random copolymer can also be controlled systematically by varying the ratio of PyDPP to TDPP in the copolymer, since the HOMO energy level becomes deeper as the PyDPP content in the random copolymer is increased. Consequently, the solar cell device made of the random copolymer with the ratio of 3:1 (TDPP:PyDPP) shows higher PCE (8.11%) than those made of corresponding homopolymers, PTDPP2T (6.70%) and PPyDPP2T (4.14%).

From these results, it can be concluded that the absorption properties of the active layers are influenced by chemical modification of polymer and third component in ternary blend. Also these absorption properties are important factors to design high performance PSCs.

Keywords: polymer solar cell, bulk heterojunction, low bandgap, ternary blend, random copolymer

Student Number: 2011-22870

Contents

List of Tables

List of Schemes

List of Figures

Chapter 1. Introduction

1.1 Polymer solar cells

1.1.1 Background of polymer solar cells

There is a great deal of attention about the development and production of global energy needs from renewable energy source, since fossil resources are finite and burning fossil fuels is accompanied by carbon dioxide emission. Solar energy has been recognized as one of the promising energy resource which delivers electricity from sun light directly with high potential. The theoretical potential, which is given by the solar energy flux hitting the earth surface, is estimated to be 6,000 times larger than global annual energy needs (~15 TW).[1,2]

The Photovoltaics (PV) is a device of converting light source to electricity using semiconductor.[3,4] The first generation PV cell was developed at Bell Laboratories in 1954.[5] This PV cell was based on Silicon (Si) and showed the power conversion efficiency (PCE) of 6%. Over the years the PCEs for crystalline Si-based PV cells have reached 25%, and until now Si is the most dominating material for PV cells.[6–8] However it is well known that the electricity of PV cells is more expensive than that of fossil and nuclear power, which is related to high manufacturing cost such as expensive vacuum systems and high temperature processes. Thus, to overcome the cost issue of Si-based PV cells, recently polymer-based organic materials are introduced

due to their potential for low temperature or vacuum-free process.[9] Also this polymer-based PV cells have advantages for fabricating lightweight, flexible and transparent devices via high-throughput roll-to-roll production process. Hence, extensive research efforts have been devoted to understanding and improving the performance of polymer-based PV cells over the last decade.[10–20]

1.1.2 Operating mechanism and device structure

As Compared with inorganic semiconductors, the dielectric constant of organic materials is low ($\varepsilon \sim 3–4$). Consequently, photoinduced excited states result in coulombically bound electron–hole (e^-/h^+) pairs (excitons).[21,22] To help the charge separation from exciton, a bilayer structure has been introduced by stacking *p*-type and *n*-type organic layers, since the bilayer structure could improve the charge separation at the interface between *p*-type and *n*-type organic semiconducting layers.[23–27] To enhance the interface surface area for efficient exciton dissociation, the bulk heterojunction (BHJ) structure is proposed by simply mixing of *p*-type and *n*-type organic materials to form a bicontinuous interpenetrating network.[28–30] Since then, the BHJ structure has become the standard architecture for organic solar cells, and PCEs over 9% have been achieved under AM 1.5G (AM = air mass) illumination.[31–41]

The operating mechanism of *p*-*n* junction polymer solar cells (PSC) is briefly mentioned in scheme 1.1. The energy conversion process has at least

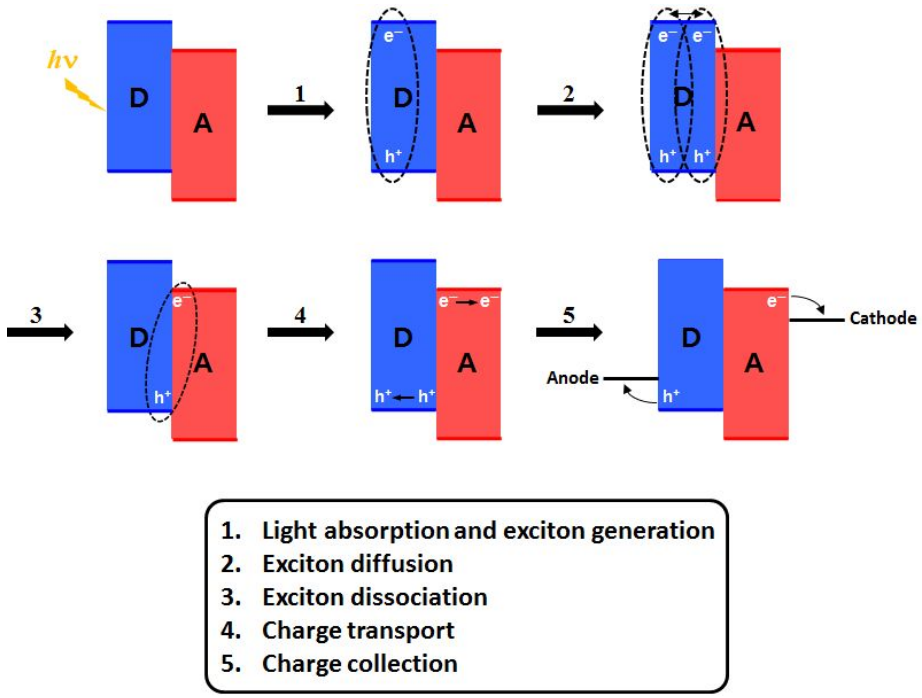

Scheme 1.1. Operation mechanism of *p*-*n* junction in PSCs.

five fundamental steps; (i) Light absorption: The incident photons are absorbed in the active layer and excitons are created. Polymer-based organic materials typically have high absorption coefficients (>10^5 cm^{-1}), therefore a layer thickness of just a few hundred nanometers is sufficient to absorb the light.[42] To maximize the light absorption, absorption ranges of polymers should be well matched to the solar spectrum. (ii) Exciton generation and diffusion: As photons of energy which is larger than the band gap of polymer are absorbed, excitons are generated and diffuse through the polymer phase, where they can decay (radiatively or non-radiatively), or meet interface of *p*-*n* junction and dissociate into free charges. Several values of exciton diffusion

length have been reported in the range of 10–15 nm.[43–45] (iii) Exciton dissociation: Exciton dissociation or charge separation refers to process of splitting the electrostatically coupled electron–hole (e^-/h^+) pairs into free charges. This exciton dissociation occurs at the interfaces between *p*-type and *n*-type organic materials. For the efficient charge separation, the difference in LUMO energy level of donor and acceptor, which acts as a driving force for exciton dissociation, should be higher than that of exciton binding energy.[46] (iv) Charge transport: Once the free charge carriers are produced, electrons and holes travel through *n*-type materials and *p*-type materials, respectively, to get collected at the electrodes. The efficiency of charge transport is determined by the electrical mobility and impedance of the organic materials.[47,48] (v) Charge collection: Finally, the charge carriers are collected from the organic material (HOMO level for holes and LUMO level for electrons) to the Fermi level of the electrode by hopping or tunneling mechanism.

The figure 1.1 shows a schematic device structure composed of indiumtin-oxide (ITO)/ poly(3,4-ethylenedioxythiophene:polystyrenesulfonic acid (PEDOT:PSS)/polymer:PCBM/Ca or LiF/Al. Transparent ITO is the most widely used material as a anode electrode which has a high-work function. On the ITO-coated glass, PEDOT:PSS is used extensively as a solution-processable hole extracting interlayer due to its high conductivity and transparency. And then active layer (polymer:PCBM) is spin coated on top of the PEDOT:PSS layer. Finally, metal electrode, such as Al, is deposited by thermal evaporation as a cathode. Specifically, between active layer and

cathode an electron transporting layer (Ca or LiF) is adopted to lower the work function of the cathode, which facilitates efficient charge extraction by forming Ohmic contact with active layer.[49,50]

The current-voltage (*J*–*V*) curve of PSCs under illumination is illustrated in Figure 1.2. The PCE of a solar cell is given by the ratio between the maximum electrical power deliverable by the cell and the light power reaching the device (P_{in}), which is standardized at 100 mW/cm^2 with a spectral intensity distribution matching the AM 1.5 condition.

$$\mathrm{PCE} = \frac{V_m * J_m}{P_{in}} = \mathrm{FF} * \frac{V_{OC} * J_{SC}}{P_{in}}$$

where the short-circuit current density (J_{SC}), the open circuit voltage (V_{OC}) and the current and voltage defining the maximum power point (J_m and V_m) can be extracted from the current versus voltage characteristics, and the fill factor (FF) can be written as:[51,52]

$$\mathrm{FF} = \frac{V_m * J_m}{V_{OC} * J_{SC}}$$

1.1.3 Donor and Acceptor materials for polymer solar cells

To date, the most popular BHJ structure of PSCs is made by mixing of conjugated polymers (*p*-type) as donors and fullerene derivatives (*n*-type) as acceptors. The development of *p*-type donor polymers has gone through

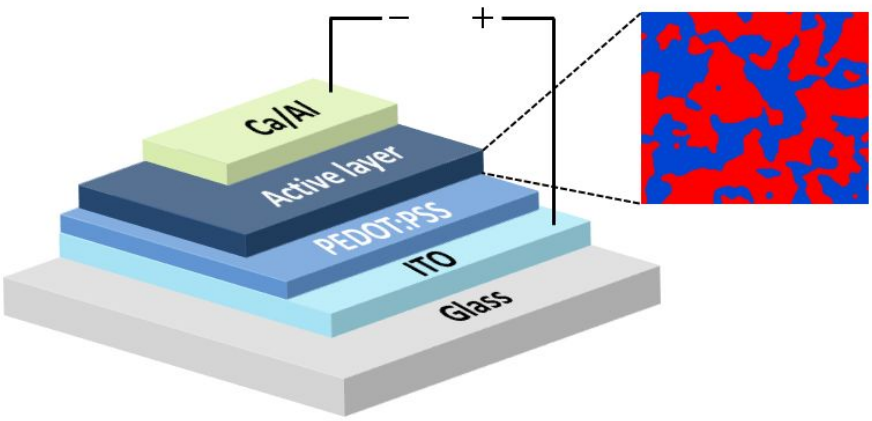

Figure 1.1. Device structure of a general BHJ PSCs.

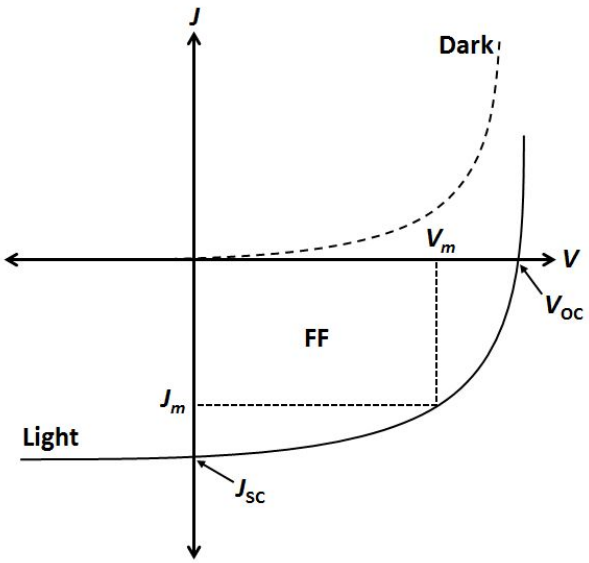

Figure 1.2. Current–voltage curves of solar cell under illumination with the parameters.

several phases of research, and Figure 1.3 shows the chemical structures of these polymers. The early classes of polymers were poly(phenylenevinylene) (PPV) derivatives. In the beginning, poly(2-methoxy,5-(2-ethyl-hexyloxy)-p-phenylenevinylene) (MEH-PPV) was used as a donor,[28] after that another PPV polymer poly(2-methoxy-5-(3,7-dimethyloctyloxy)-1,4-phenylenevinylene) (MDMO-PPV) was designed to enhance solubility. The different alkyl side chains of MDMO-PPV left the band gap and energy levels unchanged compared to MEH-PPV, but solubility and miscibility with PCBM were enhanced, which leads to PCE up to 3%.[53,54] Although many studies were focused on PPV-based polymers, the bandgaps of PPV derivatives are larger than 2 eV, thus research rapidly shifted to polythiophene, such as regioregular poly(3-hexylthiophene) (P3HT).[55–59] The bandgap of P3HT is about 1.9 eV and the external quantum efficiency (EQE) of PSC device at maximum wavelength reached more than 70%. Such high EQE can be explained by high crystallization characteristics and resulting high charge carrier mobility of regioregular P3HT. Consequently, the P3HT-based PSC have achieved the PCE of 4–5%. However, the V_{OC} of P3HT is relatively lower than that of MDMO-PPV, since the HOMO energy level of P3HT is higher than that of MDMO-PPV. The other important donor polymers are polyfluorene derivatives like poly[2,7-(9-(2-ethylhexyl)-9-hexyl-fluorene-*co*-5,5-(4',7'-di-2-thienyl-2',1',3'-benzothiadiazole)]. Interesting features of this polymer included low-lying HOMO energy level and wide bandgap, resulting in high V_{OC} but low J_{SC}: the fluorene-based solar cell shows a low PCE of 2.2% with a small J_{SC} of 4.66 mA/cm^2, but high V_{OC} of 1.04 V.[60]

In fact, the *n*-type electron acceptors such as fullerene derivatives are important as same as donor polymers for high performance PSCs, and their chemical structures are described in Figure 1.4. Parent fullerene C_{60} is the most advanced organic *n*-type semiconductor that shows electron mobilities as high as 1–10 cm^2/V s when measured in organic field effect transistors.[61–64] Also, C_{60} has been known to be highly resistant to oxidation and up to six electrons can be accommodated in the LUMO energy level.[65,66] However, due to solubility limitation of C_{60} in common organic solvent, a organo-soluble derivative, [6,6]-phenyl-C_{61}-butyric acid methyl ester ($PC_{61}BM$) and [6,6]-

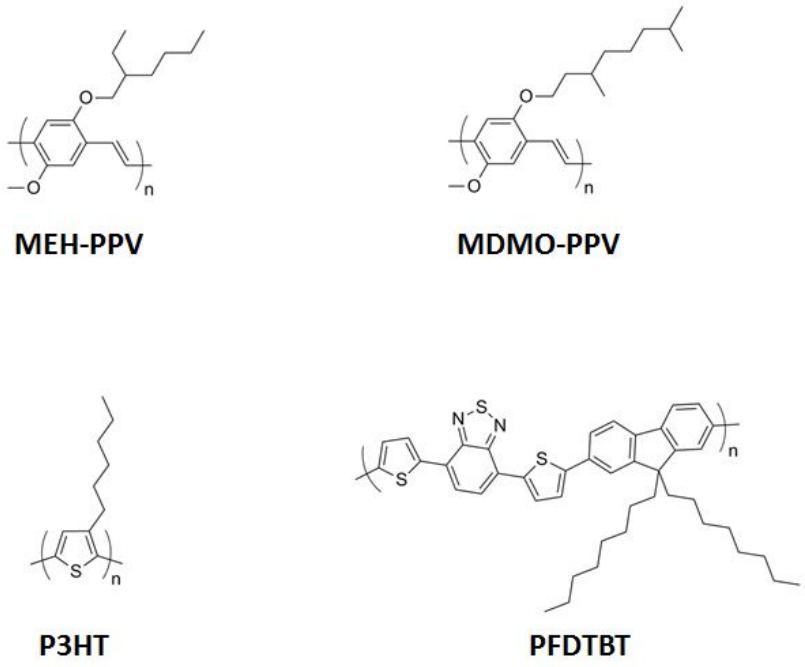

Figure 1.3. Chemical structures of *p*-type polymers used as electron donors in active layers of PSCs.

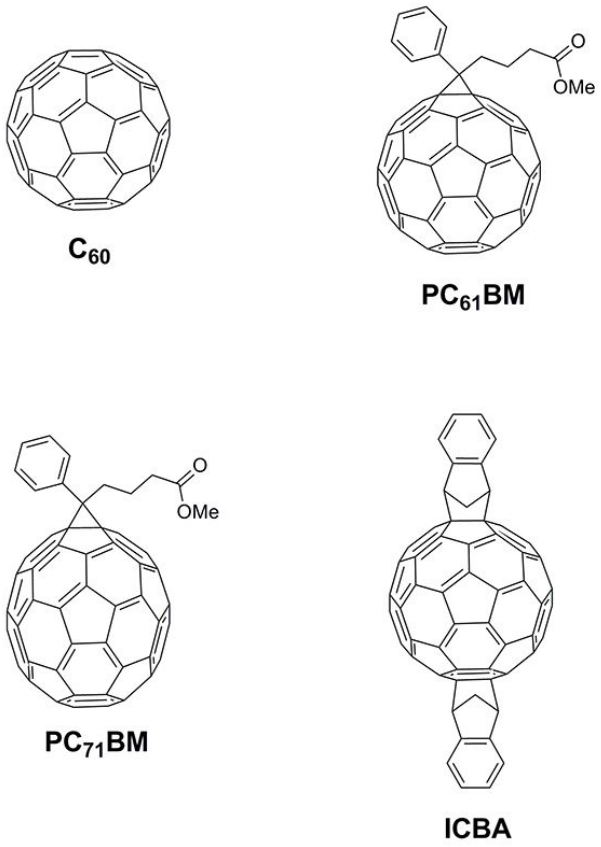

Figure 1.4. Chemical structures of *n*-type materials used as electron acceptors in active layers of PSCs.

phenyl-C_{71}-butyric acid methyl ester ($PC_{71}BM$) were synthesized. Since then $PC_{71}BM$ which possesses stronger visible absorption than $PC_{61}BM$ are widely used in the fabrication of BHJ PSCs.[67] Recently, in order to increase LUMO energy level and solubility for high V_{OC}, indene-C_{60} bisadduct (ICBA) has also been proposed.[68,69]

1.2 Strategies to enhance light absorption for high performance polymer solar cells

1.2.1 Energy levels of conjugated polymers for active layers

The fundamental requirements for high performance photovoltaic polymers include (i) a broad light absorption range, which enables more sunlight to be absorbed in the active layers;[70–72] and (ii) a low-lying HOMO to keep V_{OC} as high as possible, together with a suitable LUMO energy level to enable effective photoinduced charge transfer from the polymers to the acceptor (fullerene derivatives) in the BHJ device.[73–75] It has been known that these requirements are closely related to energy levels of conjugated donor polymer in the active layer.

First, if we assume that ITO has a transmittance of 85%, from the standard spectrum of solar irradiation (AM 1.5G), the theoretical maximum J_{SC} is approximately 14.3 mA/cm^2, with a response range of 300–650 nm (when using P3HT as the standard material). If the photocurrent response is extended to 800 nm, the theoretical maximum J_{SC} can be increased to ~23.0 mA/cm^2; moreover if the response is extended to 1000 nm, the theoretical maximum of J_{SC} can be increased to ~33.9 mA/cm^2.[76] These simple calculations clearly indicate that the absorption spectrum strongly affects photovoltaic performance, especially J_{SC}. In reality, it is hard to absorb the whole range of the solar spectrum with a single polymer material due to the limitation of absorption range. As shown in Figure 1.5, since the solar spectrum around 700 nm have the maximum of the photon flux, the

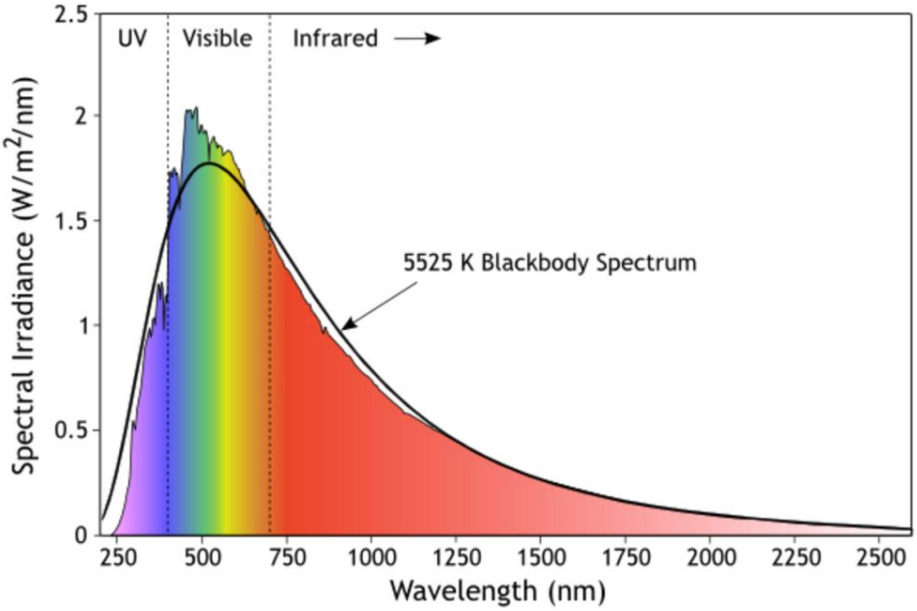

Figure 1.5. The AM 1.5 solar spectrum. (ref. 77)

semiconducting polymers with a maximum absorption near 700 nm would have the highest matching of the spectra with single absorption band.

Second, after many years of controversy about the origin of the V_{OC} in organic solar cells, what is clear now is that it is not defined by the work function of the electrodes but rather by the energy levels of the active layer materials. Several reports show no correlation of V_{OC} with the energy levels of the used cathode materials, and some even demonstrate V_{OC} values larger than the difference between the anode and cathode work functions. Recently a simple empirical expression was found that correlates V_{OC} in PSC devices with the energy difference between the HOMO energy level of the donor polymer and the LUMO energy level of the acceptor (fullerene derivatives).

$$V_{\mathrm{OC}} = \frac{1}{e} * \left[\left(E_{\mathrm{HOMO,donor}}\right) - \left(E_{\mathrm{LUMO,donor}}\right) - 0.3\ \mathrm{eV}\right]$$

Where e is the elementary charge, $E_{\mathrm{HOMO,donor}}$ is the HOMO energy level of donor polymer, $E_{\mathrm{LUMO,acceptor}}$ is the LUMO energy level of acceptor and 0.3 eV is an empirical factor for effective exciton dissociation. Therefore, if the donor polymer has a deep HOMO energy level, V_{OC} can be kept at a high value. Here, the LUMO energy difference between donor and acceptor should be at least higher than 0.3 eV for effective exciton dissociation.[78,79]

Consequently, it is not only important to synthesize polymers with a low bandgap; we also needs to consider the energy level alignment to increase the efficiency of OPV devices. The optimum energy levels of donor polymer are shown in Scheme 1.2, when PCBM (E_{LUMO} = –4.3 eV) is used as an acceptor. Generally, to obtain the optimum light harvesting and V_{OC} values, the energy levels of polymers should have HOMO energy levels between –5.2 and –5.7 eV and LUMO energy levels between –3.5 and –4.0 eV.[80,81]

1.2.2 Design concepts for low band gap polymers

There are several factors that influence the bandgap of a conjugated polymer. The Stabilization of the quinoid resonance structure is the first approach to consider. Generally, most of the conjugated polymers have two resonance structures: aromatic and quinoid. When the aromatic form and quinoid form are compared, the quinoid form has a smaller bandgap but is energetically

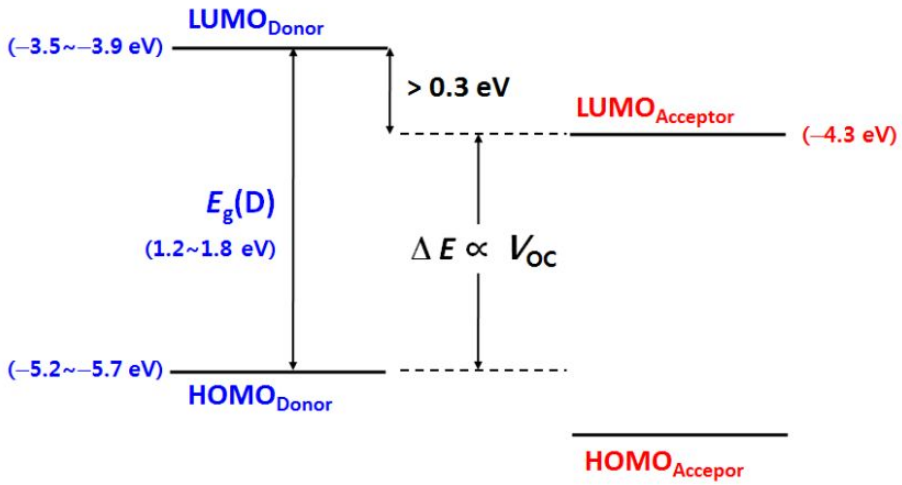

Scheme 1.2. The optimum energy levels of donor polymer for high performance PSCs.

less stable, since adopting the quinoid form requires destruction of the aromaticity and a loss in the stabilization energy. It was found that the quinoid form can be stabilized by fusing another aromatic ring to the polymer backbone.[71]

The other consideration is the effect of conjugation length because they are frequently used in designing low-band-gap polymers. Proper selection of conjugation size can facilitate π-electron delocalization and tune the band gaps and energy levels. Also it can enhance the charge carrier mobilities by preventing steric hinderance.[82–85] However, if the conjugation is too large, excessive π−π stacking interaction between the polymers may be introduced. Thus, the solubility and miscibility of the polymers with acceptor (PCBM) will drop significantly, leading to inferior performance.

Also, the low bandgap polymers are useful in structural modification because there are many sites along the backbone available for chemical functionalization. The functional group directly attached to the polymer backbone influence physical properties, especially electronic properties. For example, the HOMO energy level of P3HT is decreased from –5.10 to –4.95 eV by changing the side chain from normal alkyl to ester group,[86] while side chain with alkoxy group raises the HOMO energy level to –4.50 eV.[87]

1.2.3 Donor-acceptor (push-pull) type of low bandgap alternating copolymers

For high performance PSCs, efficient light absorption by increasing extinction coefficient and extending absorption region to overlap with the solar spectrum is required. The most effective way to broaden or narrow down absorption range of polymer is to incorporate alternative donor and acceptor unit (D–A) in the polymer, which is formed as D–A copolymer and possesses an intramolecular charge transfer between donor and acceptor units which leads to low bandgap. The principle of band gap and energy level manipulation can be explained by molecular orbital theory. As described in Scheme 1.3, the HOMO of donor unit interacts with that of acceptor unit by molecular orbitals (MOs) hybridization to form two new occupied MOs, where both units are connected with covalent bond. Also by the similar LUMO hybridization of donor and acceptor, other two new unoccupied MOs are formed. Finally, this redistribution of MOs results in a generation of higher-lying HOMO and a lower-lying LUMO and then in low

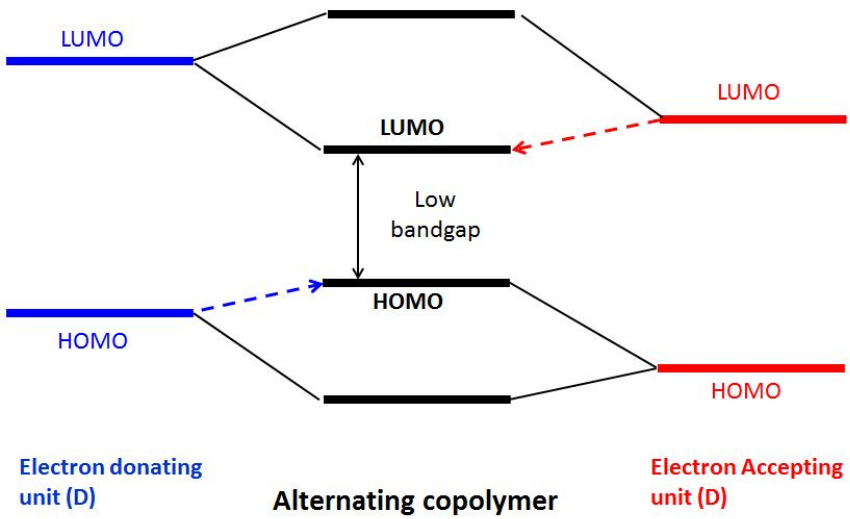

Scheme 1.3. Energy level diagram of the orbital hybridized HOMO and LUMO in D–A alternating copolymers.

bandgap.[74,76]

Over the years, a variety of high performance D−A polymers has been studied. Figure 1.6 and Figure 1.7 represent the widely used structure fragments of these polymers, such as thiophene,[88,89] thieno[3,2-*b*]thiophene,[90,91] phenylene,[92,93] naphthalene,[94] fluorene,[95–97] carbazole,[96,97] cyclopentadithiophene (CPDT),[98,99] benzodithiophene (BDT),[100–102] indacenodithiophene (IDT),[103–105] etc., for use as donor materilas and thieno[3,4-*b*]thiophene (TT),[106–108] benzothiadiazole (BT),[95,98,99] diketopyrrolopyrrole (DPP),[88,90,92,93], thienopyrroledione (TPD),[109,110] isoindigo (IID),[112–114] quinoxaline,[115,116] etc., for use as acceptor materials. Although initial concept of D−A copolymers are introduced in the 1990s

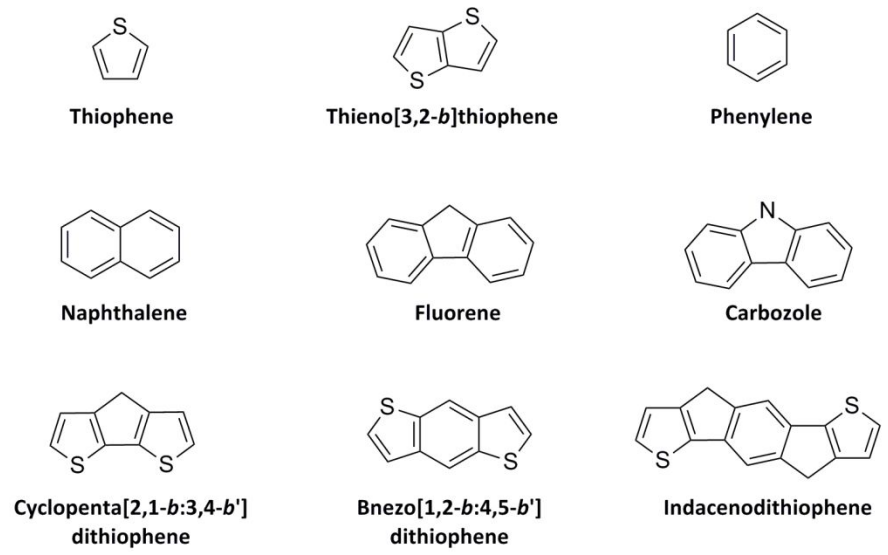

Figure 1.6. Chemical structures of D units widely used in D–A alternating copolymers.

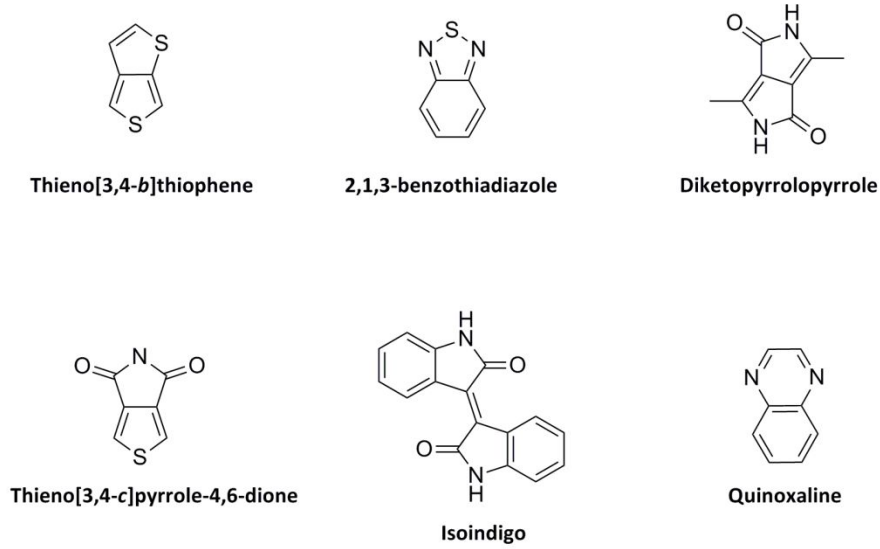

Figure 1.7. Chemical structures of A units widely used in D–A alternating copolymers.

with band gaps of 1.1 eV, it was not until 2003, fluorene- and BT-based D−A polymer PFDTBT was used in BHJ PSC.[60] Overall there has been remarkable progress in the field of organic solar cells and until now, rational design of polymers is still one of the most important key issues for further improvement of PSCs. Thus when designing alternating copolymer, we should carefully choose D or A units for desirable properties.

1.2.4 Influence of substituents on energy level of conjugated polymer

Substituents directly attached to the polymer backbone, such as fluorine, cyano group, and heteroatoms in the backbone, such as Si, Se and O, can strongly influence electronic properties (energy levels and dipole moments) of the resulting polymers. These effects have a great influence on the performance of PSC devices.

For example, the fluorine is the most electronegative atom in the periodic table, and thus it is an excellent substituent for solar cell polymers. It can lower both the HOMO and the LUMO energy levels without introducing much steric hindrance due to very strong electron-withdrawing ability with very small size. Also, fluorination changes the charge distribution along the polymer backbone and can also improve polymer crystallinity by inter- and intramolecular interactions (C−F···H, F···F and F···S).[117–119] On the contrary, Yang and co-workers reduce the bandgap of CPDT-based by introducing an oxygen atom to the CPDT unit to make the 5*H*-dithieno[3,2-*b*:2',3'-*d*]pyran unit (DTP).[120] The DTP-based polymer has a higher HOMO level than

CPDT-based polymer which is attributed to the strongly electron donating oxygen atom in the pyran ring. As a result, the optical absorption of CPDT-base polymer is extended to 900 nm, resulting in a high *J*sc of 17.8 mA/cm^2 and PCE of 7.9%.

1.2.5 Ternary blend organic solar cells

To overcome the absorption limitation of the donor polymers, various strategies are currently studied. As discussed above, design and synthesis of novel and high potential low bandgap alternating conjugated copolymers would extend light absorption to long wavelength, and then improve light harvesting. Alternatively, polymers with different bandgaps and absorption can be used into tandem cells. However, the fabrication of the tandem structure is more complex and leads to increased costs, since they are based on a complicated multi-layer stack with serious technical challenges. Those challenges are including processing of a robust intermediated layer, selection of appropriate absorbers and the optimization of the active layers' thicknesses.[121-124] Recently, a novel alternative strategy was proposed to extend the spectral sensitivity of wide bandgap polymers into the near IR region, which is called as ternary blend organic solar cell. In a ternary blend organic solar cell, which is shown in Figure 1.8, an IR sensitizer is simply mixed to the binary system composed of a wide bandgap donor polymer such as P3HT blended with fullerene derivative. For example, Huang *et al*. used 2,4- bis[4-(*N*,*N*-diisobutylamino)-2,6-dihydroxyphenyl] squaraine (SQ)

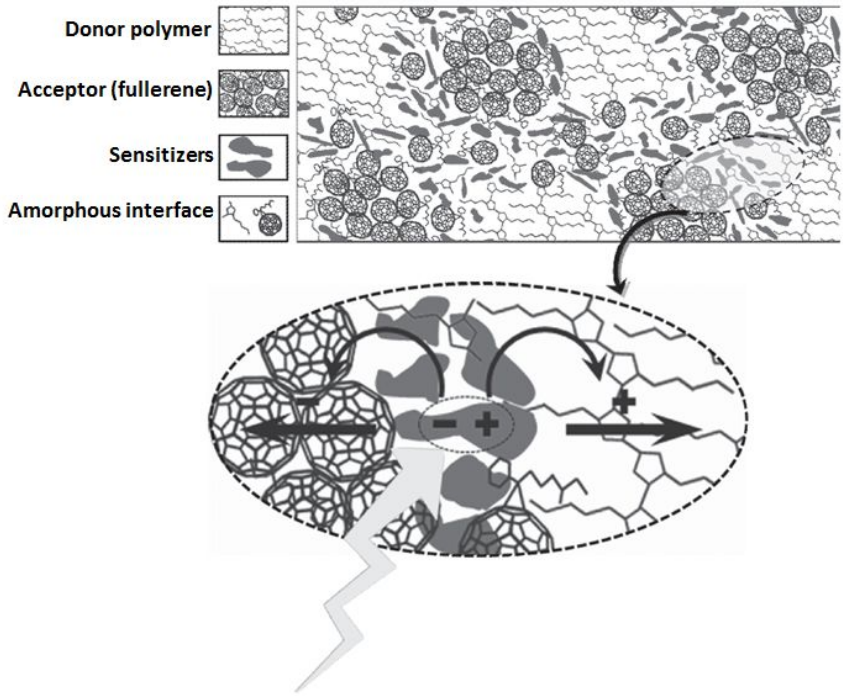

Figure 1.8. Illustration of an optimal microstructure of the ternary blends where the sensitizer positions directly at the interface between the host donor and acceptor. (ref. 125)

dye as a third compound as a donor material in P3HT/PCBM blend system.[126] The SQ dye molecule exhibits the maximum absorption peak around 647 nm, which satisfies not only complementary absorption as compared to that of P3HT, but also overlaps strongly with the photoluminescence of P3HT, enabling efficient FRET between SQ and P3HT. Further from the morphology studies, it is revealed that SQ molecules prefer to exist at the P3HT/PCBM interface and facilitate more ordered packing of P3HT fibrils. Along with the light absorption, both strong energy

transfer and better morphology also contribute to the much enhanced PCE from 3.27% to 4.51% in the device with 1 wt % SQ content.

Many previous works have focused on third component to the P3HT/PCBM blend system, because device physics of this system are most well understood.[127–132] Recently as progress in donor polymer design has changed from P3HT to alternating copolymer systems, the investigation of ternary blend organic solar cell has likewise been following this trend. In contrast to P3HT-based systems, where the host polymer is a wide bandgap material which needs a low bandgap material as a third component, these new systems are usually based on low bandgap polymers as a host donor and require the use of a wide bandgap material to obtain complementary absorption as a co-donor.[133–140]

However, the binary blend of D_1 and D_2 very often exhibits phase separation due to unfavorable interaction between two donors. The unfavorable interaction may cause severe molecular disorder and large domain size which act as the charge recombination trap site, and thereby decrease the PSC performance. Therefore it is essential for the efficient blend solar cells to combine two donors with complementary absorption and appropriate compatibility.[141] Yang *et al.*[137] reported a ternary blend solar cell based on the blend of two donor polymers (PTB7 and PBDTT-SeDPP) with different absorption range. They clearly demonstrated that the two donor polymers exhibit compatibility showing preferred molecular orientation, crystal size and domain structure. Very recently, Zhang *et al.*[140] designed high performance ternary blend solar cell with a PCE of 10.5% by adding

high crystalline small molecule (*p*-DTS-$(FBTTH_2)_2$) into PTB7-Th/$PC_{71}BM$ binary blend. They reported that two donors (*p*-DTS-$(FBTTH_2)_2$ and PTB7-Th) are miscible and that an addition of the small molecule increases the crystallinity and the face-on orientation of donor polymers in the ternary blend, which afford high hole mobility and thus increase J_{SC} and FF, although *p*-DTS-$(FBTTH_2)_2$ and PTB7-Th show similar light absorption range.

1.2.6 Random copolymers for polymer solar cells

The ternary blend approach is useful for achieving the broad light absorption because the absorption range can be widen as two different components with a complementary absorption range are used as active layer materials. However, the successful increase of the J_{SC} has rarely been reported due to difficulty in morphology control. In order to improve the J_{SC}, a new approach is required, and random copolymer is another promising candidate for designing new donor polymer for PSCs.

Random copolymer consisting of two different monomers may have broad absorption range if the absorptions of two monomers are complementary to each other (Figure 1.9).[142–149] Secondly, the molecular energy levels of random copolymer can be easily tuned by controlling the monomer composition in copolymer.[150,151] Third, a proper choice of comonomer can control the molecular packing of the copolymer: a choice of comonomer with planar molecular structure can enhance the interaction

between copolymer chain backbones.[152–154] However, the dissimilar chemical structure of comonomers and the random sequence in copolymer chain may cause an adverse effect on crystallinity, and therefore the random copolymer strategy has still an important problem to be solved. Thus, it is essential to design the molecular structure of random copolymer not to disturb crystallization.[155–158]

There are two methods to synthesize random copolymer: One is 1D/2A copolymer which consists of one D unit and two A units, and another is 2D/1A copolymer with two D units and one A unit. According to previous reports for random copolymer, the former method was used to extend the light absorption range while the latter method was used to control the crystallinity of copolymers. Our group also reported 1D/2A-type random conjugated copolymers, in which thiophene-capped diketopyrrolopyrrole (TDPP) and isoindigo were used as co-electron accepting units.[142] The random copolymers consisting of two different chromophores show broad light absorption spectrum, and the compositional variation of two chromophores with different electron withdrawing power also allow us to tune the HOMO and LUMO energy levels of the copolymer. Consequently, the random copolymer with the feed ratio of 1:1 shows higher PCE (6.04%) than those of two homopolymers due to wide absorption range of the solar spectrum from 600 to 900 nm with low lying HOMO energy level. Recently Kim *et al.* synthesized 2D/1A-type random copolymers containing TDPP as an A unit and two different D units of thiophene and selenophene (Se) to control the crystallization and crystal structure.[153] They found that the

crystallinity of the copolymer is dramatically increased with increasing the Se content in the random copolymer, and also observed that the morphology of polymer:PCBM BHJ film strongly depends on the Se content. The best PCE (7.2%) of the random copolymer with the optimal Se content is higher than that of reference homopolymer (6.8%). Based on the considerations above, random copolymer structures have great potential for increasing the photocurrent in BHJ photovoltaic devices.

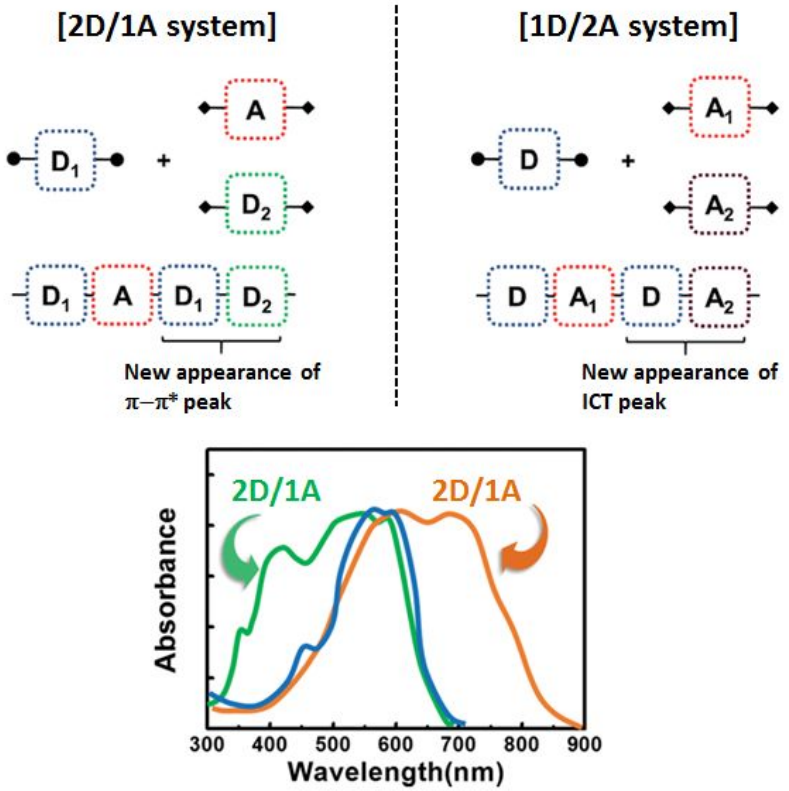

Figure 1.9. Two different approaches for achieving broad absorption by random copolymer stragegy. (ref. 159)

1.3 Objectives of this study

Recently, researchers have paid a great deal of attention to the research and development of organic solar cells, leading to a breakthrough of over 10% power conversion efficiency. One primary requirement of highly efficient conjugated polymers is a suitable match between their light absorption and the photon flux of the solar spectrum. Until now, much effort in the research community has been devoted to improving the absorption features of PSCs by fine tuning absorption characteristics.

As mentioned above, with a low bandgap and broad absorption band, the polymer can absorb more photons, which will increase the J_{SC}. Among various semiconducting polymers for PSCs, a copolymer consisting of fluorene as an electron-donating unit exhibits a high V_{OC} because of its deep HOMO energy level, but it shows relatively low J_{SC}s and PCE due to a large bandgap.[60] Thus, although the V_{OC} is sacrificed to some extent, we should design more powerful electron donating unit than fluorene by introducing oxygen atom into fluorene in order to reduce the bandgap of polymers by raising the HOMO energy level.

The use of ternary blend structure-active layer is another way to broaden absorption band of polymer without V_{OC} sacrifice. We prepared TDPP-based polymer (PTDPP2T) and small molecule ($(TDPP)_2Ph$) as donor material, and $PC_{71}BM$ as an acceptor material for ternary blend solar cell. Among various A units, TDPP has widely been used as an A unit for D–A type conjugated polymers for PSCs and OFETs due to its unique properties such

as high extinction coefficient, strong electron-accepting power and molecular planarity, which may improve charge carrier transport. Also, introduction of various branched alkyl groups into *N*-position of DPP affords solubility of DPP-based semiconducting polymers.[160–163] Especially, a low bandgap TDPP-based polymer (PTDPP2T) composed of TDPP and bithiophene (2T) shows high J_{SC} due to its low bandgap and well-developed BHJ morphology,[164] and we have already reported the TDPP-based small molecule ($(TDPP)_2Ph$),[165] which shows complementary absorption as compared to PTDPP2T. Thus, we anticipate enhancement of J_{SC} came from extended light harvesting in the solar spectrum.

Also, in order to further enhance J_{SC}, we introduce random copolymer strategy since the molecular energy levels of random copolymer can be easily tuned by controlling the monomer composition in copolymer. According to this strategy, we synthesized a new series of 1D/2A-type DPP-based random copolymer by copolymerization of 2T with TDPP and pyridine-capped DPP (PyDPP) (co-electron accepting units). Recently, PyDPP, which is more electron deficient than TDPP, has been used as a strong electron-accepting building block.[166–168] Our group[166] and Sun *et al.*[167] synthesized a PyDPP-based copolymer (PPyDPP2T) with deep HOMO and LUMO energy levels by copolymerization of 2T and PyDPP. The PPyDPP2T-based solar cell exhibits a high V_{OC} of 0.9 V with a record high electron mobility of 6.30 $cm^2\ V^{-1}\ s^{-1}$ in OTFT device. Thus we expect synergetic effect of high J_{SC} and high V_{OC}, which is originated from TDPP and PyDPP, respectively.

Chapter 2. Synthesis of 6*H*-benzo[*c*]chromene as a new electron-rich building block of conjugated alternating copolymers and its application to polymer solar cells

2.1 Introduction

Recently, remarkable progress has been made in polymer/fullerene BHJ solar cells, demonstrating that the power conversion efficiency (PCE) of PSCs reaches over 8–9%. However, it is still needed to further improve the PSC performance for commercialization. One of the most effective methods to improve the PCE is to develop new donor polymers, which have ideal energy levels and planar structures as well as good solubility in organic solvents.

To obtain high short-circuit current (J_{SC}) of PSCs, one must consider several factors: (i) broad and strong light absorption in the active layer, (ii) efficient charge separation before geminate recombination and (iii) good charge transport characteristics of conjugated copolymers. A commonly used strategy to acquire broad and strong absorption in the active layer is to synthesize a low bandgap polymer, consisting of alternating electron-donating and electron-accepting units. It has been known that the charge separation is dependent upon the dipole moment change of donor polymer from the ground state to the excited state ($\Delta\mu_{ge}$).[169,170] As proposed by Yu and other groups, a

large value of $\Delta\mu_{ge}$ suppresses geminate recombination and facilitates charge separation. Another approach to improve J_{SC} is to incorporate a planar molecular unit into the polymer backbone, which may enhance electron delocalization and promote cofacial π–π stacking, thus benefitting charge transport in the PSC device.

Among various semiconducting polymers for PSCs, a copolymer consisting of fluorene as an electron-donating unit and benzothiadiazole as an electron-accepting unit, poly{9,9-bisalkyl fluorene-2,7-diyl-alt-[4,7-bis-(thien-2-yl)-2,1,3-benzothiadiazole]-50,500diyl} (PFDTBT), exhibits a high V_{OC} of around 1 V because of its deep HOMO energy level, but it shows relatively low PCEs with moderate J_{SC}s due to a large bandgap of 1.9 eV. The other critical issue of the PFDTBT-based polymer is the solubility in organic solvent. Previously, it has been reported that bis-octyl-substituted PFDTBT has poor solubility, and therefore only a low average molecular weight (M_n = ~5k) of the polymer was obtained, which leads to a low PCE of 2%.[171] Therefore, other PFDTBTs with longer and branched side chains such as decyl (M_n = 17 k), 2-ethylhexyl (M_n = 21 k) and 3,7-dimethyloctyl35 (M_n = 20 k) were synthesized, and the devices based on these polymers showed higher PCEs of 4.0–4.5% due to better solubility and higher molecular weight.[172,173] However, the J_{SC}s of the devices are still moderate (7.0–9.0 mA cm^{-2}) probably because of a large bandgap.

Another electron accepting unit that has attracted significant interest in the past few years is thiophene-capped diketopyrrolopyrrole, which exhibits intense absorption at long wavelength and good field effect mobilities.

Recently, the Janssen group synthesized a copolymer (PFDPP2T) consisting of DPP2T and fluorene, and utilized the copolymer in the photovoltaic device.[174] Although the PFDPP2T-based device shows a high V_{OC} of ~ 0.9 V due to its deep HOMO energy level, the polymer affords a low PCE of 0.9% with a low J_{SC} of 2.41 mA cm^{-2}. One of the reasons for the low J_{SC} is probably a large bandgap of 1.79 eV, which is a common problem of the fluorene-based polymer.

In this study, we introduce an oxygen atom into a bis-octyl-substituted fluorene unit in order to develop a new electron donating unit, benzochromene (BC). BC was then polymerized with an electron-accepting unit, dithienyl benzothiadiazole (DTBT) or DPP2T to synthesize two low bandgap polymers (PBCDTBT and PBCDPP2T) (See Scheme 2.1). Since the electron donating ability of BC is stronger than fluorene, it is expected that the BC-based polymers (PBCDTBT and PBCDPP2T) exhibit narrower bandgaps than the corresponding fluorene-based polymers (PFDTBT and PFDPP2T), respectively, by raising their HOMO energy level. BC-based polymers are also expected to have better solubility due to the regio-random molecular structure in the backbone and higher M_n than the corresponding fluorene-based polymer.

2.2 Experimental

2.2.1 Materials

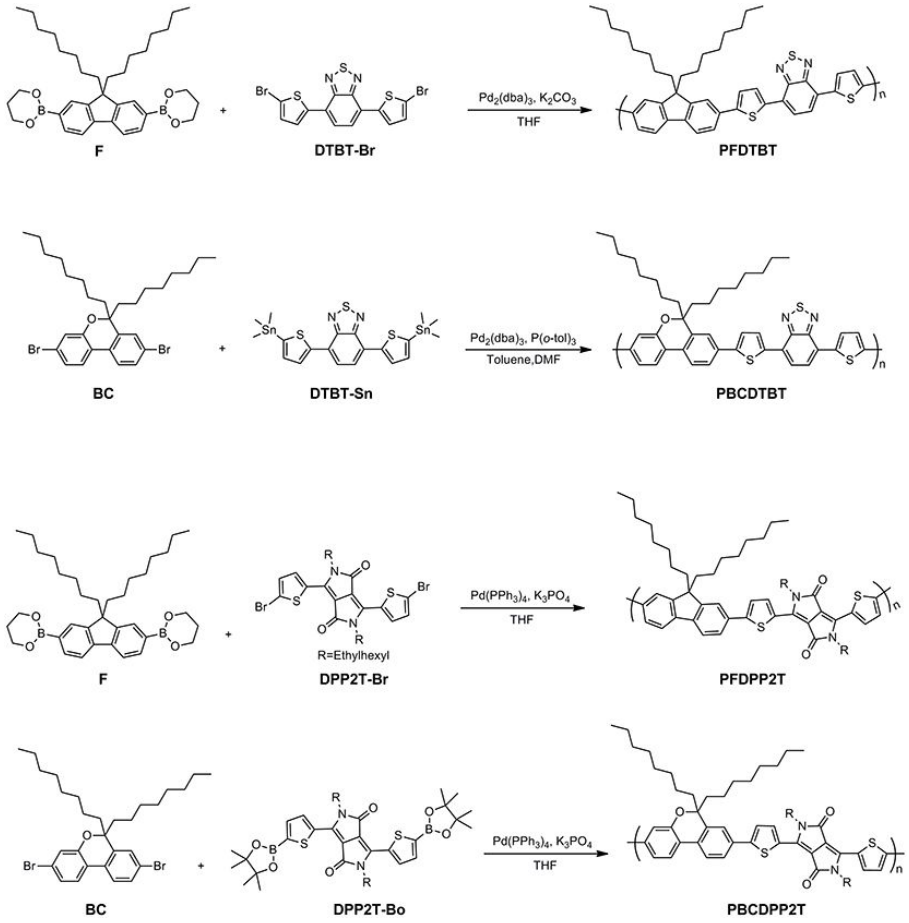

Scheme 2.1. Chemical structures of PFDTBT, PBCDTBT, PFDPP2T and PBCDPP2T.

9,9-Dioctyl fluorene-2,7-diboronic acid bis(1,3-propanediol) ester, 2,7-dibromo-9-fluorenone, sodium perborate monohydrate, octylmagnesium bromide, *p*-toluenesulfonic acid monohydrate, 2,2,6,6-tetramethylpiperdine, *n*-butyllithium and trimethyltin chloride were purchased from Sigma-Aldrich and used without further purification. [6,6]-Phenyl-C_{71}-butyric acid methyl ester ($PC_{71}BM$) was obtained from Nano-C. Poly(3,4-ethylenedioxy-thiophene):poly(styrene sulfonate) (PEDOT:PSS) (Clevious P VP AI 4083) was purchased from H. C. Stark and passed through a 0.45 μmPVDF syringe filter before spin-coating. Common organic solvents were purchased from Daejung. Tetrahydrofuran was dried over sodium/benzophenone under nitrogen and freshly distilled prior to use. All other reagents were purchased from Tokyo Chemical Industry and used as received.

2.2.2 Measurements

The chemical structures of compounds were identified by ^{1}H NMR and ^{13}C NMR (Avance DPX-300). Molar masses of compounds were measured on a mass spectrometer (HP 5890) in electron-impact mode. Molecular weight and its distribution of polymers were measured by GPC (Polymer Labs GPC 220 and Waters) with a refractive index detector. Chloroform was used as an eluent, and the molecular weight of polymers were calibrated by polystyrene standards. The optical absorption spectra were obtained by a UV–vis spectrophotometer (Shimadzu UV-3600 and Lambda 25, Perkin Elmer). Cyclic voltammetry was conducted on a potentiostat/galvanostat (VMP 3,

Biologic) in an electrolyte solution of 0.1 M tetrabutylammonium hexafluorophosphate acetonitrile. Pt wires (Bioanalytical System Inc.) were used as both counter and working electrodes, and silver/silver ion (Ag in 0.1 M $AgNO_3$ solution, Bioanalytical System Inc.) was used as a reference electrode. The HOMO energy levels of polymers were calculated by using the flowing relation: HOMO (eV) = $-[E_{ox} - E_{1/2}(\text{ferrocene}) + 4.8]$, where E_{ox} is the onset oxidation potential of the polymer and $E_{1/2}$(ferrocene) is the onset oxidation potential of ferrocene vs. Ag/Ag^+. Density functional theory (DFT) calculations were carried out at the B3LYP/6-31G(d,p) level on Gaussian 03 and 09. Dipole moments in ground and excited states were calculated with time-dependent DFT. The one dimensional XRD patterns were obtained from an X-ray diffractometer (New D8 Advance, Bruker) using Cu-Kα radiation (λ = 1.5418 Å) at a scan rate of 2° min^{-1}. The GIWAXS measurements were performed at PLS-II 9A U-SAXS beamline of Pohang Accelerator Laboratory in Korea. The thin film morphology was observed by TEM (JEM1010) operating at an acceleration voltage of 80 kV. DSC analysis was performed on a TA Instruments 2910 Modulated DSC (Dupont) under N_2 at a heating rate of 10 °C min^{-1}. Thickness of the active layers was measured by the atomic force microscopy (Nano Xpert2). These measurements were used in chapter 3 and chapter 4 with same procedure.

2.2.3 Fabrication of polymer solar cell device

The polymer solar cells were fabricated with a configuration of

ITO/PEDOT:PSS/polymer:$PC_{71}BM$/Ca/Al. PEDOT:PSS was spin-coated with 40 nm thickness on the ITO-coated glass and annealed at 150 ºC for 30 min. The blend solution with various solvent was spin-coated on the top of the PEDOT:PSS layer. The film thickness of the active layer was measured by AFM (Nano Xpert 2, EM4SYS). Calcium (20 nm) and aluminum (100 nm) was thermally evaporated on the top of the active layer under vacuum ($<10^{-6}$ Torr). The effective area of the cell was 0.1 cm^2. The same solar cell device fabrication method was used in chapter 3 and chapter 4 with same procedure.

2.2.4 Characterization of polymer solar cell

The *J–V* characteristics were measured with a Keithley 4200 source-meter under AM 1.5G (100 mW/cm^2) simulated by a Newport-Oriel solar simulator. The light intensity was calibrated using a NREL-certified photodiode prior to each measurement. The external quantum efficiencie (EQE) was measured using a lock-in amplifier with a current preamplifier (K3100, Mac Science Co.) under short circuit current state with illumination of monochromatic light. The space charge limited current (SCLC) *J–V* curves were obtained in the dark using hole-only devices (ITO/PEDOT:PSS/polymer:$PC_{71}BM$/Au), and hole mobilities were calculated using the Mott-Gurney square law, $J = (9/8)\varepsilon_0\varepsilon_r\mu(V^2/L^3)$, where ε_0 is vacuum permittivity, ε_r is the dielectric constant of polymer, μ is the charge carrier mobility, V is the effective applied voltage, and L is the thickness of the film. The same characterization of polymer solar cell was used in chapter 3 and chapter 4.

2.2.5 Synthesis of monomers and polymers

2.2.5.1 Synthesis of copolymers based on benzothiadiazole copolymerized with fluorene and 6*H*-benzo[*c*]chromene

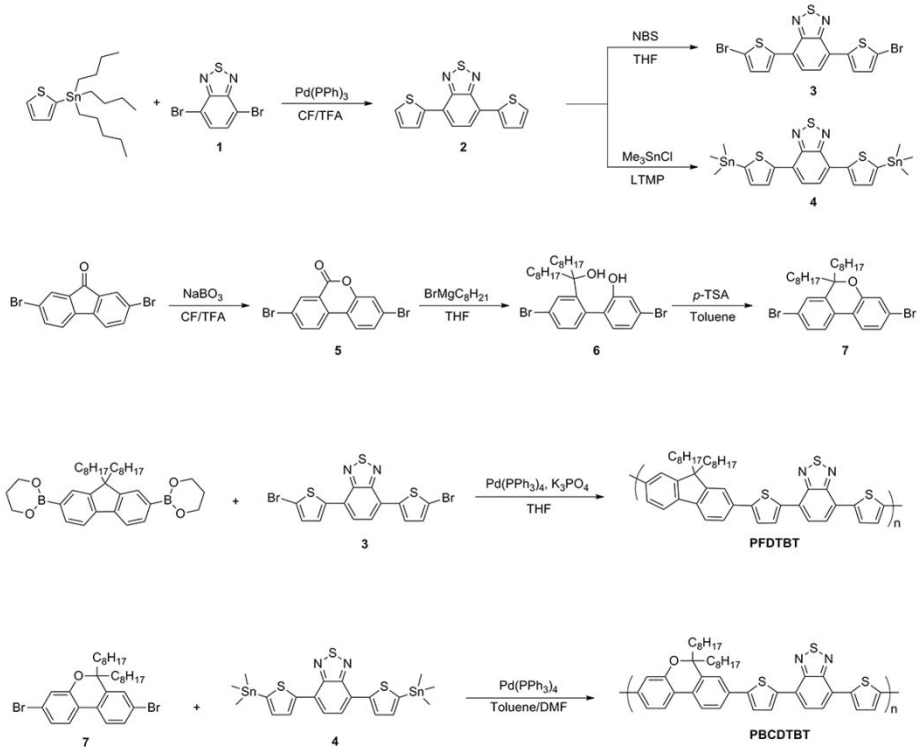

Scheme 2.2. Synthetic scheme of 6*H*-benzo[*c*]chromene and copolymers based on benzothiadiazole copolymerized with fluorene and 6*H*-benzo[*c*]chromene.

Synthesis of 4,7-dibromobenzo[*c*]-[1,2,5]thiadiazole (1): To a three-necked 250 mL round-bottom flask equipped for stirring was added 2,1,3-benzothiadiazole (6.8 g, 50.0 mmol) and 50 mL of hydrobromic acid. The mixture was heat to 110 ℃, and bromine (8.3 mL, 150.0 mmol) was added dropwise to the mixture. After stirring for 30 min, another portion of hydrobromic acid (20 mL) was added. The reaction mixture was refluxed at 110 °C for 3 h under stirring. After cooled to room temperature, the mixture was filtered. The solid residue was washed thoroughly with water and dried under vacuum. Recrystallization from chloroform yielded a yellow solid as a product. Yield: 82 %. ^{1}H NMR (300 MHz, $CDCl_3$): δ (ppm) 7.73 (s, 2H).

Synthesis of 4,7-di(thiophen-2-yl)benzo[*c*]-[1,2,5]thiadiazole (2): 1 (5.0 g, 17 mmol), 2-(tributylstannyl)thiophene (14.6 g, 39 mmol) and $Pd(PPh_3)_2Cl_2$ (1.194 g, 1.7 mmol) were dissolved into THF (125 mL) under argon. After purged by argon for 30 min, the reaction mixture was heated to 75 °C and heated at reflux for 19 h, before cooling to room temperature. H_2O was added and the mixture was extracted into CH_2Cl_2. The combined organic solution was washed with brine, dried over anhydrous $MgSO_4$, and concentrated under reduced pressure after filtration. The resulting dark brown residue was purified by column chromatography (silica gel, hexane/$CH2Cl_2$, 4:1, v/v). The final product was recrystallized from ethanol to afford orange needle-like crystals. Yield: 65 %. ^{1}H NMR (300 MHz, $CDCl_3$): δ (ppm) 8.13 (d, 2H), 7.89 (s, 2H), 7.46 (d, 2H), 7.22 (d, 2H).

Synthesis of 4,7-bis(5-bromothiophen-2-yl)benzo[*c*][1,2,5]thiadiazole (3): To a stirred solution of 2 (1.44 g, 4.8 mmol) in THF, NBS (2.05 g, 4.8 mmol) was added in darkness. The mixture was stirred at room temperature for 12 h. The product was extracted into chloroform and the organic phase and dried over $MgSO_4$. The solvent was removed to afford the product as dark red crystals that were recrystallized from chloroform. Yield: 59%. ^{1}H NMR (300 MHz, $CDCl_3$): δ (ppm) 7.80 (d, 4H), 7.13 (d, 2H).

Synthesis of 4,7-bis(5-(trimethylstannyl)thiophen-2-yl)benzo[*c*][1,2,5]thiadiazole (4): 2,2,6,6-tetramethylpiperdine (1.46 mL, 8.66 mmol) was dissolved into dry THF (20 mL) under argon. *n*-butyllithium (3.46 mL of a 2.5 M solution in hexane, 8.66 mmol) was added into the solution rapidly at −78 °C. The resulting solution was stirred at −78 °C for 30 min, and was warmed to room temperature and stirred for 10 min, to afford lithium 2,2,6,6-tetramethylpiperidide (LTMP). The solution was cooled to −78 °C and **2** (1.0 g, 3.33 mmol) in THF (15 mL) was added in a dropwise manner, during which time the colorless solution turned purple. The resulting solution was stirred at −78 °C for 45 min; and trimethyltin chloride (8.32 mL of a 1.0 M solution in THF, 8.33 mmol) was then added in a dropwise manner, during which time the solution turned from purple to orange. The solution was then warmed to room temperature and was stirred for 12 h. Brine was added and the mixture was extracted into CH_2Cl_2, washed with brine, dried over anhydrous M_gSO_4, and concentrated under reduced pressure after filtration. The residue was recrystallized from ethanol to give orange needle-like

crystals (yield: 90%). ^{1}H NMR (300 MHz, $CDCl_3$): δ (ppm) 8.18 (d, 2H), 7.88 (s, 2H), 7.30 (d, 2H), 0.43. (s, 18H).

Synthesis of 3,8-dibromo-6H-benzo[*c*]chromen-6-one (5): 2,7-dibromo-9*H*-fluoren-9-one (1.00 g, 2.96 mmol) was dissolved in a solvent mixture of 15 mL of chloroform and 15 mL of trifluoroaceticacid, followed by addition of sodium perborate monohydrate (0.68 g, 6.80 mmol) in one portion. After the reaction mixture was stirred at room temperature for 12 h, it was poured into 150 mL of dichloromethane and then extracted with water, sodium bicarbonate and brine. The organic phase was collected and dried over MgSO4. The product was sequentially recrystallized with toluene and then chloroform to afford light yellow powder. Yield: 56%. ^{1}H NMR (300 MHz, $CDCl_3$): δ (ppm) 8.49 (s, 1H), 7.92 (s, 2H), 7.85 (d, 1H), 7.51 (d, 1H), 7.48–7.44 (m, 1H). ^{13}C NMR (125 MHz, $CDCl_3$): δ (ppm) 159.19, 151.38, 138.18, 133.35, 132.89, 128.15, 124.23, 123.86, 123.41, 123.21, 122.48, 121.08, 116.44. HRMS (EI, *m*/*z*): calculated for $C_{13}H_6Br_2O_2$: 351.87, found: 351.87.

Synthesis of Synthesis of 4,4'-dibromo-2'-(9-hydroxyheptadecan-9-yl)-[1,1'-biphenyl]-2-ol (6): Compound **5** (0.50 g, 1.41 mmol) was dissolved in dry THF (20 mL) under argon and kept at 0 °C. 1 M diethyl ether solution of octylmagnesium bromide (3.26 mL, 3.26 mmol) was slowly added into the solution. The resulting solution was then warmed to room temperature and stirred for 10 h. The reaction mixture was quenched by addition of 12 mL of water and 3 mL of hydrochloric acid, and then extracted with DCM. After the

organic phase was dried over $MgSO_4$, the solvent was evaporated under reduced pressure. The crude product was purified by column chromatography on silica gel using ethyl acetate and hexane mixture (1:8, v/v) as an eluent to obtain light yellow oil. Yield: 75%. ^{1}H NMR (300 MHz, $CDCl_3$): δ (ppm) 7.66 (d, 1H), 7.42 (m, 1H), 7.13 (d, 1H), 7.07 (m, 1H), 6.84–6.91 (m, 2H), 5.29 (s, 1H), 1.68 (s, 1H), 1.25–1.17 (m, 24H), 0.89–0.84 (m, 6H). ^{13}C NMR (125 MHz, $CDCl_3$): δ (ppm) 153.79, 147.20, 134.67, 132.58, 131.11, 130.88, 130.20, 129.33, 123.30, 122.98, 122.19, 119.67, 78.35, 42.19, 41.31, 31.83, 31.81, 30.32, 29.89, 29.72, 29.47, 29.37, 29.25, 29.18, 24.02, 23.47, 22.63, 22.61, 14.08. HRMS (EI, *m*/*z*): calculated for $C_{29}H_{42}Br_2O_2$: 580.16, found: 580.15.

Synthesis of Synthesis of 3,8-Dibromo-6,6-dioctyl-6*H*-benzo[*c*]chromene (7): Compound **6** (0.58 g, 1 mmol) was dissolved in toluene (20 mL) in a two-neck flask under argon. After *p*-toluenesulfonic acid monohydrate (0.57 g, 3 mmol) was added into the solution, the mixture was stirred at 120 °C for 15 h. The solution was cooled down to room temperature and extracted with DCM. After the organic phase was dried over $MgSO_4$, the solvent was evaporated under reduced pressure. The residue was purified by column chromatography on silica gel using hexane as an eluent to afford colorless oil Yield: 88%. ^{1}H NMR (300 MHz, $CDCl_3$): δ (ppm) 7.53 (d, 1H), 7.48 (m, 1H), 7.41–7.44 (d, 1H), 7.20 (d, 1H), 7.10–7.07 (m, 2H), 1.83–1.81 (m, 4H), 1.29–1.21 (m, 24H), 0.88–0.83 (m, 6H). ^{13}C NMR (125 MHz, $CDCl_3$): δ (ppm) 153.68, 138.67, 130.64, 127.87, 127.67, 124.36, 123.74,

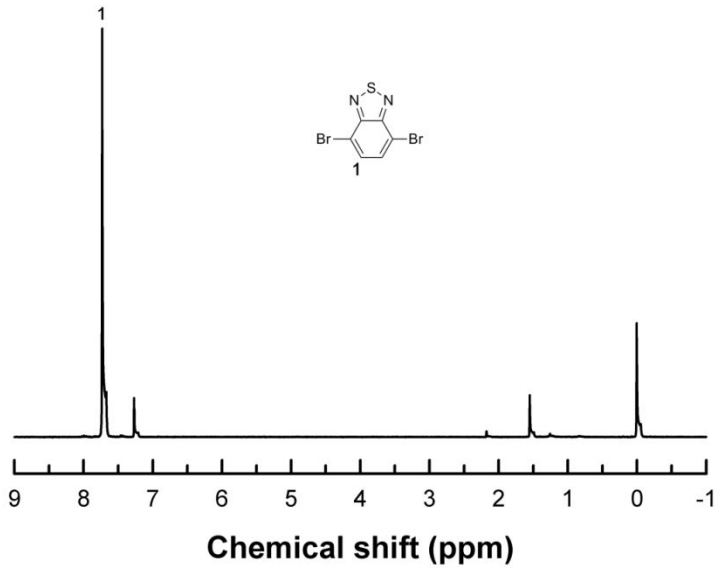

Figure 2.1. ^{1}H NMR spectrum of compound **1** in Scheme 2.2.

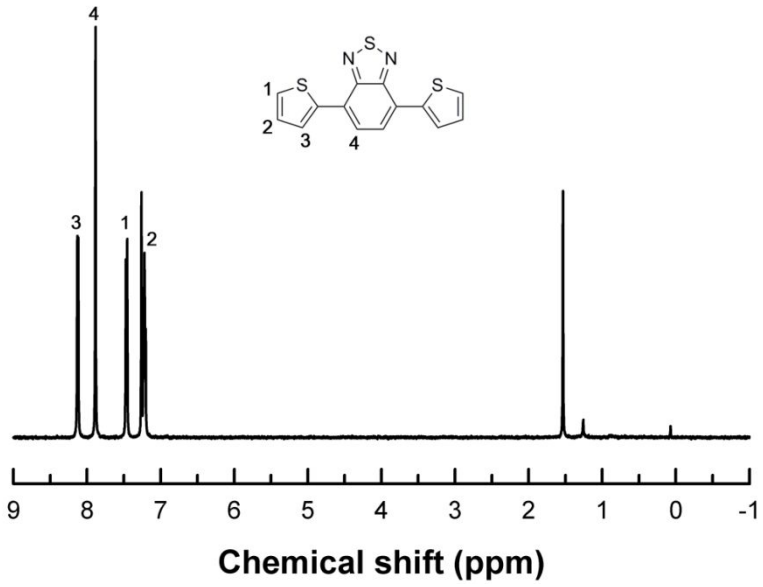

Figure 2.2. ^{1}H NMR spectrum of compound **2** in Scheme 2.2.

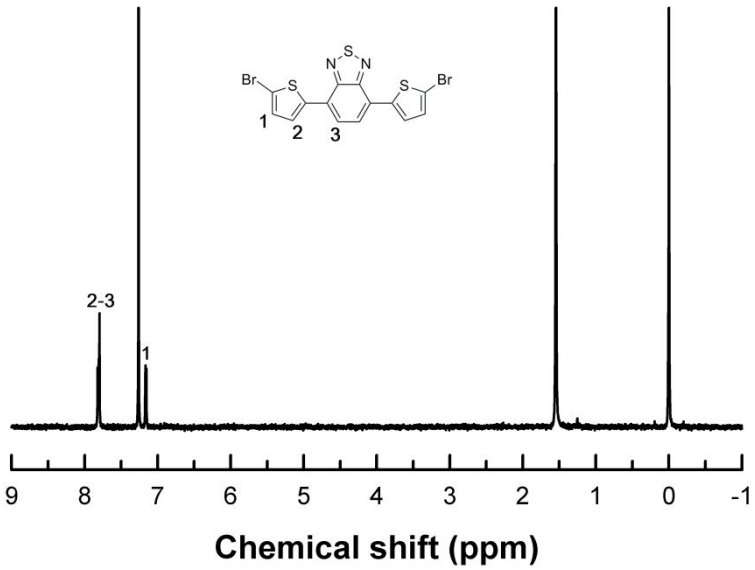

Figure 2.3. ^{1}H NMR spectrum of compound **3** in Scheme 2.2.

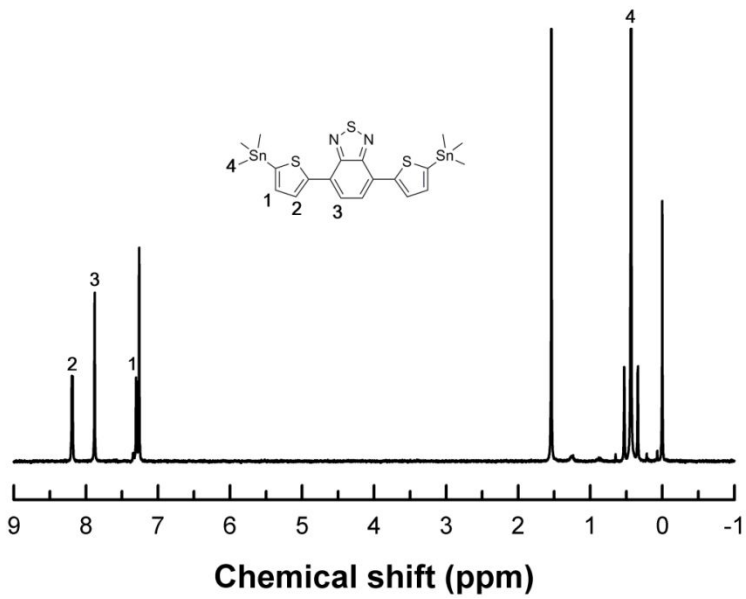

Figure 2.4. ^{1}H NMR spectrum of compound **4** in Scheme 2.2.

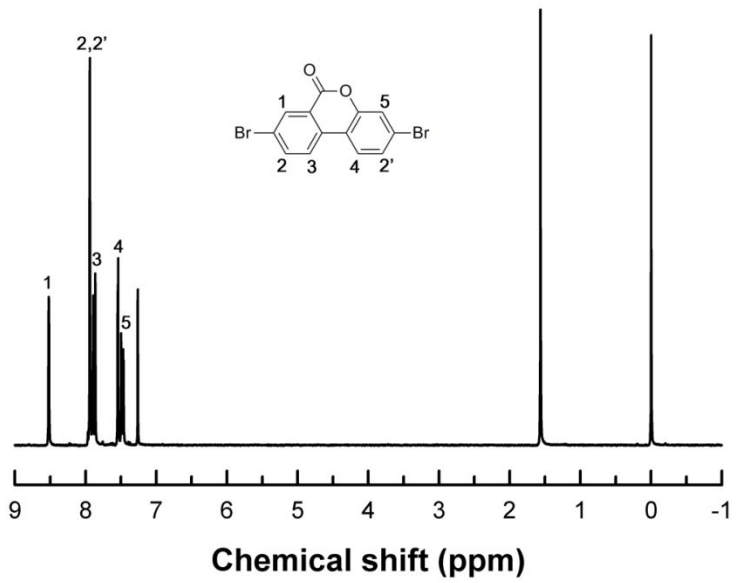

Figure 2.5. ^{1}H NMR spectrum of compound **5** in Scheme 2.2.

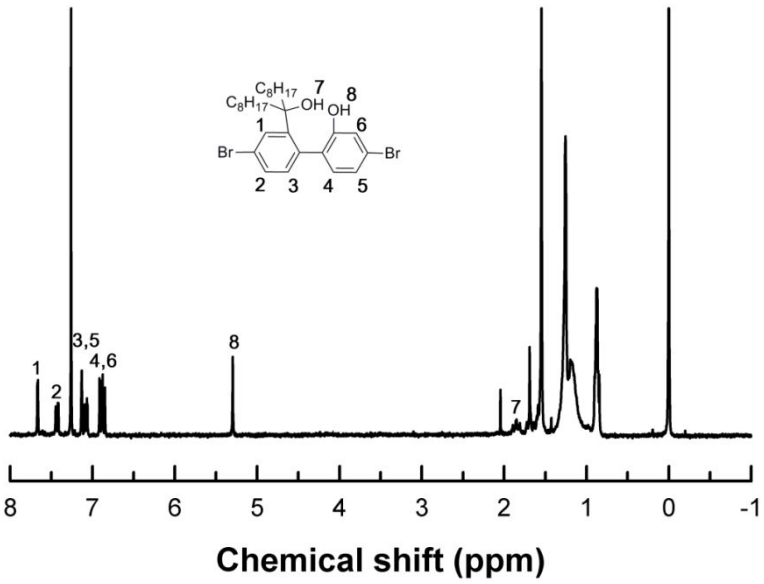

Figure 2.6. ^{1}H NMR spectrum of compound **6** in Scheme 2.2.

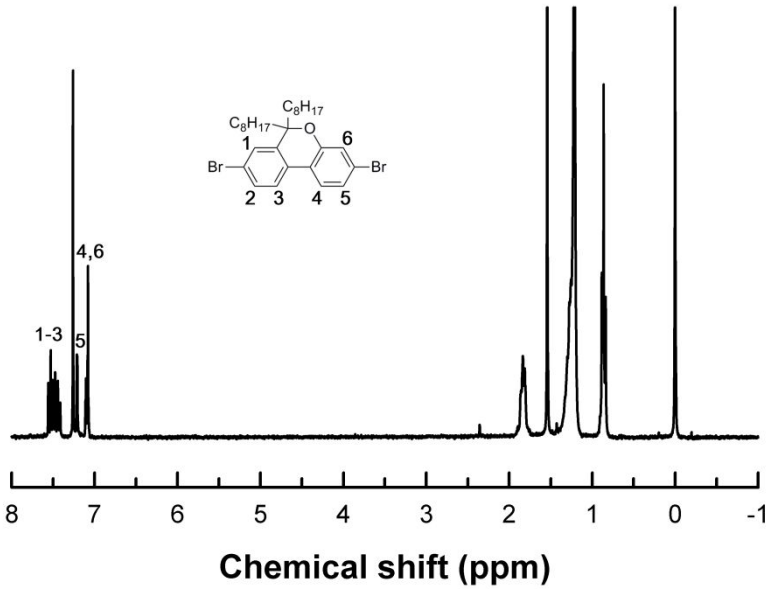

Figure 2.7. ^{1}H NMR spectrum of compound **7** in Scheme 2.2.

123.54, 122.76, 121.74, 120.92, 119.84, 82.99, 38.86, 31.81, 29.82, 29.36, 29.20, 23.54, 22.63, 14.08; HRMS (EI, *m*/*z*): calculated for $C_{29}H_{40}Br_2O$: 562.14, found: 562.14.

Polymerization of PFDTBT: PFDTBT was synthesized by the Suzuki coupling. A mixture of 9,9-dioctylfluorene-2,7-diboronicacid-bis-(1,3-propanediol)ester (0.15 g, 0.27 mmol), DTBT-Br (0.12 g, 0.27 mmol) and P(*o*-tol)$_3$ (0.02 g, 0.06 mmol) was dissolved in a mixture of aqueous K_3PO_4 solution (2 M, 3.3 mL) and THF (10 mL). After the solution was flushed with argon for 10 min, $Pd_2(dba)_3$ (0.02 g, 0.02 mmol) was added quickly into the reaction mixture and sealed. The reaction mixture was stirred at 140 °C for 3 h in a microwave reactor. After being cooled to room temperature, the organic

phase was poured into methanol during stirring. The precipitate was filtered through a Soxhlet thimble and subjected to Soxhlet extraction sequentially with methanol, acetone, ethyl acetate, hexane and chloroform. The polymer was recovered from the chloroform fraction, and precipitated into methanol to afford a reddish-purple solid Yield: 69%. ^{1}H NMR (300 MHz, $CDCl_3$): δ (ppm) 8.13 (br, 1H), 7.89 (br, 1H), 7.66 (d, 3H), 7.46 (br, 1H), 7.34 (br, 2H), 2.04 (br, 3H), 1.11 (br, 16H), 0.78 (br, 8H).

Polymerization of PBCDTBT: PBCDTBT was synthesized by the Stille coupling. A mixture of BC (0.11 g, 0.19 mmol), DTBT-Sn (0.12 g, 0.19 mmol) and P(*o*-tol)$_3$ (0.01 g, 0.03 mmol) was dissolved in a mixture of toluene (9 mL) and DMF (1 mL). After the solution was flushed with argon for 10 min, $Pd_2(dba)_3$ (0.01 g, 0.01 mmol) was added quickly into the reaction mixture and sealed. The reaction mixture was stirred at 130 °C for 2 h in a microwave reactor. After being cooled to room temperature, the organic phase was poured into methanol during stirring. The precipitate was filtered through a Soxhlet thimble and subjected to Soxhlet extraction sequentially with methanol, acetone, ethyl acetate, hexane and chloroform. The polymer was recovered from the chloroform fraction, and precipitated into methanol to afford a bluish-purple solid. Yield: 51%. ^{1}H NMR (300 MHz, $CDCl_3$): δ (ppm) 7.10 (br, 29H), 4.86 (br, 1H), 2.04 (br, 21H), 1.25 (br, 15H), 0.82 (br, 28H).

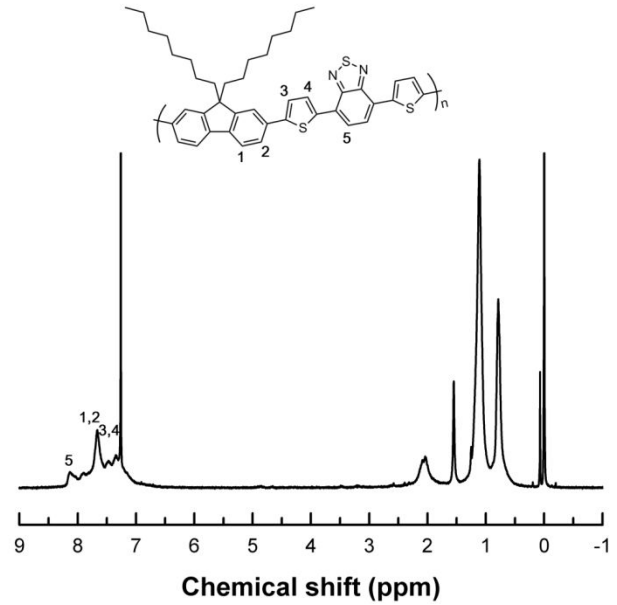

Figure 2.8. ^{1}H NMR spectrum of **PFDTBT** in Scheme 2.1.

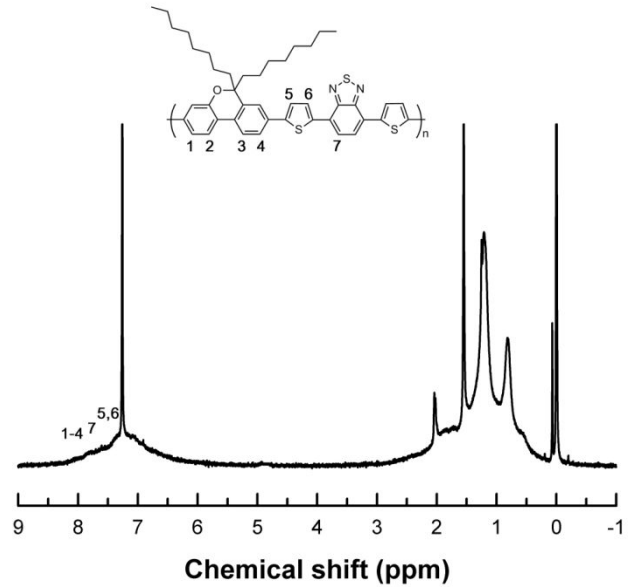

Figure 2.9. ^{1}H NMR spectrum of **PBCDTBT** in Scheme 2.1.

2.2.5.2 Synthesis of copolymers based on thiophene-capped diketopyrrolopyrrole copolymerized with fluorene and 6*H*-benzo[*c*]chromene

Synthesis of 3,6-Di(thien-2-yl)pyrrolo[3,4-*c*]pyrrole-1,4(2*H*,5*H*)-dione (8): To *t*-amyl alcohol (250 mL), sodium metal pieces (2.56 g, 108 mmol) were slowly added to the reaction mixture over a 1.5 h and the temperature of solution was increased to 120 °C. After all the sodium metal pieces were dissolved, thiophene-2-carbonitrile (11.9 g, 108 mmol) and dimethyl succinate (5.29 g, 36.2 mmol) was added to the solution. The reaction mixture was stirred overnight at 120 °C and then poured into acidic MeOH (400 mL MeOH and 20 mL conc. HCl). Filtration of the suspension yielded the product as a dark red solid. This product was used in next reactions without further purification. Yield: 47%.

Synthesis of 3,6-Bis-(thiophen-2-yl)-*N*,*N*'-bis(2-ethylhexyl)-1,4-dioxo-pyrrolo [3,4-*c*]pyrrole (9): To the compound **8** (5.00 g, 16.6 mmol) in DMF (150 mL), anhydrous K_2CO_3 (6.43 g, 49.9 mmol) were added and stirred at 120 °C for 1 h. And then the 2-ethylhexyl bromide (9.36 g, 49.9 mmol) was added dropwise, and the reaction mixture was further stirred overnight at 130 °C. After being cooled to room temperature, the solution was poured into water, and stirred for 30 min. The product was extracted with chloroform, then washed with water, and dried over MgSO4. The product was purified by column chromatography on silica gel (hexane/toluene as eluent) to yield the compound **9.** Yield:11%. ^{1}H NMR (300 MHz, $CDCl_3$): δ (ppm) 8.88 (d, 2H), 7.62 (d, 2H), 7.27 (d, 2H), 4.03 (d, 4H), 1.85–0.87 (m, 30H).

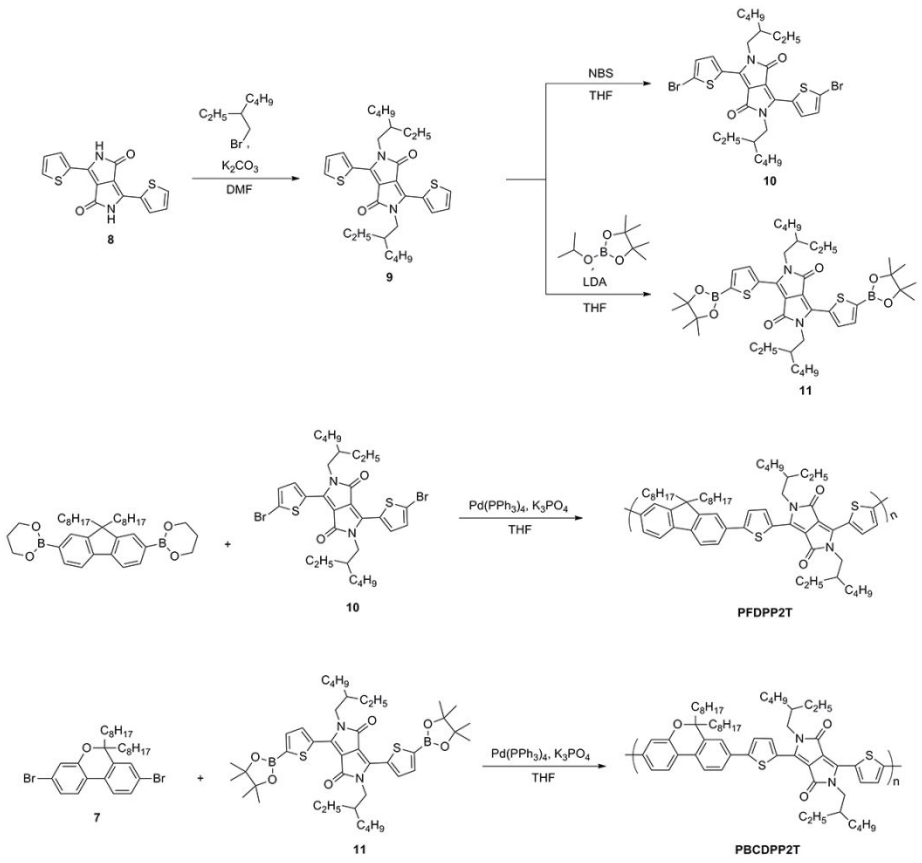

Scheme 2.3. Synthetic scheme of copolymers based on thiophene-capped diketopyrrolopyrrole copolymerized with fluorene and 6*H*-benzo[*c*]chromene

Synthesis of 3,6-Bis-(5-bromo-thiophen-2-yl)-*N*,*N*'-bis(2-decyltetradecyl)-1,4-dioxo-pyrrolo[3,4-*c*]pyrrole (10): To the compound **9** (1 g, 1.03 mmol) in $CHCl_3$ (30 mL), NBS (0.38 g, 2.11 mmol) was added slowly in the dark and stirred overnight at room temperature. After pouring into water, the product was extracted with $CHCl_3$ and dried over $MgSO_4$. The solvent was evaporated under reduced pressure and the product was purified by column chromatography on silica gel (hexane/DCM as eluent) and recrystallization from acetone. Yield: 81%. ^{1}H NMR (300 MHz, $CDCl_3$): δ (ppm) 8.63 (d, 2H), 7.22 (d, 2H), 3.98 (d, 4H), 1.85–0.87 (m, 30H).

Synthesis of 2,5-Bis(2-ethylhexyl)-3,6-bis[5-(4,4,5,5-tetramethyl-1,3,2-dioxoborolan-2-yl)thiophene-2-yl]-2,5-dihydropyrrolo[3,4-*c*]pyrrole-1,4-dione (11): *n*-Butyllithium in *n*-hexane (2.55 mL, 6.38 mmol) was added slowly at 0 °C to diisopropylamine (700 mg, 0.98 mL, 6.94 mmol) in 28 mL of dry THF under argon atmosphere. The freshly prepared LDA solution was added at –25 °C within 15 min to a 9 mL THF solution of **9** (1.50 g, 2.86 mmol) and 2-isopropoxy-4,4,5,5-tetramethyl-1,3,2-dioxoborolane (1.64 g, 1.80 mL, 8.79 mmol). After 1 h of stirring at 0 °C, the reaction was quenched with 10 mL of 1 M HCl solution. After extraction with chloroform, the solvent was removed under vacuum. The residue was dissolved in 25 mL of DCM, and the solution was poured into 400 mL of cold acetone under vigorous stirring. The precipitate was filtered off and washed with cold acetone to afford as a pink solid of **11**. Yield: 78%. ^{1}H NMR (300 MHz, $CDCl_3$): δ (ppm) 8.82 (d, 2H), 7.67 (d, 2H), 4.03 (m, 4H), 1.82 (m, 2H), 1.36–1.24 (m, 40H),

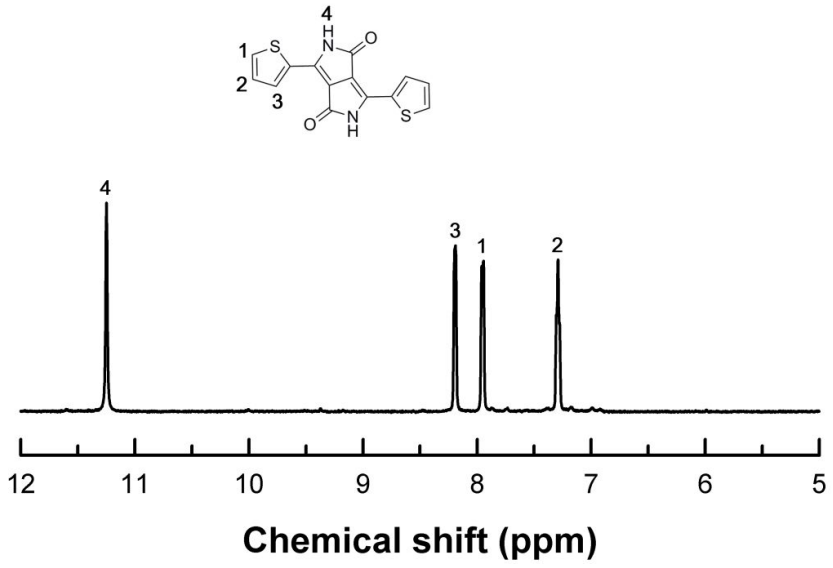

Figure 2.10. ^{1}H NMR spectrum of compound **8** in Scheme 2.3.

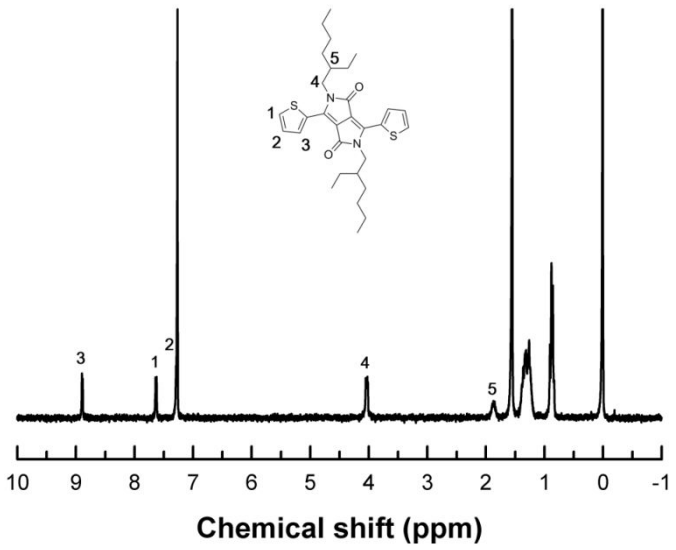

Figure 2.11. ^{1}H NMR spectrum of compound **9** in Scheme 2.3.

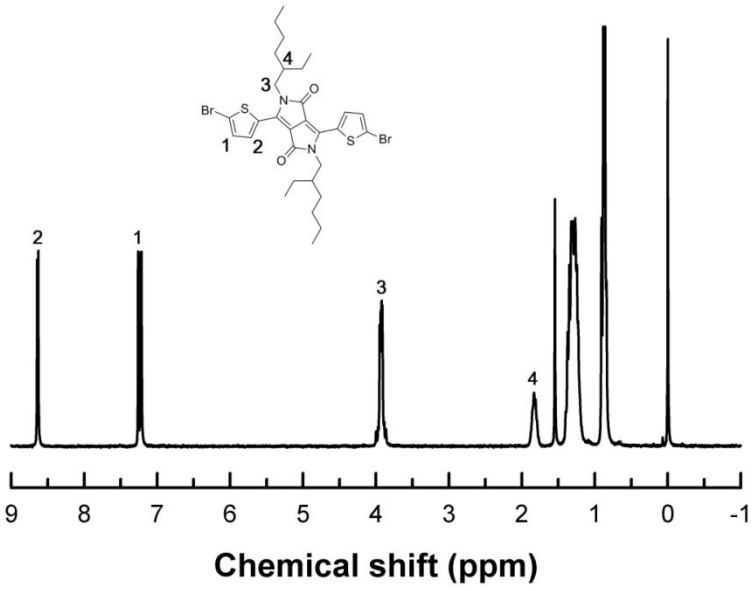

Figure 2.12. [1]H NMR spectrum of compound **10** in Scheme 2.3.

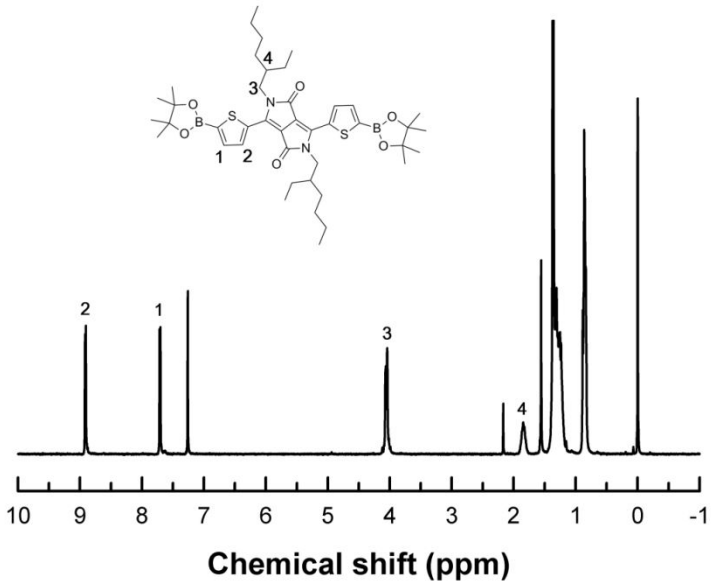

Figure 2.13. [1]H NMR spectrum of compound **11** in Scheme 2.3.

0.86 (m, 12H).

Polymerization of PFDPP2T: PFDPP2T was synthesized by the Suzuki coupling. A mixture of 9,9-dioctylfluorene-2,7-diboronicacid-bis-(1,3-propanediol)ester (0.15 g, 0.27 mmol) and compound **9** (0.18 g, 0.27 mmol) was dissolved in a mixture of aqueous K_2CO_3 solution (2 M, 3.3 mL) and THF (10 mL). After the solution was flushed with argon for 10 min, $Pd(PPh_3)_4$ (0.02 g, 0.02 mmol) was added quickly into the reaction mixture and sealed. The reaction mixture was stirred at 140 °C for 3 h in a microwave reactor. After being cooled to room temperature, the organic phase was poured into methanol under stirring. The precipitate was filtered through a Soxhlet thimble and subjected to Soxhlet extraction sequentially with methanol, acetone, ethyl acetate, hexane and chloroform. The polymer was recovered from the chloroform fraction, and the fraction is then precipitated into methanol to afford a dark blue solid. Yield: 56%. ^{1}H NMR (300 MHz, $CDCl_3$): δ (ppm) 9.01 (br, 1H), 7.64 (br, 4H), 4.14 (br, 2H), 2.00 (br, 3H), 1.42 (br, 9H), 0.94 (br, 22H).

Polymerization of PBCDPP2T: PBCDPP2T was synthesized by following the same procedure as used in the synthesis of PFDPP2T. Compound **6** (0.11 g, 0.19 mmol) and **10** (0.15 g, 0.19 mmol) were used as monomers, and a dark green solid was obtained as a product (0.12 g, 50%). ^{1}H NMR (300 MHz, $CDCl_3$): δ (ppm) 9.09 (br, 1H), 7.39 (br, 4H), 4.01 (br, 2H), 1.96 (br, 4H), 1.24 (br, 38H).

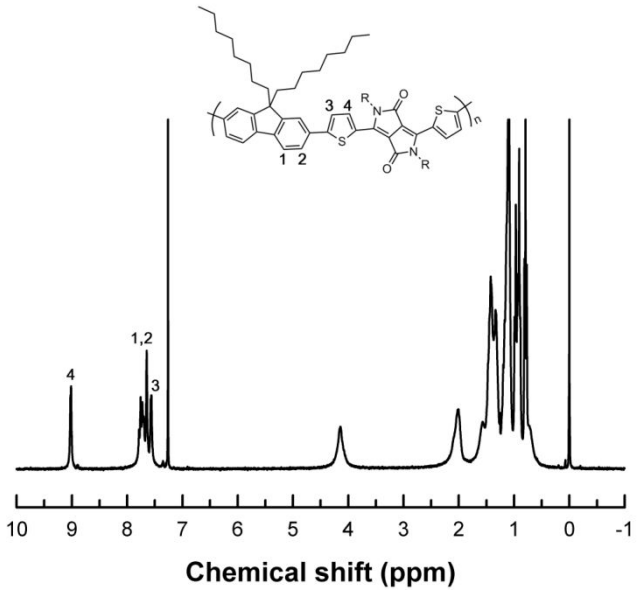

Figure 2.14. ^{1}H NMR spectrum of **PFDPP2T** in Scheme 2.3.

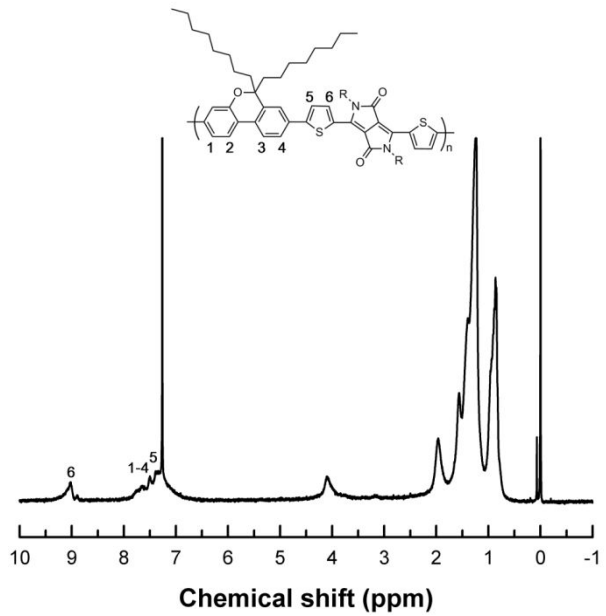

Figure 2.15. ^{1}H NMR spectrum of **PBCDPP2T** in Scheme 2.3.

2.3 Results and discussion

Three polymers, PFDTBT, PFDPP2T and PBCDPP2T, were synthesized by the Suzuki coupling, and PBCDTBT was synthesized by Stille coupling reaction. The M_ns of PFDTBT and PFDPP2T are 19.0 and 12.4 kDa with polydispersity indices of 2.6 and 2.1, respectively, while PBCDTBT and PBCDPP2T have the M_n of 46.0 and 18.6 kDa with polydispersity indices of 2.2 and 1.9, respectively, as measured by gel permeation chromatography (Table 2.1).

When the UV–vis spectra of PFDTBT and PBCDTBT are compared, as shown in Figure 2.16 (a), PBCDTBT absorbs more photons in the range of 550–700 nm with higher molar extinction coefficient (ε_{max}) than PFDTBT. Furthermore, PBCDTBT exhibits a strong vibronic shoulder in solution, indicating that PBCDTBT is significantly aggregated in the solution state. When the UV–vis spectra of two polymers in the film state are compared, as shown in Figure 2.16 (b), it reveals that PBCDTBT exhibits higher ε_{max} and broader absorption than PFDTBT. Thus, it is easily expected that more excitons are generated in PBCDTBT than in PFDTBT when they are exposed to light. Since a strong vibronic shoulder appears in the film of PBCDTBT while the PFDTBT film does not exhibit the vibronic shoulder, it is concluded that PBCDTBT has a more ordered structure than PFDTBT in the solid state. When the optical bandgap (E_g^{opt}) of PBCDTBT is estimated from the absorption edge of the thin film, the E_g^{opt} of PBCDTBT (1.77 eV) is slightly lower than that of PFDTBT (1.81 eV). The two absorption bands of

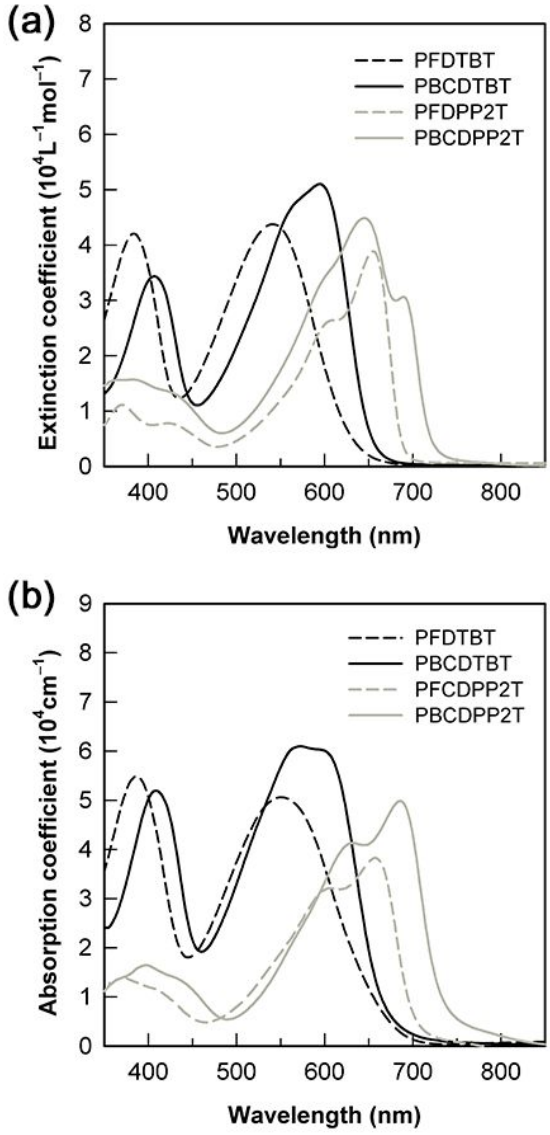

Figure 2.16. UV–vis absorption spectra of DTBT- and DPP-based polymers in chloroform solution (a) and in film (b).

PBCDTBT are red-shifted in both solution and film state as compared to PFDTBT. PBCDPP2T also shows lower E_g^{opt} (1.64 eV) with higher ε_{max} than that of PFDPP2T (1.73 eV), because the electron-donating power of BC is stronger than fluorene.

When the electrochemical properties of polymers are studied by cyclic voltammetry (CV), as shown in Figure 2.17, the HOMO energy levels of PBCDTBT (–5.28 eV) and PBCDPP2T (–5.31 eV) are higher than those of PFDTBT (–5.43 eV) and PFDPP2T (–5.55 eV), respectively. This is easily understood because the electron-donating power of BC in PBCDTBT and PBCDPP2T is stronger than that of fluorene in PFDTBT and PFDPP2T. It should be noted here that the strong electron-donating unit in a donor polymer raises the HOMO energy level. Since the LUMO energy levels of PFDTBT,

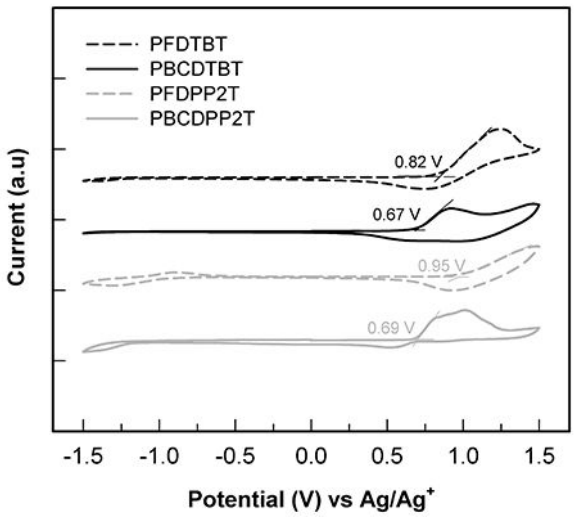

Figure 2.17. Cyclic voltammograms of DTBT- and DPP-based polymers.

PBCDTBT, PFDPP2T and PBCDPP2T are –3.62 eV, –3.51 eV, –3.82 eV and –3.67 eV, respectively, as listed in Table 2.1, the LUMO–LUMO offsets between the donor polymers and $PC_{71}BM$ (–4.2 eV) are larger than 0.3 eV, which are sufficient for effective exciton dissociation.

When the solar cell performances are measured with the conventional device structure (glass/ITO/PEDOT:PSS/polymer:$PC_{71}BM$/Cs/Al), as shown in Figure 2.20 and Table 2.4, the best device based on PBCDTBT exhibits a promising PCE of 5.74% with a J_{SC} of 12.51 mA cm^{-2}, a V_{OC} of 0.87 V and a FF of 52% while PFDTBT shows a PCE of 2.56% with a J_{SC} of 6.35 mA cm^{-2}, a V_{OC} of 0.94 V and a FF of 43%. Another BC-based polymer, PBCDPP2T, also shows higher PCE (2.01%) than that of the fluorene-based counterpart, PFDPP2T (0.95%). Here, the devices with fluorene-based polymers were optimized by following the method reported in the literature while the devices with BC-based polymers were optimized by varying the blend ratio of polymer to $PC_{71}BM$, the mixing ratio of solvents and the amount of DIO additive (See Figure 2.18–2.19 and Table 2.2–2.3). Since the V_{OC} is proportional to the energy difference between the LUMO energy level of $PC_{71}BM$ and the HOMO energy level of the donor polymer, it is reasonable that the V_{OC}s of PFDTBT (0.94 V) and PFDPP2T (0.91 V) are higher than those of PBCDTBT and PBCDPP2T, respectively, considering that the HOMO energy levels of fluorene-based polymers are deeper than those of BC-based polymers. Although the V_{OC} is sacrificed to some extent upon introduction of oxygen into the fluorene unit, the J_{SC}s of PBCDTBT (12.51 mA cm^{-2}) and PBCDPP2T (5.79 mA cm^{-2}) are two times larger than those of PFDTBT (6.35 mA cm^{-2}) and PFDPP2T (2.84 mA cm^{-2}), respectively, which

Table 2.1. Characteristics of DTBT- and DPP-based polymers.

Polymer	M_n (kg/mol)	PDI	UV–vis absorption		E_g^{opt} (eV)[a]	HOMO (eV)	LUMO (eV)[b]
			$\lambda_{max,\ CHCl3}$ (nm)	$\lambda_{max,\ film}$ (nm)			
PFDTBT	19.0	2.6	384, 542	386, 555	1.81	–5.43	3.62
PBCDTBT	46.0	2.2	406, 594	409, 570	1.77	–5.28	–3.51
PFDPP2T	12.4	2.1	604, 654	601, 652	1.73	–5.55	–3.82
PBCDPP2T	18.6	1.9	642, 687	631, 685	1.64	–5.31	–3.67

[a]Determined from the onset of UV–vis absorption spectra.

[b]Calculated from LUMO=HOMO+E_g^{opt}

can be further identified by comparing the external quantum efficiencies (EQE) of the four polymers as blended with $PC_{71}BM$ (Figure 2.20 (b)). Integration of EQE spectra of PFDTBT, PBCDTBT, PFDPP2T and PBCDPP2T blends yields J_{SC} = 6.11 mA cm^{-2}, J_{SC} = 11.86 mA cm^{-2}, J_{SC}=2.61 mA cm^{-2} and J_{SC}=5.49 mA cm^{-2}, respectively, which are nearly consistent with the J_{SC} values obtained from *J–V* measurement.

Three factors may be considered for higher J_{SC} of the BC-based polymer solar cell: molecular weight, UV–vis absorption and blend morphology. First, a high molecular weight of the donor polymer is beneficial for effective charge transport, because it may facilitate formation of a bicontinuous phase structure. To examine the effect of molecular weight on photovoltaic properties, we synthesized two PFDTBTs with different molecular weights (8.3k and 19.0k) and compared their solar cell performances. The best device based on PFDTBT with M_n = 19.0k shows a PCE of 2.56% with J_{SC} = 6.35 mA cm^{-2}, V_{OC} = 0.94 V and FF = 0.43, while the device based on lower molecular weight PFDTBT (M_n = 8.3k) exhibits a PCE of 2.29% with J_{SC} =6.11 mA cm^{-2}, V_{OC} = 0.94 V and FF = 0.40 (Figure. 2.21), indicating that the molecular weight does not strongly affect the photovoltaic properties when the molecular weight exceeds 8.3 k. It has also been reported that the photovoltaic properties of PFDTBT are saturated when M_n > 10 k.[175] Second, strong and broad light absorption is also an important factor for achieving high J_{SC}. The stronger and broader light absorption of PBCDTBT and PBCDPP2T contributes to larger J_{SC} than PFDTBT and PFDPP2T, respectively (Figure 2.16). Third, the morphology of the polymer:$PC_{71}BM$

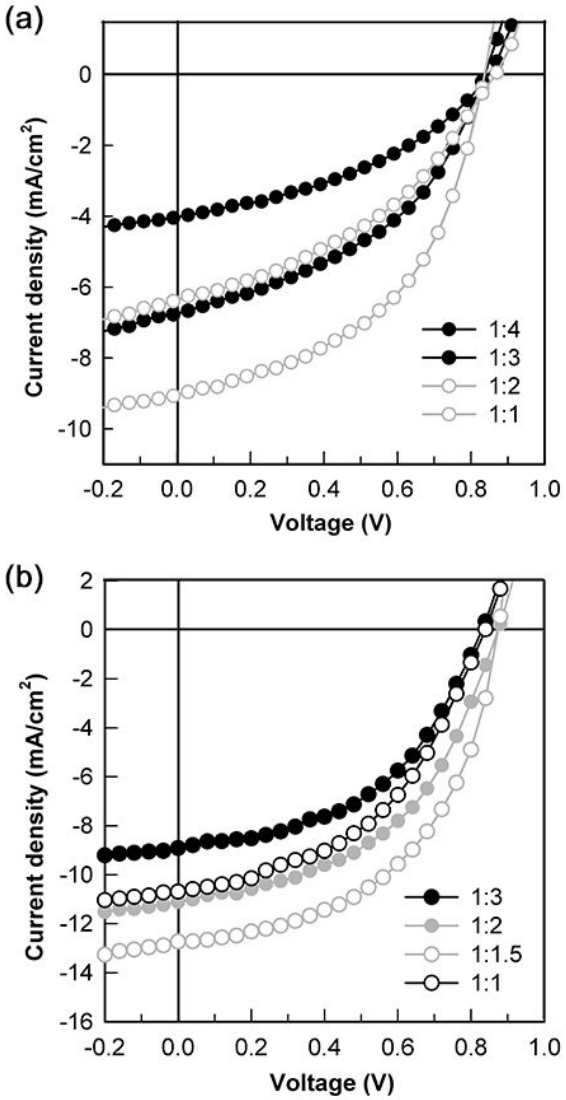

Figure 2.18. *J–V* curves of PBCDTBT/$PC_{71}BM$ BHJ solar cells under AM 1.5G, 100 mW/cm^2 cast from DCB with 2 vol% DIO (a) and CF/DCB mixture solvent (CF:DCB=1:2) with 2 vol% DIO (b).

Table 2.2. Photovoltaic properties of PBCTBT:$PC_{71}BM$ under standard AM 1.5G illumination cast from DCB or DCB/CF mixture solvent with 2 vol% DIO.

Solvent	PBCDTBT: $PC_{71}BM$ (w/w)	V_{OC} (V)	J_{SC} (mA/cm^2)	FF	PCE (%)
DCB	1:4	0.85	4.02	0.39	1.27±0.05
	1:3	0.84	6.75	0.43	2.30±0.10
	1:2	0.84	9.04	0.48	3.60±0.12
	1:1	0.85	6.73	0.37	2.08±0.05
CF:DCB=1:2	1:3	0.83	8.88	0.47	3.46±0.11
	1:2	0.87	11.10	0.48	4.63±0.17
	1:1.5	0.87	12.51	0.52	5.56±0.14
	1:1	0.84	10.68	0.45	4.04±0.13

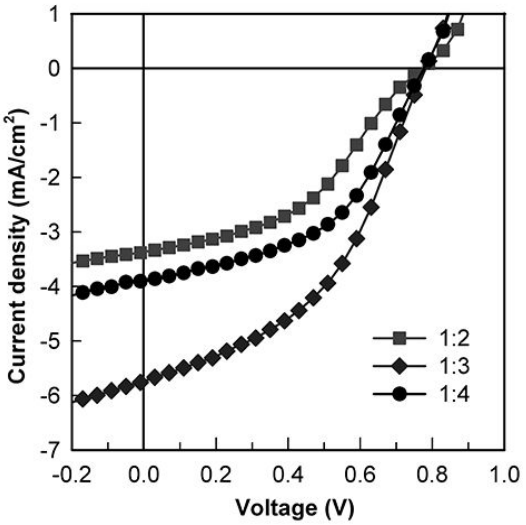

Figure 2.19. *J–V* curves of PBCDPP2T/$PC_{71}BM$ BHJ solar cells under AM 1.5G, 100 mW/cm^2 cast from DCB with 4 vol% DIO.

Table 2.3. Photovoltaic properties of PBCDPP2T:$PC_{71}BM$ under standard AM 1.5G illumination cast from DCB with 4 vol% DIO.

PBCDTBT: $PC_{71}BM$ (w/w)	V_{OC} (V)	J_{SC} (mA/cm^2)	FF	PCE (%)
1:4	0.78	3.36	0.43	1.11±0.09
1:3	0.78	5.79	0.45	2.01±0.15
1:2	0.79	3.89	0.47	1.46±0.12

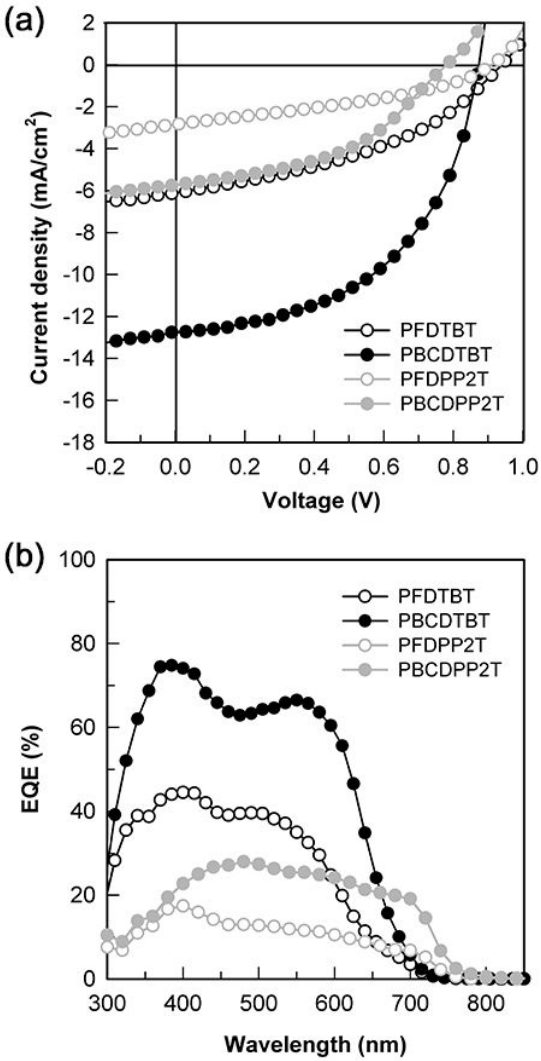

Figure 2.20. *J–V* curves of DTBT-based polymer/$PC_{71}BM$ and DPP-based polymer/$PC_{71}BM$ BHJ solar cells under AM 1.5G, 100 mW/cm^2 (a) and external quantum efficiency spectra of corresponding solar cells (b) under optimum condition.

Table 2.4. Photovoltaic properties of DTBT- and DPP-based devices under standard AM 1.5G illumination and charge carrier mobilities under dark conditions

Polymers	Polymer: $PC_{71}BM$ (w/w)	Thickness (nm)	V_{OC} (V)	J_{SC} (mA/cm^2)	FF	μ_h ($cm^2/V\ s$)[a]	μ_h ($cm^2/V\ s$)[b]	PCE (%)
PFDTBT	1:4	80±5	0.94	6.26	0.40	5.0×10^{-4}	9.0×10^{-3}	2.41±0.07
PBCDTBT	1:1.5	77±5	0.86	12.48	0.51	1.0×10^{-3}	5.2×0^{-4}	5.56±0.14
PFDPP2T	1:4	75±5	0.91	2.64	0.34	7.4×10^{-6}	4.4×10^{-6}	0.85±0.08
PBCDPP2T	1:3	70±5	0.78	5.58	0.42	2.0×10^{-5}	8.7×10^{-6}	1.85±0.12

[a]Hole mobility in pristine polymer as measured by SCLC method.

[b]Hole mobility in the blend of polymer:$PC_{71}BM$ as measured by SCLC method.

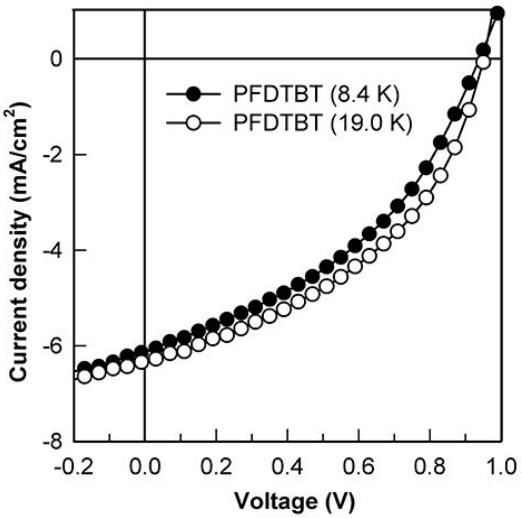

Figure 2.21. *J–V* curves of BHJ solar cells fabricated from two PFDTBTs with different molecular weights blended with $PC_{71}BM$ under AM 1.5G, 100 mW/cm^2.

blend is also a critical factor to control J_{SC}. Since the transmission electron microscopy (TEM) images of BC-based polymer blends exhibit nanoscale phase separation with a fibril-like network structure while fluorene-based polymer blends show coarser morphology with larger domain sizes (Figure 2.22), it is expected that the BC-based polymer blends are more effective for both charge separation and charge transport.

To analyze the effect of oxygen atom in PBCDTBT and PBCDPP2T on PSC device performance in more detail, we determined the maximum exciton generation rate (G_{max}) and exciton dissociation probability ($P(E,T)$) of the four

polymers according to the method previously reported, and compared them with each other.[176] The Figure 2.23 shows the dependence of photocurrent density (J_{ph}) on effective voltage (V_{eff}). Here J_{ph} is defined as $J_{ph} = J_L - J_D$, where J_L and J_D are the current density under illumination at 100 mW cm^{-2} and dark conditions, respectively, and V_{eff} is defined as $V_{eff} = V_0 - V_a$, where V_0 is the voltage at the point of $J_{ph} = 0$ and V_a is the applied bias voltage. Since it can be assured that all of photogenerated excitons are dissociated into free charge carriers at high V_{eff} due to sufficient electric field, the G_{max} can be determined from the saturation current density (J_{sat}): $J_{sat} = qG_{max}L$, where q is the electronic charge and L is the thickness of the active layer. When the value of G_{max} is calculated from the above relation and Figure 2.23, the value of G_{max} for PBCDTBT (8.55×10^{27} m^{-3} s^{-1} with $J_{sat} = 115$ A m^{-2}) is larger than that of PFDTBT (5.66×10^{27} m^{-3} s^{-1} with $J_{sat} = 77$ A m^{-2}). This is probably because PBCDTBT shows higher ε_{max} and broader absorption than PFDTBT. The exciton dissociation probability ($P(E,T)$), which is a function of the electric field (E) and temperature (T), can also be determined from the relation $J_{ph} = qG_{max}P(E,T)L$. Figure 2.24 shows a plot of $P(E,T)$ against V_{eff}, where the dashed-line indicates V_{eff} and the corresponding $P(E,T)$ under short-circuit conditions. The $P(E,T)$ values of PFDTBT and PBCDTBT under short-circuit conditions are 79% and 85%, respectively, suggesting that excitons photogenerated in PBCDTBT dissociate more efficiently than those in PFDTBT. The DPP-based polymer shows the same result as the BT-based polymer, as shown in Figure 2.23 and Figure 2.24: PBCDPP2T exhibits larger G_{max} (5.89×10^{27} m^{-3} s^{-1}) and higher $P(E,T)$ (82%) than those of the fluorene-

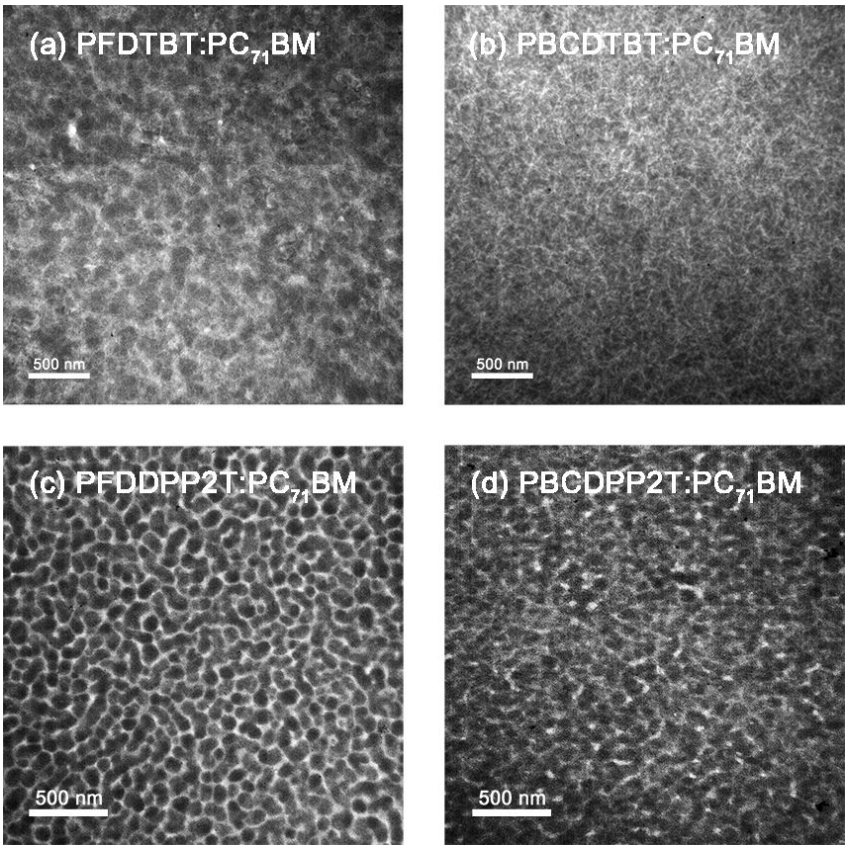

Figure 2.22. TEM images of DTBT-based polymer/$PC_{71}BM$ and DPP-based polymer/$PC_{71}BM$ blend films.

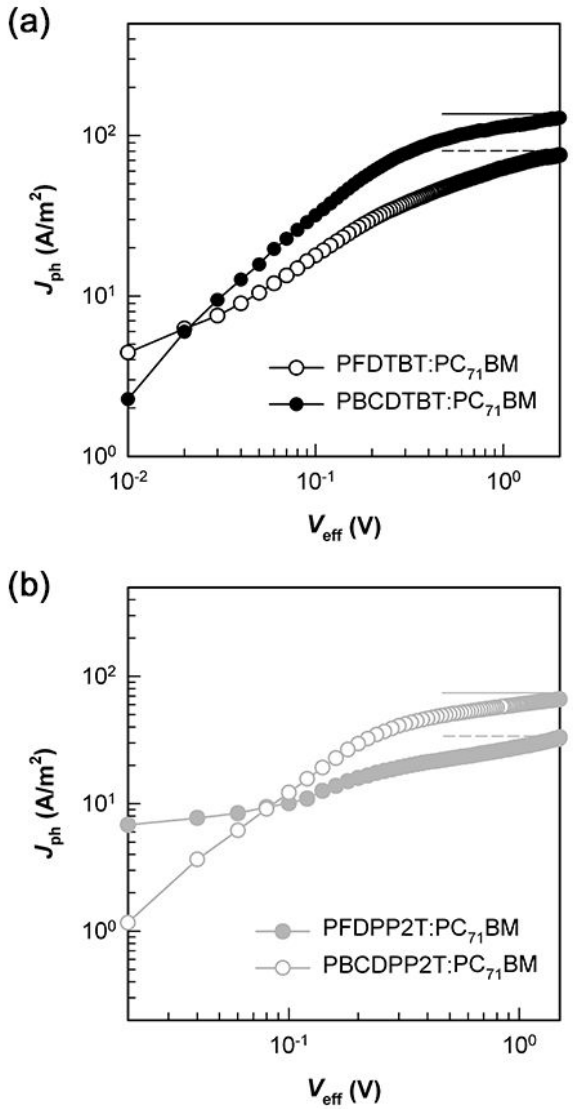

Figure 2.23. Photocurrent density (J_{ph}) plotted against effective voltage (V_{eff}) of DTBT-based polymer/$PC_{71}BM$ (a) and DPP-based polymer/$PC_{71}BM$ (b) under optimized conditions.

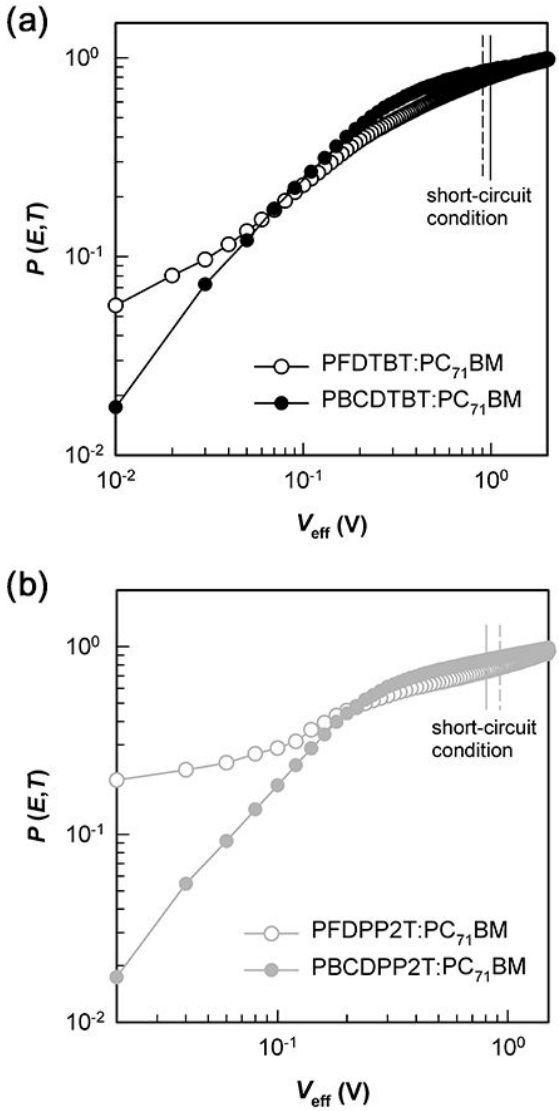

Figure 2.24. Exciton dissociation probability ($P(E,T)$) plotted against effective voltage for DTBT-based polymers/$PC_{71}BM$ devices (a) and DPP-based polymers/$PC_{71}BM$ (b) under optimum condition.

based counterpart, PFDPP2T (2.42×10^{27} m^{-3} s^{-1} and 75%).

It has been reported that the difference between the dipole moment from ground state to excited state ($\Delta\mu_{ge}$) in conjugated polymers largely affects the device performance of PSCs.[169,170] Since a large value of $\Delta\mu_{ge}$ in the donor polymer makes the excited state highly polarized, it facilitates electron transfer from donor polymer to acceptor. In other words, Coulombic binding energy of the exciton is reduced by larger $\Delta\mu_{ge}$. When the $\Delta\mu_{ge}$ was calculated for one repeating unit of the four polymers using DFT/TDDFT at B3LYP/6-31G level, the $\Delta\mu_{ge}$ values of BC-based polymers are larger than the corresponding fluorene-based polymers (see Tables 2.5 and Tables 2.6), indicating that excitons in BC-based polymers are more easily separated into free charge carriers than fluorene-based polymers, which are very consistent with the value of $P(E,T)$.

Another important factor to control J_{SC} is the crystallinity of the donor polymer, because a high crystalline polymer affords efficient charge carrier transport to the electrode after exciton dissociation. When the crystallinities of two polymers are examined by wide angle X-ray diffraction (XRD), as shown in Figure 2.25, the XRD patterns of BC-based two polymers clearly show distinctive Bragg diffraction, while those of fluorene-based polymers do not show a discernible peak,[177] indicating that BC-based polymers are highly crystalline whereas fluorene-based polymers are amorphous. To investigatethe molecular orientation of the polymers blended with $PC_{71}BM$, the grazing incident wide angle X-ray scattering (GIWAXS) experiments are performed. The PBCDTBT:$PC_{71}BM$ blend clearly shows (100), (200), (300) and (010)

Table 2.5. Calculated ground and excited state dipole moment of PFDTBT and PBCDTBT with DFT/TDDDFT B3LYP/6-31G level using Gaussian 09.

Dipole	μ_x (D)	μ_y (D)	μ_z (D)	Total (D)	$\Delta\mu_{eg}$ (D) [a]
$\mu_{g,\ PFDTBT}$	–0.7574	–0.3529	0.0736	0.8388	7.9709
$\mu_{e,\ PFDTBT}$	–7.3490	–4.8328	–0.0580	8.7959	
$\mu_{g,\ PBCDTBT}$	0.6615	–0.6416	0.2454	0.9536	9.3158
$\mu_{e,\ PBCDTBT}$	–7.4460	–5.2298	0.2063	9.1014	

[a] $\Delta\mu_{eg}$ represents the difference between the ground and excited state dipole moments, as calculated by $\Delta\mu_{eg}=[(\mu_{gx}-\mu_{ex})^2+(\mu_{gy}-\mu_{ey})^2+(\mu_{gz}-\mu_{ez})^2]^{1/2}$.

Table 2.6. Calculated ground and excited state dipole moment of PFDPP2T and PBCDPP2T with DFT/TDDDFT B3LYP/6-31G level using Gaussian 09.

Dipole	μ_x (D)	μ_y (D)	μ_z (D)	Total (D)	$\Delta\mu_{eg}$ (D) [a]
$\mu_{g,\ PFDPP2T}$	1.4228	0.1144	0.0806	1.4296	0.4973
$\mu_{e,\ PFDPP2T}$	0.9381	0.2200	0.0445	0.9645	
$\mu_{g,\ PBCDPP2T}$	–0.0421	–0.2382	–1.0961	1.1224	2.8065
$\mu_{e,\ PBCDPP2T}$	–0.5253	–0.3425	0.9310	1.1225	

[a] $\Delta\mu_{eg}$ represents the difference between the ground and excited state dipole moments, as calculated by $\Delta\mu_{eg}=[(\mu_{gx}-\mu_{ex})^2+(\mu_{gy}-\mu_{ey})^2+(\mu_{gz}-\mu_{ez})^2]^{1/2}$.

diffraction peaks in the q_z direction, while the diffraction peaks of (100) and (200) are also observed in the q_{xy} direction, indicating that PBCDTBT has both face-on and edge-on molecular orientation on the substrate. However, the PFDTBT:$PC_{71}BM$ blend does not exhibit discernible diffraction peaks in both q_z and q_{xy} directions, indicating amorphous characteristics (Figure 2.26).

To correlate crystallinity to charge transport, the hole mobilities of the four polymers and their blends with $PC_{71}BM$ are measured by the standard method using a single charge carrier device and compared with each other. The space-charge limited current (SCLC) *J–V* curves were obtained under dark conditions using a hole-only device (ITO/PEDOT:PSS/polymer or polymer:$PC_{71}BM$/Au), from which the hole mobility was calculated using the Mott–Gurney law (Figure 2.27, Figure 2.28 and Table 2.4). When the hole mobilities of BC-based polymers and their blends with $PC_{71}BM$ are compared with those of fluorene-based polymers and their blends with $PC_{71}BM$, the hole mobilities of BC-based polymers and their blends are higher than those of fluorene-based polymers and their blends, respectively. Considering that BC-based polymers, PBCDTBT and PBCDPP2T, have higher crystallinity than fluorene-based polymers, PFDTBT and PFDPP2T, the higher hole mobilities of BC-based polymers are attributed to higher crystallinity as compared to fluorene-based polymers. In short, higher J_{SC}s of BC-based polymers arise from larger photon absorption, higher G_{max}, more effective charge separation, higher hole mobility and better developed morphology as compared to fluorene-based polymers.

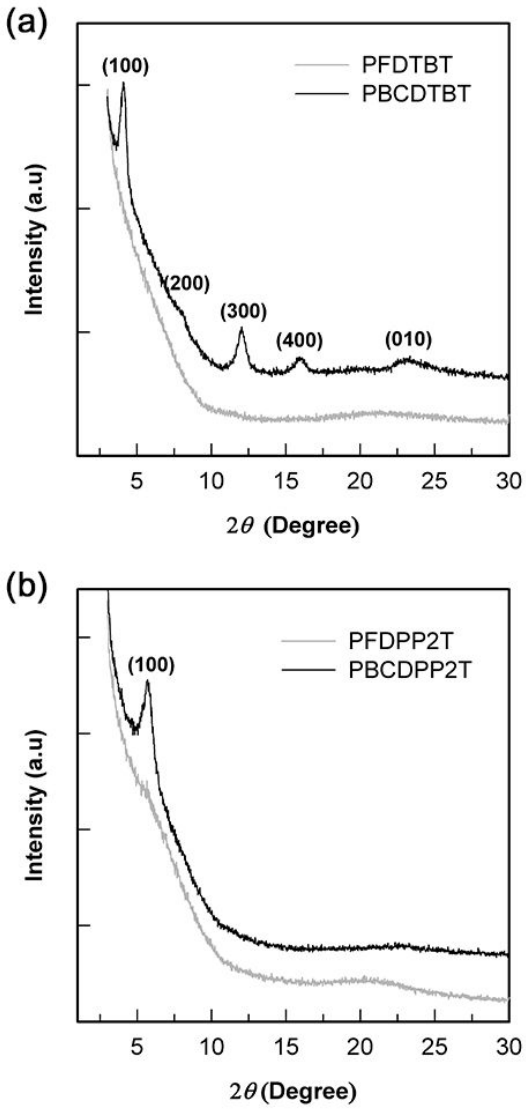

Figure 2.25. XRD diffractograms of DTBT-based polymers (a) and DPP-based polymers (b) in thin film.

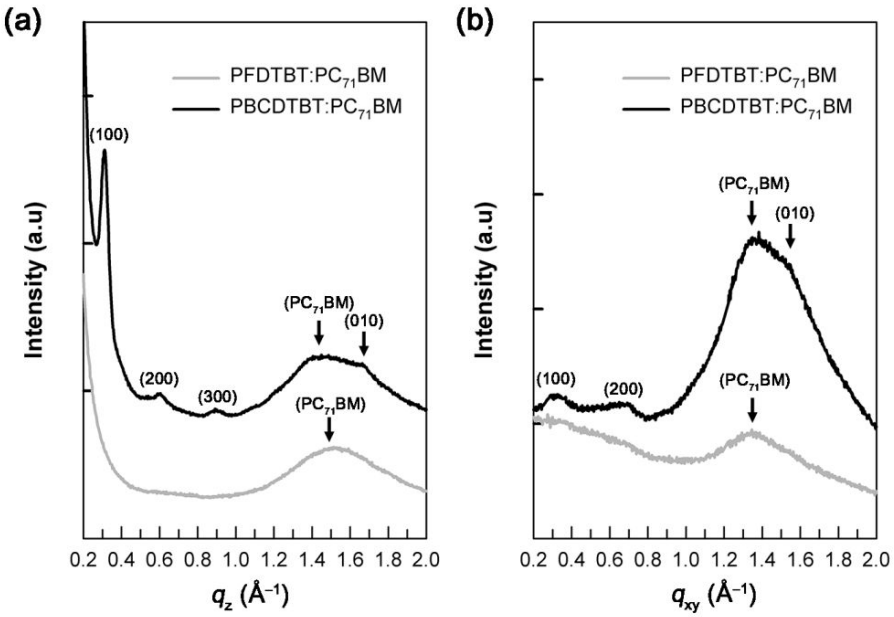

Figure 2.26. GIWAXS patterns of DTBT-based blend thin film under optimized condition: out-of-plane (a) and in-plane scan (b).

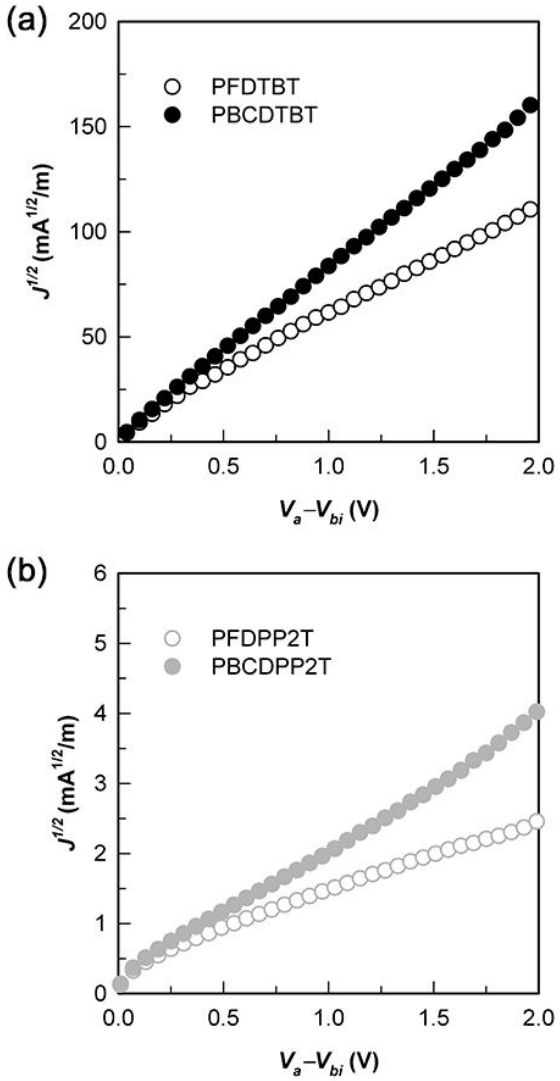

Figure 2.27. Dark *J*–*V* characteristics of pristine DTBP-based polymers (a) and DPP-based polymers (b) with hole-only device.

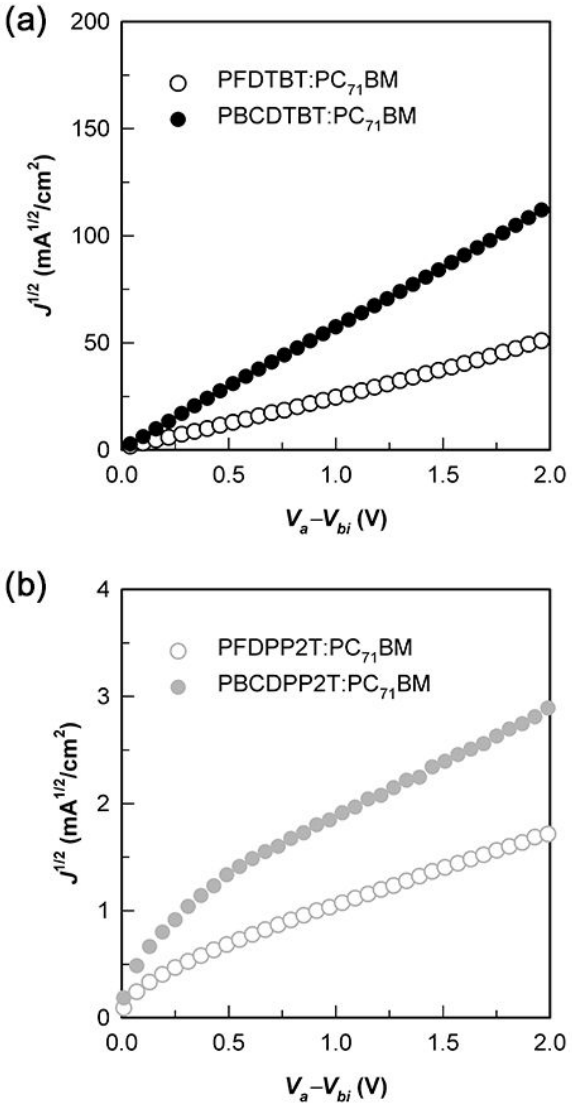

Figure 2.28. Dark *J–V* characteristics of DTBT-based polymer:$PC_{71}BM$ (a) and DPP-based polymer:$PC_{71}BM$ blends (b) with a hole-only device.

2.4 Summary

In this study, we synthesized a new electron-donating unit, BC, by introducing an oxygen atom into fluorene, which was then polymerized with electron-deficient DTBT and DPP2T, for the purpose of reducing the bandgap and enhancing the solubility of the conjugated polymer. The bandgaps of BC-based polymers, PBCDTBT and PBCDPP2T, are lower than those of fluorene-based counterparts, PFDTBT and PFDPP2T, respectively, due to the introduction of the electronegative oxygen atom in fluorene. Since BC-based polymers exhibit stronger and broader light absorption, higher exciton generation rate as evidenced by larger G_{max}, more effective charge generation rate due to larger $\Delta\mu_{ge}$ and higher mobility due to higher crystallinity than the corresponding fluorene-based counterparts, BC-based polymers show higher J_{SC} than fluorene-based polymers. Particularly, the PSC based on PBCDTBT:$PC_{71}BM$ shows a promising PCE of 5.74% with a J_{SC} of 12.51 mA cm^{-2}, a V_{OC} of 0.87 V and a FF of 52%.

Chapter 3. Ternary blend composed of two organic donors and one acceptor for active layer of organic solar cells

3.1 Introduction

One of the most successful approaches for high performance PSCs is to develop new low bandgap polymers. Molecular design of low bandgap polymer for PSCs has mostly utilized the electron push-pull concept in copolymer consisting of electron donating and electron accepting unit over low bandgap last decade. This approach allows us to tune the absorption range, bandgap and molecular energy levels of D–A type alternating copolymer by choosing appropriate combination of D and A unit. Although many D and A units have been developed, only a few D–A alternating copolymers show the PCE over 9% in single-junction device.[31–41] Therefore another strategy is needed to further enhance the device performance by overcoming the limitation of D–A type copolymer.

Ternary blend BHJ solar cells provide attractive and effective alternative to enhance photon harvest by incorporating multiple organic materials with simplicity of fabrication. In early studies, the efficiency enhancement of ternary blend solar cells is originated from increasing in the spectral response by the introduction of an additional donor having an absorption range which is

complementary to that of the parent donor and acceptor.[127–129] On the other hand, until recently, the V_{OC} of such devices was thought to be pinned by the energy levels difference; LUMO energy level of the acceptor and the higher HOMO energy level between two donors in the active layers. On the contrary, Thompson and co-workers demonstrated that the V_{OC} of ternary blend solar cells need not be pinned by the smallest energy level difference of the constituents.[132] In fact, with proper selection of materials combination for ternary blend active layers, the V_{OC} of these solar cells can be continuously tuned with composition between those derived from the HOMO energy levels of the individual donors.[125,141] Thus in ternary blend system, J_{SC} improvement from complementary absorption by third compound is clear, while there remains interesting issue about V_{OC}.

For the consideration of ternary blends, the polymer/polymer blends generally have a strong tendency to undergo enthalpy-driven phase separation. Thus, these attempts frequently result in lateral phase separation with domain sizes in the micrometer regime. The performances of polymer:small molecule/fullerene ternary blend solar cells can, theoretically, be better than the performances of polymer:polymer blend solar cells.[178] It has been reported that a low bandgap polymer (PTDPP2T) composed of TDPP and 2T absorbs the light of long wavelength range (670–840 nm) and the device made of PTDPP2T shows a high power conversion efficiency (PCE) of 7.1% with well-developed fibril structure when blended with $PC_{71}BM$.[164] Previously, we also reported a series of TDPP-based A–D–A type small molecules,[165] $(TDPP)_2$, $(TDPP)_2T$ and $(TDPP)_2Ph$, where A is TDPP and D is an electron-

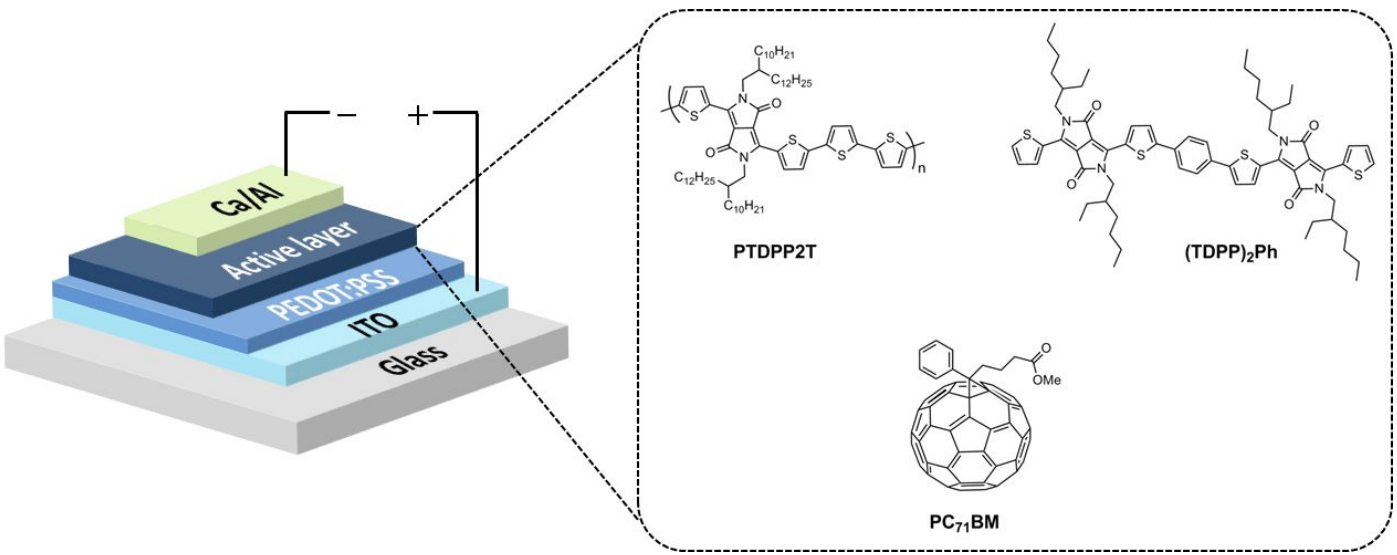

Scheme 3.1. Chemical structures of PTDPP2T, $(TDPP)_2Ph$ and $PC_{71}BM$.

donating unit such as thiophene and phenylene (Ph). Due to weak electron-donating power of Ph unit, the $(TDPP)_2Ph$ shows the widest bandgap with 550–700 nm absorption and highest PCE of 4.01% with a high V_{OC} of 0.93 V.

In this work, we report a ternary blend composed of DPP-based polymer (PTDPP2T), DPP-based small molecule $(TDPP)_2Ph$ and $PC_{71}BM$ as an active layer material (See Scheme 3.1). Unlike most of previous D_1/D_2/A-type ternary blends with dissimilar molecular structures of two donor compounds, our donor materials have the same electron accepting unit of DPP in both PTDPP2T and $(TDPP)_2Ph$, and therefore two donors are expected to be miscible at the molecular level. While the PTDPP2T:$PC_{71}BM$-based PSC exhibits a PCE of 6.60%, the ternary blend (PTDPP2T:$(TDPP)_2Ph$:$PC_{71}BM$)-based solar cell shows 13% higher PCE of 7.48%. This PCE enhancement is mainly due to the increase of J_{SC} arising from additional absorption of $(TDPP)_2Ph$.

3.2 Experimental

3.2.1 Materials

$Pd(PPh_3)_4$, *n*-butyllithium, trimethyltin chloride and 1,4-Benzenediboronic acid bis(pinacol) ester were purchased from Sigma-Aldrich and used without further purification. [6,6]-Phenyl-C_{71}-butyric acid methyl ester ($PC_{71}BM$) was obtained from Nano-C. Poly(3,4-ethylenedioxy-thiophene):poly(styrene sulfonate) (PEDOT:PSS) (Clevios P VP AI 4083) was purchased from H. C.

Stark and passed through a 0.45 μm PVDF syringe filter before spin-coating. Common organic solvents were purchased from Daejung. Tetrahydrofuran (THF) was dried over sodium/benzophenone under nitrogen condition and freshly distilled prior to use. All other reagents were purchased from Tokyo Chemical Industry and used as received.

3.2.2 Synthesis of monomers and polymers

3.2.2.1 Synthesis of small molecule composed of thiophene-capped diketopyrrolopyrrole and phenylene

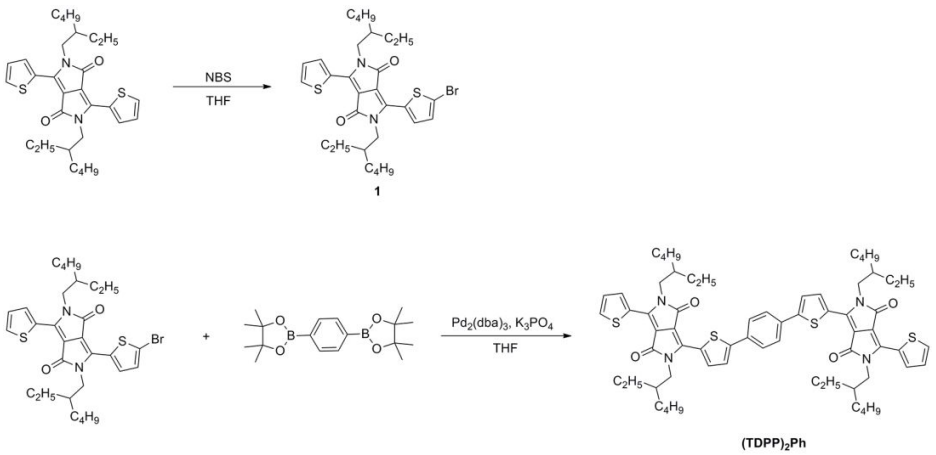

Scheme 3.2. Synthetic scheme of small molecule composed of thiophene-capped diketopyrrolopyrrole and phenylene

Synthesis of 3-(5-bromothiophen-2-yl)-2,5-bis(2-ethylhexyl)-6-(thiophen-2-yl)pyrrolo[3,4-c]pyrrole-1,4(2*H*,5*H*)-dione (1): Compound **9** (500 mg, 0.95 mmol) in chapter 2 was desolved in THF and stirred at 0°C. Protected from light, NBS (153 mg, 0.85 mmol) in THF was added to the mixture and kept at 0°C for 3h. Then reaction was warmed to room temperature and stirred overnight. The mixture was partitioned between DCM and water. The organic phase was dried by anhydrous $MgSO_4$, and then the solvent was evaporated under vacuum. The residue was purified by column chromatography on a silica gel (toluene/hexane=4/1) to afford the title compound as a purple solid. Yield: 53%. ^{1}H NMR ($CDCl_3$, 400 MHz): δ (ppm) 8.90 (d, 1H), 8.63 (d, 1H), 7.64 (d, 1H), 7.26 (d, 2H), 4.03 (m, 4H), 1.84−1.83 (m, 2H), 1.35−1.25 (m, 16H), 0.90−0.83 (m, 12H).

Synthesis of $(TDPP)_2Ph$: $Ph(TDPP)_2$ was synthesized by the Suzuki coupling. The compounds 12 (0.30 g, 0.33 mmol) and 1,4-Benzenediboronic acid bis(pinacol) ester (153 mg, 0.15 mmol) were dissolved in a mixture of aqueous K_2CO_3 solution (2 M, 2 mL) and THF (8 mL). After the solution was flushed with N_2 for 20 min, 10 mg of $Pd(PPh_3)_4$ was added. The reaction mixture was stirred at 150 °C for 3 h in a microwave reactor. The residue was purified by column chromatography on silica gel (100% dichloromethane as eluent). The product $(TDPP)_2$ Ph was obtained as a reddish blue solid. Yield: 73%. ^{1}H NMR (300 MHz, $CDCl_3$): δ (ppm) 8.97 (d, 2H), 8.91 (d, 2H), 7.72 (s, 4H), 7.63 (d, 2H), 7.53 (d, 2H), 7.29 (d, 2H), 4.14–3.98 (m, 8H), 1.94–1.88 (m, 4H), 1.42–1.27 (m, 32H), 0.95–0.88 (m, 24H). ^{13}C NMR (125 MHz,

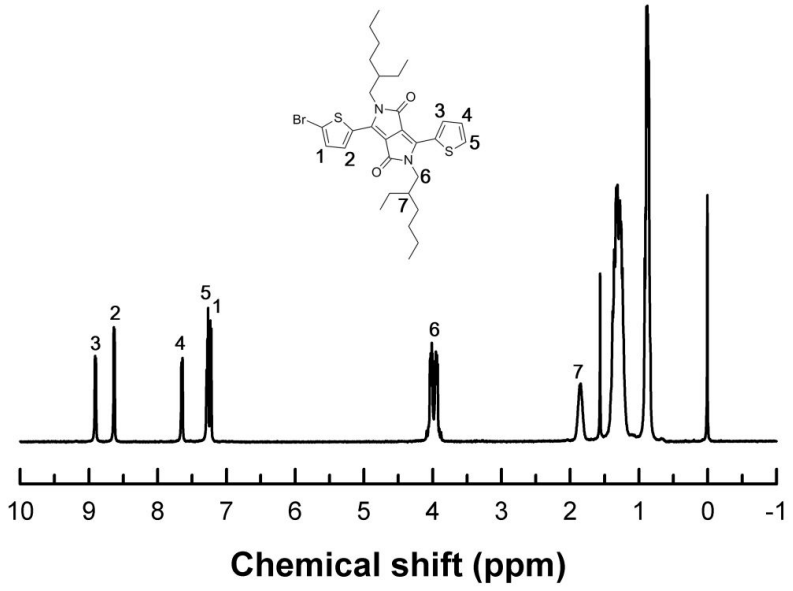

Figure 3.1. ^{1}H NMR spectrum of compound **1** in Scheme 3.2.

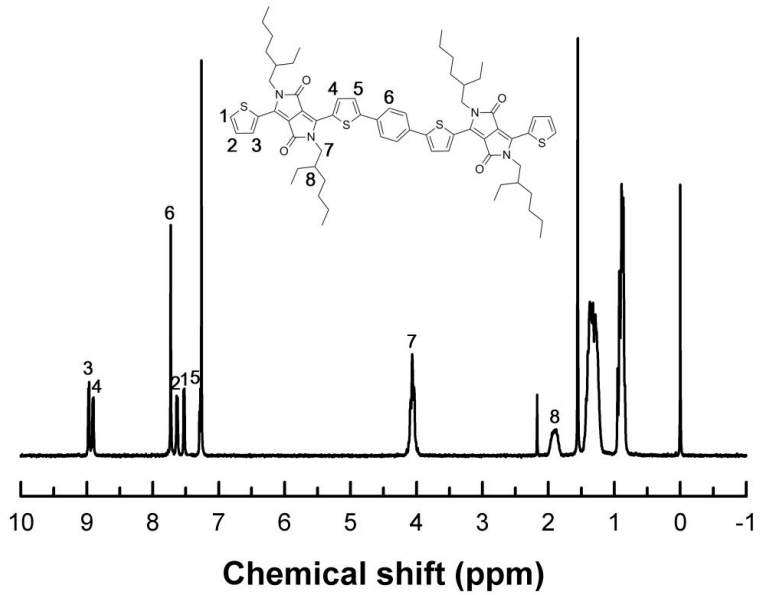

Figure 3.2. ^{1}H NMR spectrum of **$(TDPP)_2Ph$** in Scheme 3.2.

$CDCl_3$): δ (ppm) 161.79, 148.54, 140.25, 139.89, 136.82, 135.28, 133.43, 130.53, 129.90, 129.29, 128.45, 126.68, 124.85, 108.34, 108.19, 45.98, 39.30, 30.40, 28.57, 23.74, 23.09, 14.06, 10.60; HRMS (FAB, *m*/*z*): $[M + H]^+$ calcd for $C_{66}H_{82}N_4O_4S_4$, 1123.64; found, 1123.52.

3.2.2.2 Synthesis of polymer composed of thiophene-capped diketopyrrolopyrrole and bithiophene

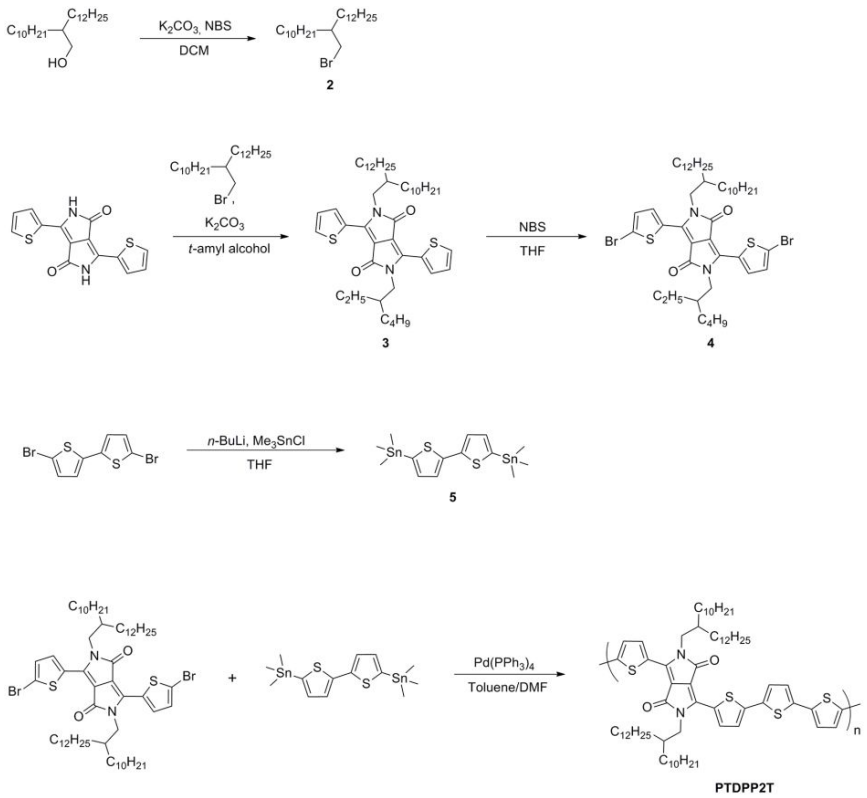

Scheme 3.3. Synthetic scheme of polymer composed of thiophene-capped diketopyrrolopyrrole and bithiophene

Synthesis of 1-bromo-2-decyltetradecyl (2): 2-decyl-1-tetradecanol (3.5 g, 10 mmol) and triphenylphosphine (5.2 g, 21 mmol) were dissolved in dichloromethane (50 ml) and cooled in ice-water bath. To the mixture n-bromosuccinimide (5.5 g, 31 mmol) was added slowly, then stirred at room temperature for 12 h. After evaporation of solvents in vacuum, the products were dissolved in hexane. Purification by column chromatography on silica gel using hexane as a eluent. After the solvent was evaporated, the product was obtained as a colorless oil Yield: 2.3 g, (80%). ^{1}H NMR (300 MHz, $CDCl_3$): δ (ppm) 3.45 (d, 2H), 1.59 (m, 1H), 1.4–1.2 (m, 40H), 0.88 (t, 6H).

Synthesis of 3,6-Bis-(thiophen-2-yl)-*N*,*N*'-bis(2-decyltetradecyl)-1,4-dioxo-pyrrolo [3,4-*c*]pyrrole (3): To the compound **8** (5.0 g, 16.6 mmol) of chapter 2 in DMF (150 mL), anhydrous K_2CO_3 (6.43 g, 49.9 mmol) were added and stirred at 120 °C for 1 h. And then the 2-decyltetradecyl bromide (**2**) (20.1 g, 49.9 mmol) was added dropwise, and the reaction mixture was further stirred overnight at 130 °C. After being cooled to room temperature, the solution was poured into water, and stirred for 30 min. The product was extracted with chloroform, then washed with water, and dried over $MgSO_4$. The product was purified by column chromatography on silica gel (hexane/toluene). Yield: 1.7 g, 11%. ^{1}H NMR (300 MHz, $CDCl_3$): δ (ppm) 8.88 (d, 2H), 7.62 (d, 2H), 7.27 (d, 2H), 4.03 (d, 4H), 1.85–0.87 (m, 94H).

Synthesis of 3,6-Bis-(5-bromo-thiophen-2-yl)-*N*,*N*'-bis(2-decyltetradecyl)-1,4-dioxo-pyrrolo[3,4-*c*]pyrrole (4): To the compound **3** (1

g, 1.03 mmol) in $CHCl_3$ (30 mL), NBS (0.38 g, 2.11 mmol) was added slowly in the dark and stirred overnight at room temperature. After pouring into water, the product was extracted with $CHCl_3$ and dried over $MgSO_4$. The solvent was evaporated under reduced pressure and the product was purified by column chromatography on silica gel (hexane/toluene as eluent) and recrystallization from acetone. Yield: 81%. ^{1}H NMR (300 MHz, $CDCl_3$): δ (ppm) 8.63 (d, 2H), 7.22 (d, 2H), 7.52 (d, 2H), 3.98 (d, 4H), 1.85–0.87 (m, 94H).

Synthesis of 5,5'-Bis(trimethylstannyl)-2,2'-bithiophene (5): To 5,5'-dibromo-2,2'-bithiophene (1 g, 3.09 mmol) in anhydrous THF (15 mL), 2.5 M of *n*-BuLi in hexane (2.8 mL, 7.0 mmol) was added dropwise at –78 °C. After stirring for 30 min, the solution was further stirred for 30 min at room temperature. The solution was then cooled to –78 °C again before 1 M of trimethyltin chloride in hexane (7.7 mL, 7.7 mmol) was added. After warming up to room temperature and stirring overnight, the resulting mixture was poured into water and extracted with diethyl ether. The organic phase was collected and dried over $MgSO_4$. Recrystallization from methanol affords compound **5**. Yield: 64%. ^{1}H NMR (300 MHz, $CDCl_3$): δ (ppm) 7.28 (d, 2H), 7.09 (d, 2H), 0.38 (m, 18H).

Polymerization of PTDPP2T: The compound **4** (150 mg, 0.13 mmol) and **5** (65 mg, 0.13 mmol) were dissolved in toluene (10 mL). After the solution was flushed with N_2 for 20 min, 4 mg of $Pd(PPh_3)_4$ was added. The reaction mixture was stirred for 4 h at 150°C in a microwave reactor. After being

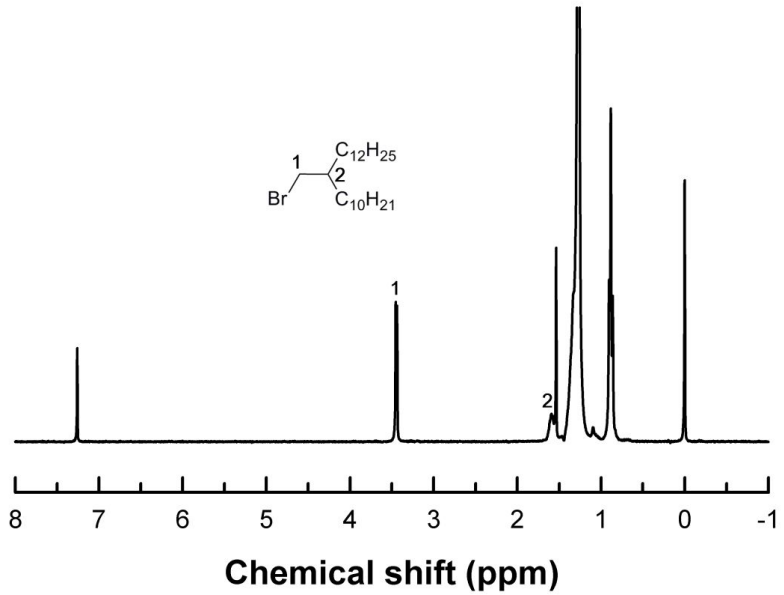

Figure 3.3. [1]H NMR spectrum of decyltetradecyl bromide in Scheme 3.3.

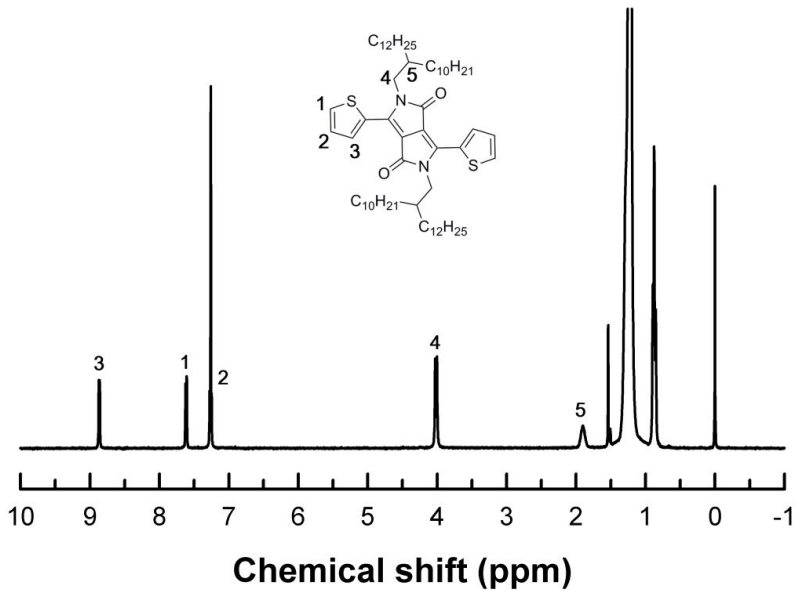

Figure 3.4. [1]H NMR spectrum of compound **3** in Scheme 3.3.

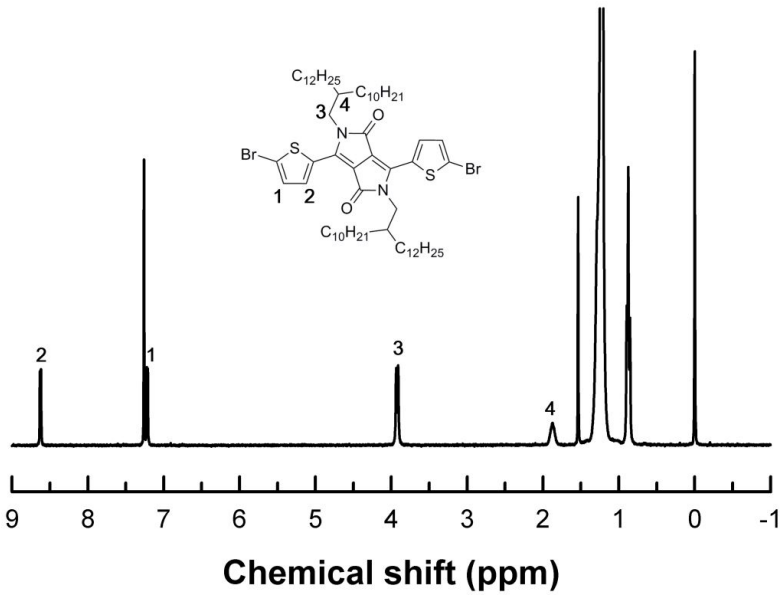

Figure 3.5. [1]H NMR spectrum of compound **4** in Scheme 3.3.

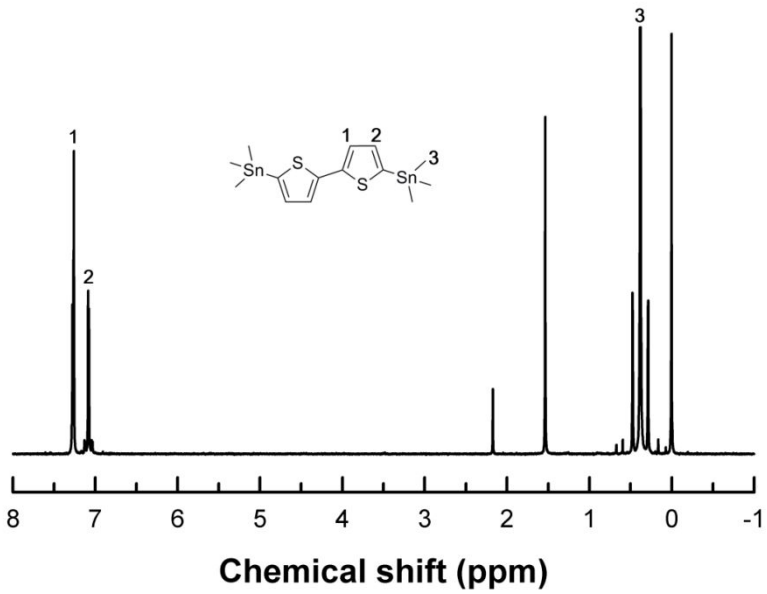

Figure 3.6. [1]H NMR spectrum of compound **5** in Scheme 3.3.

cooled to room temperature, the mixture was poured into methanol. The crude product was filtered through a Soxhlet thimble, and then subjected to Soxhlet extraction with methanol, ethyl acetate, hexane, DCM and chloroform. The polymer was recovered from chloroform fraction, and the fraction was precipitated into methanol to afford the product as green solid (120 mg, 81%).

3.3 Results and discussion

The PTDPP2T and $(TDPP)_2Ph$ were prepared by Stille coupling and Suzuki coupling reaction, respectively. For Stille coupling, toluene/DMF co-solvent was used to obtain high molecular weight of polymer. To ensure good solubility of the polymers, we substituted 2-decyltetradecyl group on DPP unit. When the M_n and PDI of PTDPP2T was measured by gel permeation chromatography using chloroform as eluent at 50 °C, the PTDPP2T has high M_n of 13.5 k with a PDI of 1.66. The synthesized polymer, PTDPP2T is soluble in chloroform, chlorobenzene and *o*-dichlorobenzene at 50 °C, while the synthesized small molecule, $(TDPP)_2Ph$, is soluble common organic solvents, including chloroform, dichloromethane, tetrahydrofuran and toluene at room temperature.

Figure 3.7 (a) illustrates the UV−vis absorption spectra of PTDPP2T, $(TDPP)_2Ph$ and three blends with different blend ratio, where the blends with addition of 5, 10 and 15wt% $(TDPP)_2Ph$ to PTDPP2T are denoted by B5, B10 and B15, respectively. The UV-vis spectrum of PTDPP2T shows broad absorption of 600–900 nm with the absorption onset at 940 nm, corresponding

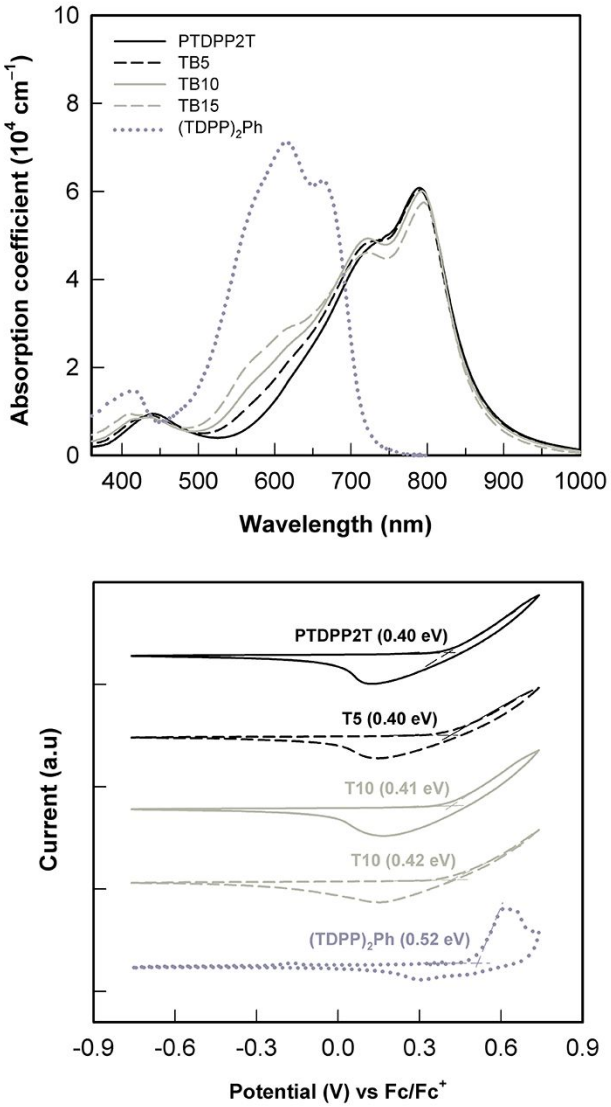

Figure 3.7. UV–vis absorption spectra (a) and cyclic voltammograms (b) of PTDPP2T/$(TDPP)_2Ph$ blends in solid state.

Table 3.1. Characteristics of PTDPP2T/ $(TDPP)_2Ph$ blends.

PTDPP2T/$(TDPP)_2Ph$ (w/w)	A_{max}[a] (10^4 cm^{-1})	E_g^{opt} (eV)[b]	HOMO (eV)	LUMO (eV)[c]
1/0 (PTDPP2T)	-	1.32	–5.20	–3.88
1/0.05 (TB5)	2.52	1.32	–5.20	–3.88
1/0.1 (TB10)	2.96	1.32	–5.21	–3.89
1/0.15 (TB15)	3.28	1.32	–5.24	–3.92
0/1 ($(TDPP)_2Ph$)	6.54	1.66	–5.32	–3.66

[a]Maximum absorption coefficient at λ=610 nm.

[b]Determined from the onset of UV–vis absorption spectra.

[c]Calculated from LUMO=HOMO+E_g^{opt}.

to an E_g^{opt} of 1.32 eV, while $(TDPP)_2Ph$ exhibits strong absorption in the range of 450–700 nm with the onset absorption at shorter wavelength (747 nm), corresponding to an E_g^{opt} of 1.66 eV, indicating that the absorptions of PTDPP2T and $(TDPP)_2Ph$ are considerably complement. The absorption features of two donor molecules lead us to expect that $(TDPP)_2Ph$ effectively harvests the photons of shorter wavelength region which PTDPP2T cannot absorb in the blend of $(TDPP)_2Ph$ and PTDPP2T. Another interesting feature form Figure 2a is that the optical bandgaps of blends are almost the same as PTDPP2T (1.32 eV) while the absorption features of blends are different from PTDPP2T: The absorption intensity at ~600 nm increases as the $(TDPP)_2Ph$ content in the blend increases from 0 to 15%. Therefore it is expected that the

additional absorption in the range of 550–650 nm by $(TDPP)_2Ph$ enhances the J_{SC} of blend-based PSCs. When we measured the HOMO energy levels of blends by cyclic voltammetry (Figure 3.7 (b) and Table 3.1), the HOMO energy level becomes slightly deeper as the content of $(TDPP)_2Ph$ in the blend increases.

For measurement of photovoltaic performance of the blend solar cells, BHJ photovoltaic devices were fabricated with the conventional configuration, ITO/PEDOT:PSS/active layer/Ca/Al, where the active layer was composed of PTDPP2T, $(TDPP)_2Ph$ and $PC_{71}BM$. The active layers were carefully optimized by varying the solvent condition, the blend ratio of two donors and the weight ratio of donor to acceptor. When we varied the amount of DCB addition (2.5, 5.0 and 7.5 vol%) in CF to optimize the solvent condition, we found that the addition of 5 vol% DCB in CF affords the best performance of blend solar cells (Figure 3.9–3.11 and Table 3.3–3.5). To examine the effect of $(TDPP)_2Ph$ addition on the photovoltaic performance of ternary blend solar cells, we varied the amount of $(TDPP)_2Ph$ addition from 5, 10, and 15 wt% relative to the weight of PTDPP2T, after the weight ratio of PTDPP2T to $PC_{71}BM$ was first fixed at 1:2. The photovoltaic properties of all blend solar cells are shown in Figure 3.8–3.11 and listed in Table Table 3.2–3.5. As the amount of $(TDPP)_2Ph$ addition increases, the PCE increases first and then decreases, showing the maximum PCE at 10 wt% addition of $(TDPP)_2Ph$: The solar cell made of TB10 (10% addition of $(TDPP)_2Ph$ to PTDPP2T) exhibits the highest PCE (7.48%) with the highest J_{SC} (16.16 mA cm^{-2}) while the solar cell based on PTDPP2T shows lower PCE of 6.60% with lower J_{SC} of 14.92

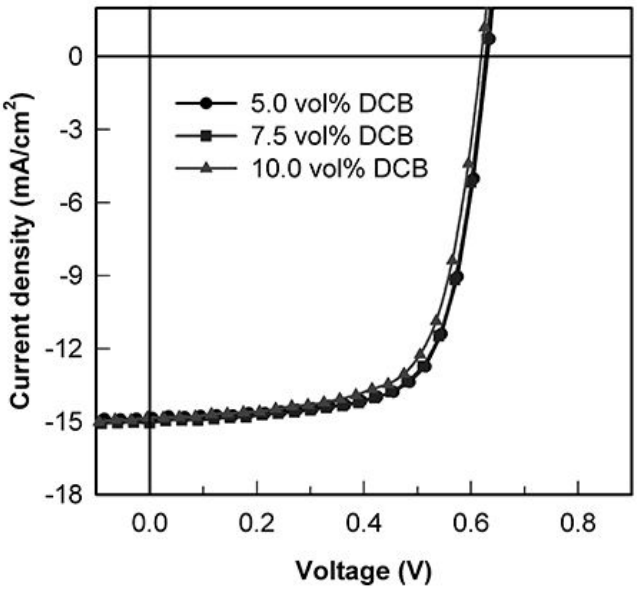

Figure 3.8. *J–V* curves of PTDPP2T:$PC_{71}BM$ BHJ solar cells under AM 1.5G, 100 mW/cm^2 cast from CF/DCB co-solvent with different DCB concentration.

Table 3.2. Photovoltaic properties of PTDPP2T:$PC_{71}BM$ under standard AM 1.5G illumination cast from CF/DCB co-solvent with different DCB concentration.

DCB concentration (vol%)	J_{SC} (mA/cm^2)	V_{OC} (V)	FF	PCE (%)
5.0 vol% DCB	14.91	0.63	0.70	6.60
7.5 vol% DCB	15.05	0.63	0.70	6.70
10.0 vol% DCB	14.93	0.62	0.67	6.21

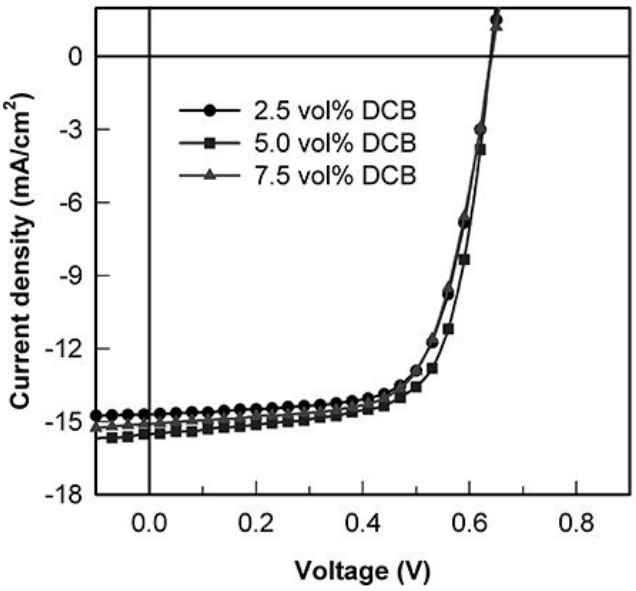

Figure 3.9. *J–V* curves of TB5:$PC_{71}BM$ BHJ solar cells under AM 1.5G, 100 mW/cm^2 cast from CF/DCB co-solvent with different DCB concentration.

Table 3.3. Photovoltaic properties of TB5:$PC_{71}BM$ under standard AM 1.5G illumination cast from CF/DCB co-solvent with different DCB concentration.

Solvent	J_{SC} (mA/cm^2)	V_{OC} (V)	FF	PCE (%)
2.5 vol% DCB	14.66	0.63	0.70	6.47
5.0 vol% DCB	15.55	0.63	0.70	6.93
7.5 vol% DCB	15.11	0.63	0.68	6.51

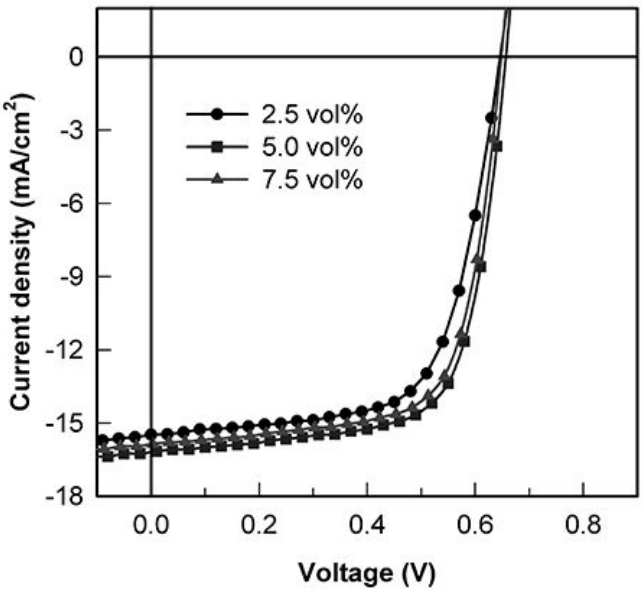

Figure 3.10. *J–V* curves of TB10:$PC_{71}BM$ BHJ solar cells under AM 1.5G, 100 mW/cm^2 cast from CF/DCB co-solvent with different DCB concentration.

Table 3.4. Photovoltaic properties of TB10:$PC_{71}BM$ under standard AM 1.5G illumination cast from CF/DCB co-solvent with different DCB concentration.

Solvent	J_{SC} (mA/cm^2)	V_{OC} (V)	FF	PCE (%)
2.5 vol% DCB	15.51	0.64	0.68	6.77
5.0 vol% DCB	16.16	0.65	0.71	7.48
7.5 vol% DCB	15.86	0.64	0.70	7.14

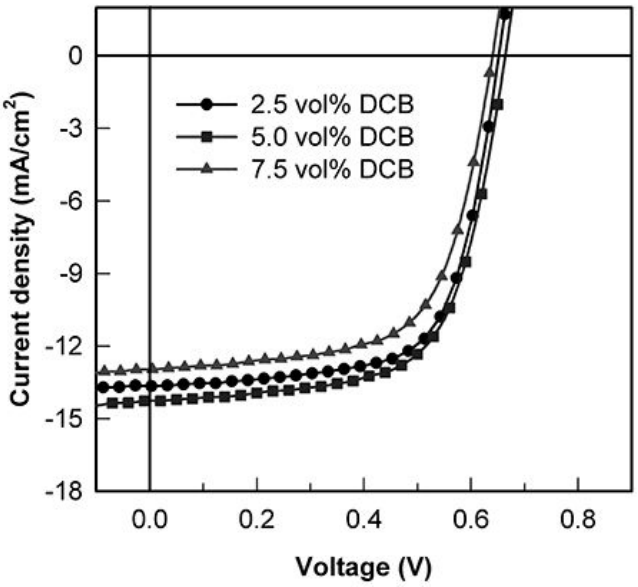

Figure 3.11. *J–V* curves of TB15:$PC_{71}BM$ BHJ solar cells under AM 1.5G, 100 mW/cm^2 cast from CF/DCB co-solvent with different DCB concentration.

Table 3.5. Photovoltaic properties of TB15:$PC_{71}BM$ under standard AM 1.5G illumination cast from CF/DCB co-solvent with different DCB concentration.

Solvent	J_{SC} (mA/cm^2)	V_{OC} (V)	FF	PCE (%)
2.5 vol% DCB	13.63	0.65	0.68	6.03
5.0 vol% DCB	14.23	0.66	0.65	6.13
7.5 vol% DCB	12.93	0.64	0.65	5.39

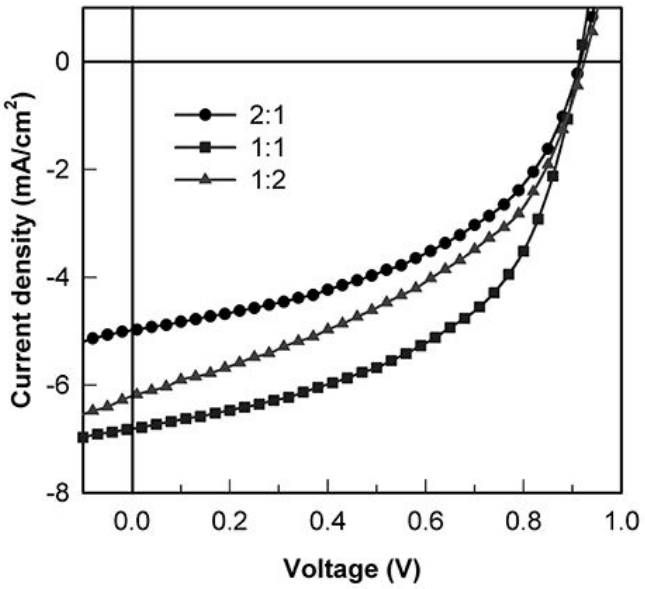

Figure 3.12. *J–V* curves of $(TDPP)_2Ph:PC_{71}BM$ BHJ solar cells under AM 1.5G, 100 mW/cm^2 cast from 5 vol% DCB in CF.

Table 3.6. Photovoltaic properties of $(TDPP)_2Ph:PC_{71}BM$ under standard AM 1.5G illumination cast from 5 vol% DCB in CF.

$(TDPP)_2Ph:PC_{71}BM$	J_{SC} (mA/cm^2)	V_{OC} (V)	FF	PCE (%)
2:1	4.94	0.91	0.48	2.16
1:1	6.79	0.91	0.51	3.17
1:2	6.17	0.91	0.44	2.48

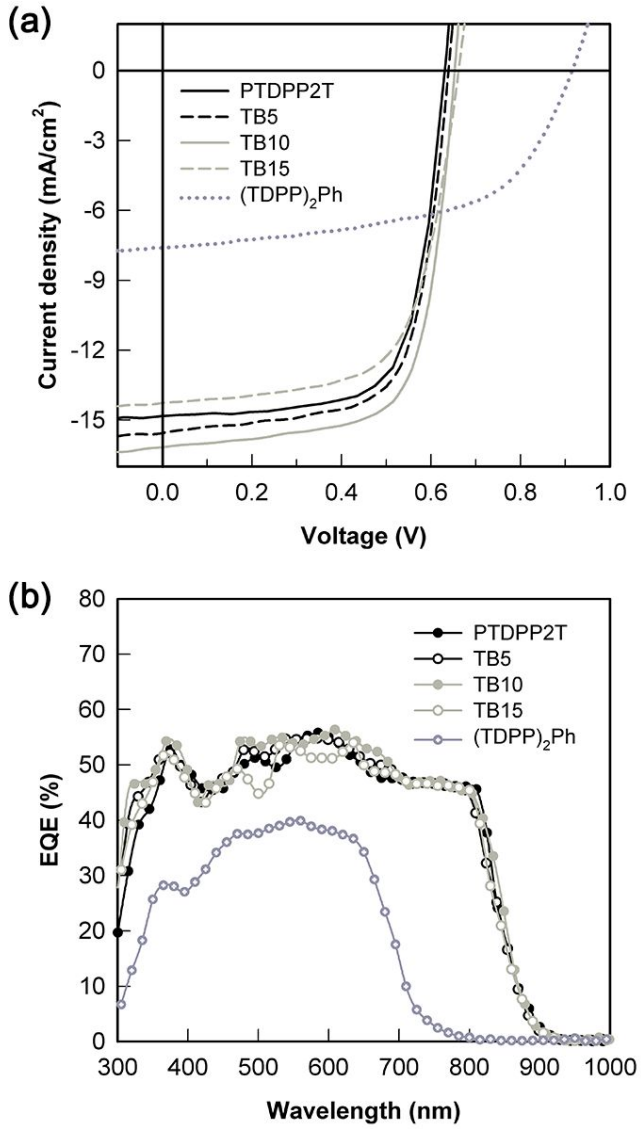

Figure 3.13. *J–V* curves (a) and external quantum efficiency spectra (b) of binary and ternary blend solar cells.

Table 3.7. Photovoltaic properties of binary and ternary blend devices under standard AM 1.5G illumination and charge carrier mobilities under dark conditions.

PTDPP2T:$(TDPP)_2Ph$: $PC_{71}BM$ (w:w:w)	Thickness (nm)	J_{SC} (mA/cm^2)	V_{OC} (V)	FF	μ_h (cm^2/V s)[b]	$PCE_{max(ave)}$ (%)
1:0:2 (PTDPP2T)	120±5	14.91 (14.88)[a]	0.62	0.70	7.53×10^{-3}	6.60 (6.48)
1:0.05:2 (T5)	120±5	15.55 (15.32)[a]	0.63	0.70	-	6.93 (6.71)
1:0.10:2 (T10)	122±5	16.16 (16.02)[a]	0.65	0.71	1.03×10^{-2}	7.48 (7.33)
1:0.15:2 (T15)	115±5	14.23 (13.97)[a]	0.66	0.65	4.44×10^{-3}	6.13 (5.83)
0:1:1 ($(TDPP)_2Ph$)	100±5	6.79 (6.62)[a]	0.91	0.51	6.69×10^{-4}	3.17 (2.91)

[a]Integrated from EQE data.

[b]Hole mobility of binary and ternary blends as measured by SCLC method.

mA cm^{-2} (Figure 3.13 and Table 3.7). We also observed that the V_{OC}s of ternary blend solar cells increase gradually (TB5=0.63 V, TB10=0.65 V and TB15=0.66 V) with addition of $(TDPP)_2Ph$, because the HOMO energy level of blend donor becomes deeper as the concentration of $(TDPP)_2Ph$ increases in the active layer.

To identify the reason for the highest J_{SC} of TB10-based solar cell, we first measure and G_{max} of all blends (Figure 3.16 (b)). The G_{max} is estimated from the saturation current of the J_{ph} vs. the V_{eff}. Here, J_{ph} is defined as $J_{ph}=J_L-J_D$, where J_L and J_D are the current densities under illumination and dark, respectively. V_{eff} is defined as $V_{eff}=V_0-V_a$, where V_0 and V_a are the voltage when J_{ph} equals zero and applied bias voltage, respectively. The values of G_{max} for PTDPP2T, TB10 and $(TDPP)_2Ph$ are 7.03×10^{27}, 7.37×10^{27}, and 4.87×10^{27} $m^{-3}s^{-1}$, respectively, suggesting that the higher J_{SC} of TB10 is attributed mainly to additional absorption of $(TDPP)_2Ph$ in the range of 550–700 nm.

It is well recognized that the molecular orientation, crystallinity and domain size of organic donor materials in the active layer are the important parameters to control the photovoltaic performance. Particularly, the morphology of active layer is very critical for ternary blend solar cells, because the miscibility of two donor materials is another important factor to determine the photovoltaic performance. For this purpose, the miscibility of PTDPP and $(TDPP)_2Ph$ was investigated by using differential scanning calorimetry. As shown in Figure 3.14, during the heating process the PTDPP2T exhibits strong melting endothermic peaks (T_m) at 320 °C, and the

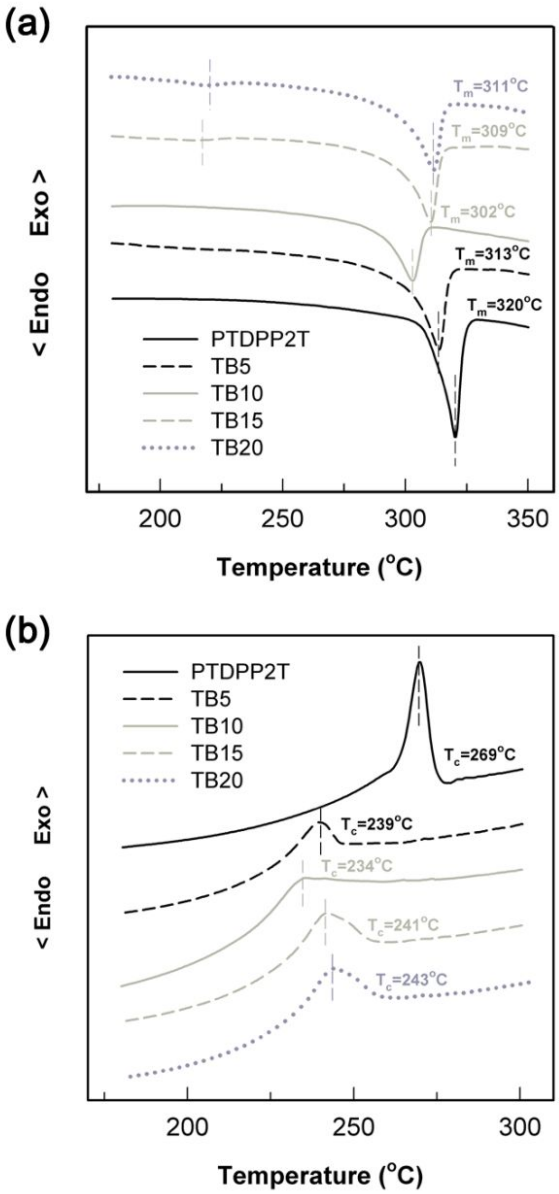

Figure 3.14. DSC heating (a) and cooling (b) thermograms of PTDPP2T and PTDPP2T/$(TDPP)_2$Ph blends.

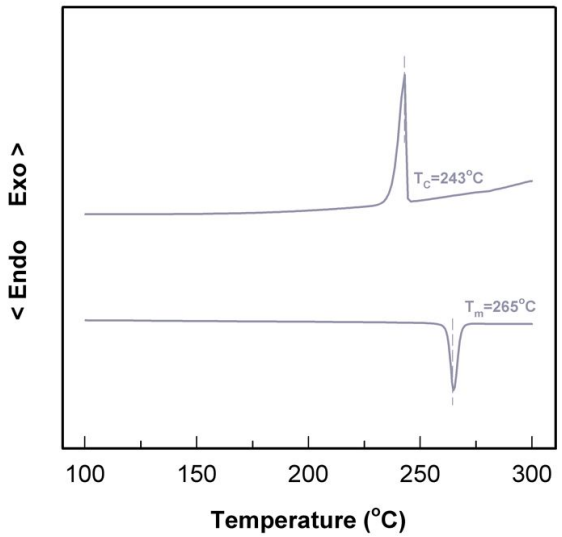

Figure 3.15. DSC thermograms of $(TDPP)_2Ph$.

T_m of PTDPP2T is depressed from 320 °C to 302 °C as the $(TDPP)_2Ph$ content is increased from 0 to 10 wt% (TB10). However as the weight ratio of $(TDPP)_2Ph$ exceeds 10 wt% (TB15), T_m of PTDPP2T begins to increase, and new endothermic peak of $(TDPP)_2Ph$ appears (Figure 3.15). It is indicating that the PTDPP2T are miscible with $(TDPP)_2Ph$ at low concentration of $(TDPP)_2Ph$ (<10 wt), while these two donor materials are immiscible when the amount of $(TDPP)_2Ph$ is increased to 15 wt%. Thus the concentration of $(TDPP)_2Ph$ is a critical parameter in the performance of ternary blend solar cell.

In order to investigate the crystalline properties of blends, X-ray diffraction (XRD) experiments were performed. One-dimensional XRD (1D-

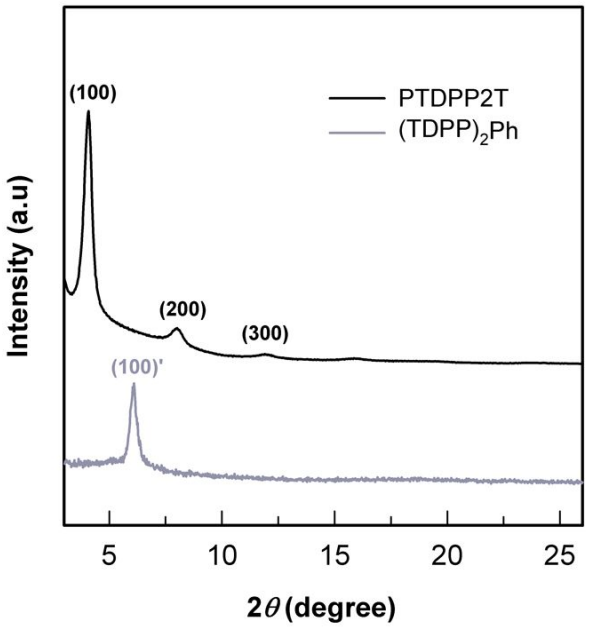

Figure 3.16. XRD diffractograms of PTDPP2T (a) and $(TDPP)_2Ph$ (b) in thin film.

Table 3.8. Interchain distance of PTDPP2T and $(TDPP)_2Ph$.

Donor material	2θ (degree)	d (Å)
PTDPP2T	4.06	21.7
$(TDPP)_2Ph$	6.8	14.5

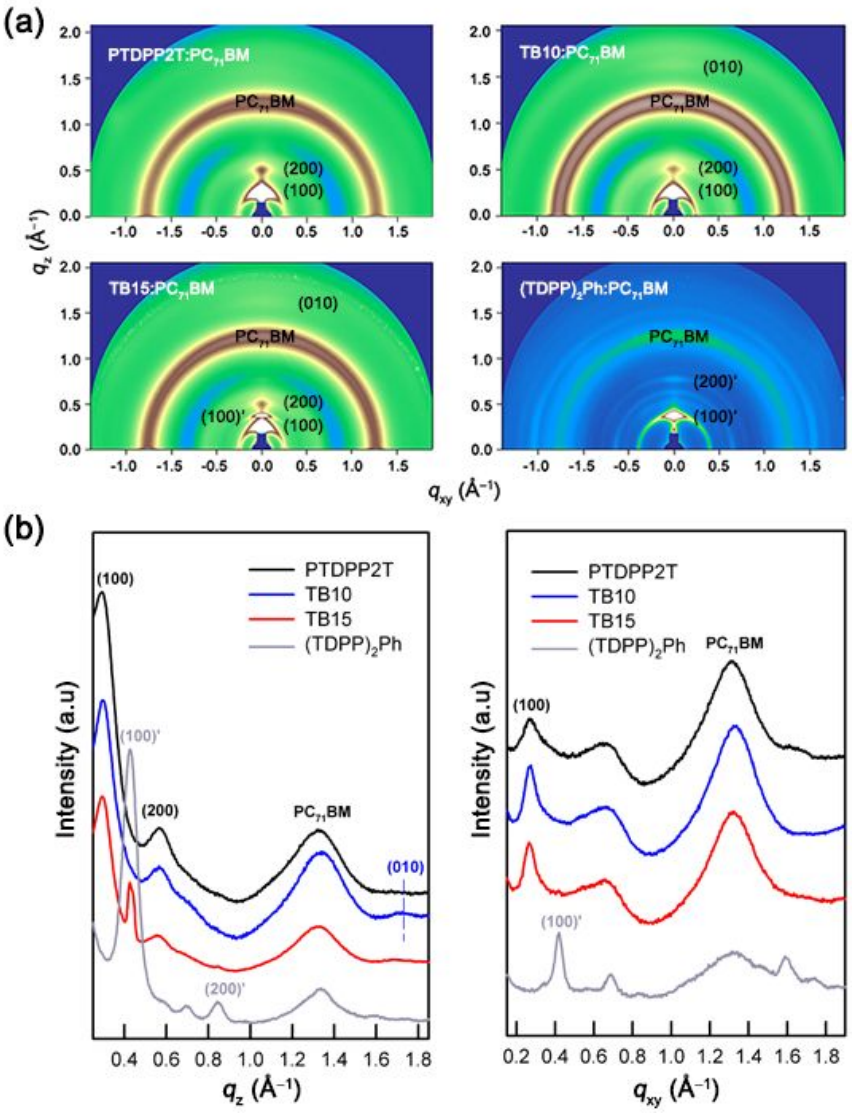

Figure 3.17. 2D-GIWAXS patterns of PTDPP2T:$(TDPP)_2Ph$:$PC_{71}BM$ blend films (a) and in-plane and out-of-plane line cuts of the corresponding GIWAXS images (b).

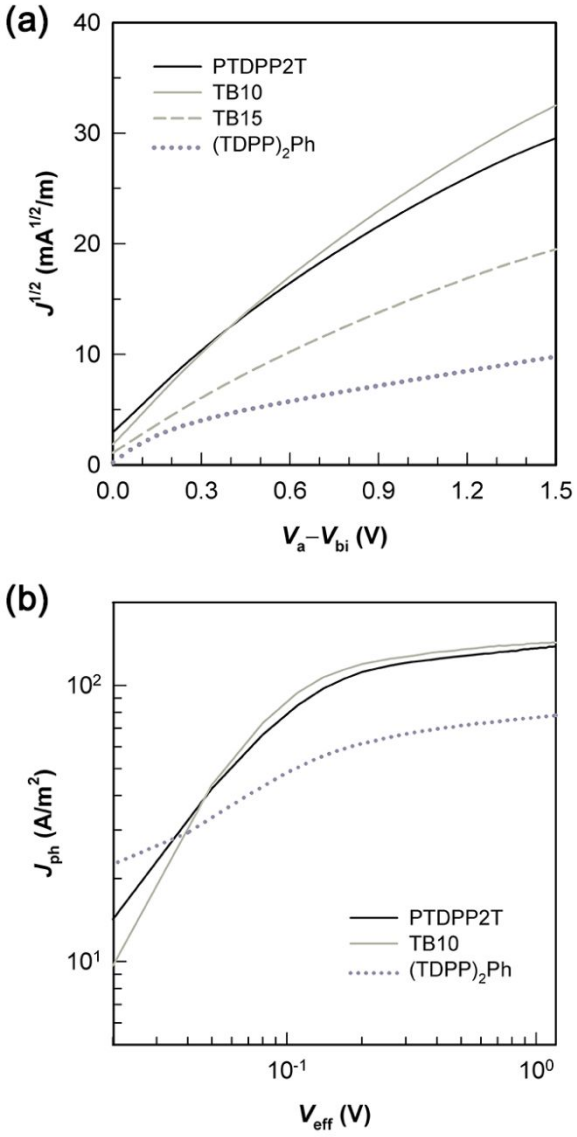

Figure 3.18. Photocurrent density (J_{ph}) plotted against effective voltage (V_{eff}) (a) and dark J–V characteristics of PTDPP2T:$(TDPP)_2Ph$:$PC_{71}BM$ blends (b) with hole only device under optimized condition.

XRD) patterns of pristine PTDPP2T and $(TDPP)_2Ph$ reveal that PTDPP2T exhibits strong diffraction peaks at 2θ = 4.06, 8.12 and 12.18, corresponding to the typical (*h*00) diffraction with interchain distance of 21.7 Å, while $(TDPP)_2Ph$ does only (100) diffraction peak at 2θ = 6.08 with shorter interchain distance of 14.5 Å (Figure 3.16 and Table 3.8). This is probably because $(TDPP)_2Ph$ has shorter alkyl chain of ethylhexyl than PTDPP2T with decyltetradecyl chain. To further understand the change in molecular packing and structure ordering when blended with $PC_{71}BM$, we performed two-dimensional 2D-GIWAXS experiment. When GIWAXS patterns and line-cut profiles of two binary blends (PTDPP2T:$PC_{71}BM$ and $(TDPP)_2Ph$:$PC_{71}BM$) and ternary blends (PTDPP2T:$(TDPP)_2Ph$:$PC_{71}BM$) with different amount of $(TDPP)_2Ph$ are compared, as shown in Figure 3.17, two binary blends exhibit distinct (*h*00) peaks at q_z=0.291 $Å^{-1}$ and q_z=0.423 $Å^{-1}$ for PTDPP2T:$PC_{71}BM$ and $(TDPP)_2Ph$:$PC_{71}BM$, respectively. The addition of 10 wt% $(TDPP)_2Ph$ into PTDPP2T:$PC_{71}BM$ does not cause any discernible change in (*h*00) diffractions in q_z direction except for appearance of (010) diffraction peak, indicating that the addition of $(TDPP)_2Ph$ induces close packing of PTDPP2T in the π–π direction. The denser packing of PTDPP2T in the π–π direction may increase the hole transporting mobility in the active layer (1.03×10^{-2} cm^2 V^{-1} s^{-1}) (Figure 3.18 (a) and Table 3.7). When the amount of $(TDPP)_2Ph$ is further increased to 15 wt% in the blend, another peak in addition to the (100) and (200) diffraction peaks of PTDPP2T is clearly observed at q_z=0.423 $Å^{-1}$, which corresponds to (100) diffraction peak of $(TDPP)_2Ph$ as denoted by (100)′ in Figure 3.17. The above result indicates that the TB15 blend exhibits

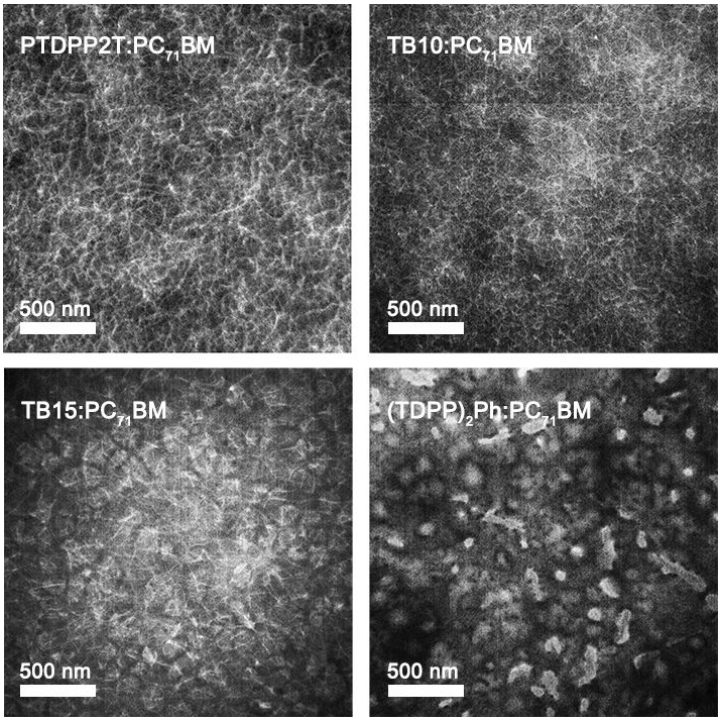

Figure 3.19. TEM images of binary and ternary blend films spin-coated from 5vol% DCB in CF.

macrophase separation into PTDPP2T and $(TDPP)_2Ph$ phases while the TB10 blend does not show macrophase separation. In other words, the blends with a small amount of $(TDPP)_2Ph$ (<10 wt%) are miscible, but the blend containing $(TDPP)_2Ph$ higher than 10 wt% is phase separated. The macrophase separation of TB15 blend is accompanied by a decrease of hole mobility (4.44×10^{-3} cm^2 V^{-1} s^{-1}) (Figure 3.18 (a) and Table 3.7).

When the morphologies of binary blends are examined by TEM, the PTDPP2T:$PC_{71}BM$ blend exhibits interconnected network structure with well-developed fibrils, while the $(TDPP)_2Ph$:$PC_{71}BM$ blend exhibits phase

separation with macro-scale islands of $(TDPP)_2Ph$ (Figure 3.19). Recently Janssen group synthesized several DPP-based polymers and controlled the fibril width by controlling the polymer solubility in solvent.[164,179] They have found that the fibril width narrower than 12 nm results in high J_{SC} and thus high PCE. The ternary blend (TB10) with 10 wt% of $(TDPP)_2Ph$ also forms well-developed fibril structure with the fibril size narrower than the binary blend (PTDPP2T:$PC_{71}BM$), whereas the ternary blend (TB15) exhibits a large size of $(TDPP)_2Ph$ domains, indicating that PTDPP2T and $(TDPP)_2Ph$ are miscible.

3.4 Summary

Ternary blend organic solar cell is a promising candidate for BHJ solar cells. However, improving the PCE is quite challenging since the ternary system is difficult to control the phase separation behavior. In this study, we fabricated the ternary blend organic solar cell composed of two donors ($(TDPP)_2Ph$, and PTDPP2T) and one acceptor ($PC_{71}BM$). Due to the third component of $(TDPP)_2Ph$ as a donor, ternary blend of TB10 shows additional absorption in the range of 550–650 nm. Also when the weight ratio of $(TDPP)_2Ph$ is below 10 wt%, the $(TDPP)_2Ph$ can be mixed into polymer matrix (PTDPP2T) and induce face-on orientation of PTDPP2T which facilitates the charge transport. Consequently, an enhanced PCE of 7.48% for ternary blend of TB10 is obtained due to improvement of the J_{SC} (16.16 mA/cm^2) as compared with PTDPP2T:$PC_{71}BM$ (14.91 mA/cm^2, 6.60%) binary system.

Chapter 4. Conjugated random copolymers consisting of pyridine- and thiophene-capped diketopyrrolopyrrole as co-electron accepting units to enhance both J_{SC} and V_{OC} of polymer solar cells

4.1 Introduction

To get a lower bandgap, a more electron-donating unit and a more electron-deficient unit can be selected, whereas the HOMO and LUMO levels can also be governed by varying the electron donating ability of the donor unit and the electron affinity of the acceptor unit, respectively. Also, most of the D−A copolymers possess an intramolecular charge transfer (ICT) absorption band at long wavelength direction. However, the strong ICT effect between the donor and acceptor units will inevitably weaken the absorption of the short wavelength polymers and therefore cause undesired trade-off between J_{SC} and V_{OC} of the solar cells. Thus, a way to enhance the absorption of D−A copolymers in short wavelength range without sacrificing other properties becomes an important and challenging issue.

Recently, the third components have been introduced into the traditional D−A conjugated polymers to synthesize random copolymers, which can

control balance among the polymer properties such as energy levels, bandgap, and their correlation with J_{SC} and V_{OC} to optimize the molecular structure for high photovoltaic performance. Thus according to this strategy, we synthesized a new series of 1D/2A-type DPP-based random copolymer by copolymerization of 2T (electron donating unit) with TDPP and PyDPP (co-electron accepting units) (Scheme 4.1). Here, TDPP and PyDPP show complementary absorption. Unlike most of 1D/2A-type random copolymers containing two different A units, the two A units (TDPP and PyDPP) in our random copolymers have the same DPP core but different flanking units (thiophene and pyridine). Thus, the molecular structure of the random copolymer may not be significantly different from those of the corresponding homopolymers, implying that random sequence of the two A units in random copolymer may not disturb its crystallization. As a result, the random sequence does not affect J_{SC} because the random copolymer may exhibit the crystallinity as high as the corresponding homopolymers. The V_{OC} of random copolymer can systematically be controlled by varying the feed ratio of PyDPP to TDPP for polymerization. The V_{OC} increases with increasing the PyDPP content in the random copolymer, because the HOMO energy level becomes deeper as the PyDPP content in the random copolymer increases due to stronger electron withdrawing power of pyridine.

4.2 Experimental

4.2.1 Materials

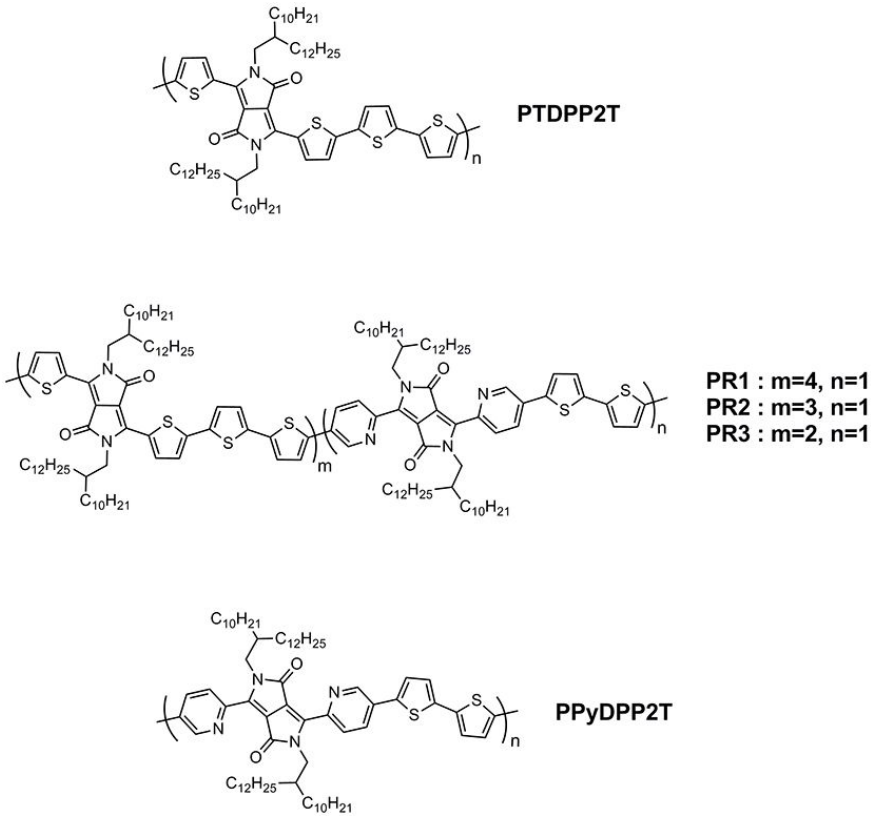

Scheme 4.1. Chemical structures of PTDPP2T, PR1, PR2, PR3 and PPyDPP2T.

$Pd(PPh_3)_4$, *n*-butyllithium and trimethyltin chloride were purchased from Sigma-Aldrich and used without further purification. [6,6]-Phenyl-C71-butyric acid methyl ester ($PC_{71}BM$) was obtained from Nano-C. Poly(3,4-ethylenedioxythiophene):poly(styrenesulfonate) (PEDOT:PSS) (Clevios P VP AI 4083) was purchased from H. C. Stark and passed through a 0.45 μm PVDF syringe filter before spin-coating. Common organic solvents were purchased from Daejung. Tetrahydrofuran was dried over sodium/benzophenone under nitrogen condition and freshly distilled prior to use. All other reagents were purchased from Tokyo Chemical Industry and used as received.

4.2.2 Synthesis of monomers and polymers

Synthesis of 3,6-Di(5-bromopyridin-2-yl)pyrrolo[3,4-*c*]pyrrole-1,4(2*H*,5*H*)-dione (1): 5-Bromopyridine-2-carbonitrile (6.19 g, 34 mmol) was added to a solution of potassium *tert*-butoxide (4.14 g, 37 mmol) in 2-methyl-2-butanol (70mL) at room temperature and the mixture was then heated to 110 °C. Diethyl succinate (2.61 g, 15 mmol) in 2-methyl-2-butanol (30 mL) was added drop-wise over 1 hr. The reaction mixture was stirred for 20 hr at 100 °C before cooling down to room temperature. Water (100 mL) was added to the mixture and the solid was filtered off, washed with methanol and water, and dried at 100 °C in vacuum oven to afford the product. The product is insoluble in common NMR solvents and was used in the next step without further purification. Yield: 50%.

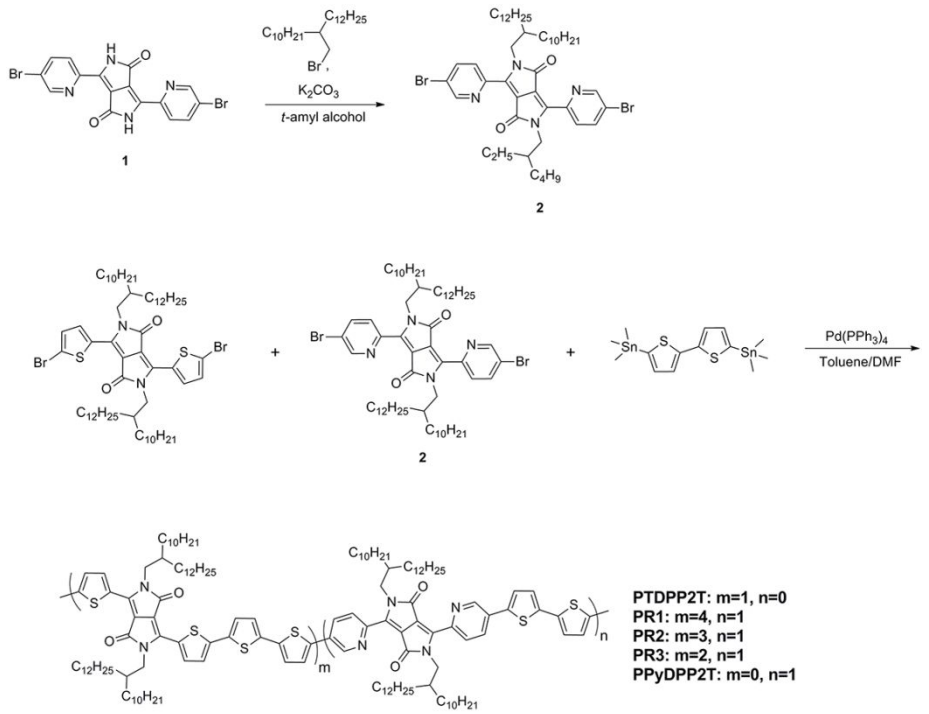

Scheme 4.2. Synthetic scheme of random copolymers composed of thiophene- and pyridine-capped diketopyrrolopyrrole as co-electron accepting

Synthesis of 3,6-Di(5-bromopyridin-2-yl)pyrrolo[3,4-*c*]pyrrole-1,4(2*H*,5*H*)-dione (2): The compound **1** (1.2 g, 2.7 mmol), potassium carbonate (1.0 g, 7.2 mmol), and 2-decyltetradecyl bromide (3.5 g, 8.8 mmol) in chapter 3 were stirred in DMF (30 mL) for 18 hr at 70 °C under argon. After cooling down to room temperature, the mixture was poured into water (50 ml) and extracted with ethyl acetate. The combined organic phase was dried over anhydrous Na_2SO_4 and filtered. After removing solvent in vacuum, the obtained crude product was purified by column chromatography on silica gel using toluene as the eluent to give the pure target product. Yield: 690 mg

(25.4%). ^{1}H NMR (300 MHz, $CDCl_3$): δ 8.93 (d, 2H), 8.74 (d, 2H), 8.01 (d, 2H), 4.28 (d, 4H), 1.61 (m, 2H), 1.24 (m, 64H), 0.93–0.81 (m, 12H).

Polymerization of PTDPP2T: The PTDPP2T was synthesized by following the same procedure in chapter 3.

Polymerization of PPyDPP2T: The compound **17** (145 mg, 0.13 mmol) and **18** (65 mg, 0.13 mmol) were dissolved in toluene (10 mL). After the solution was flushed with N_2 for 20 min, 4 mg of $Pd(PPh_3)_4$ was added. The reaction mixture was stirred for 4 h at 150°C in a microwave reactor. After being cooled to room temperature, the mixture was poured into methanol. The crude product was filtered through a Soxhlet thimble, and then subjected to Soxhlet extraction with methanol, ethyl acetate, hexane, DCM and chloroform. The polymer was recovered from chloroform fraction, and the fraction was precipitated into methanol to afford the product as green solid (105 mg, 71%).

Polymerization of PR1: A mixture of TDPP (0.184 g, 0.162 mmol), PyDPP (0.045 g, 0.040 mmol) and 2T (0.100 g, 0.203 mmol) was dissolved in a mixture of toluene (9 mL) and DMF (1 mL). After the solution was flushed with argon for 10 min, $Pd(PPh_3)_4$ (0.005g, 0.004 mmol) was added quickly in the reaction mixture and sealed, and stirred at 150 ºC for 3 h in a microwave reactor. After being cooled to room temperature, the organic phase was poured into methanol during stirring. The precipitate was filtered through a Soxhlet thimble and subjected to Soxhlet extraction sequentially with methanol,

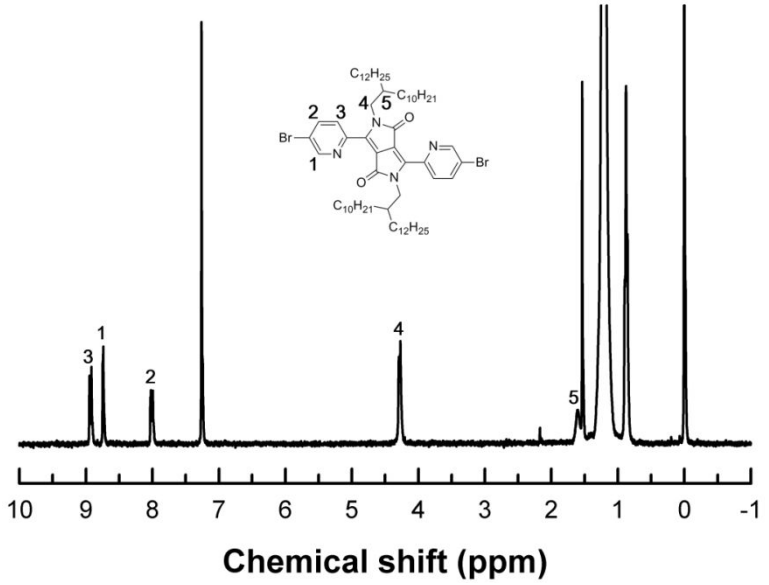

Figure 4.1. [1]H NMR spectrum of compound **2** in Scheme 4.2.

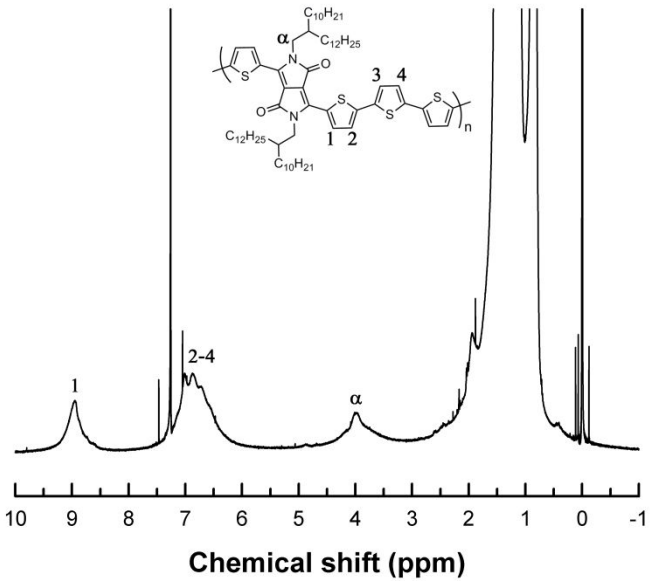

Figure 4.2. [1]H NMR spectrum of **PTDPP2T** in Scheme 4.2.

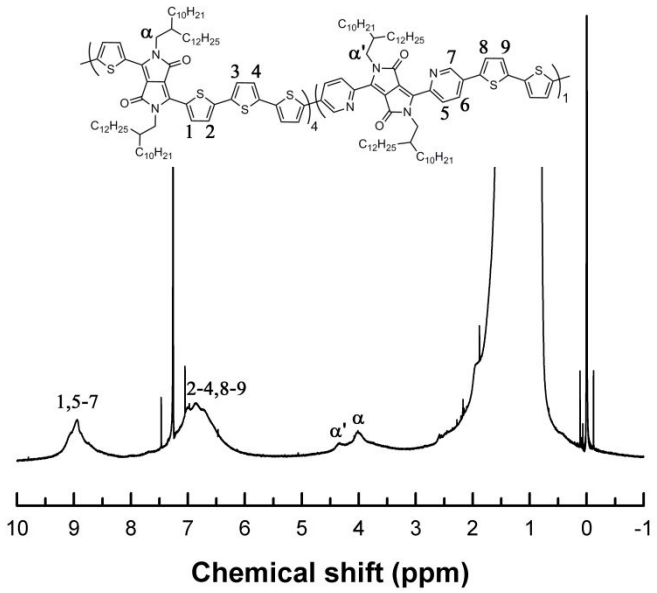

Figure 4.3. ^{1}H NMR spectrum of **PR1** in Scheme 4.2.

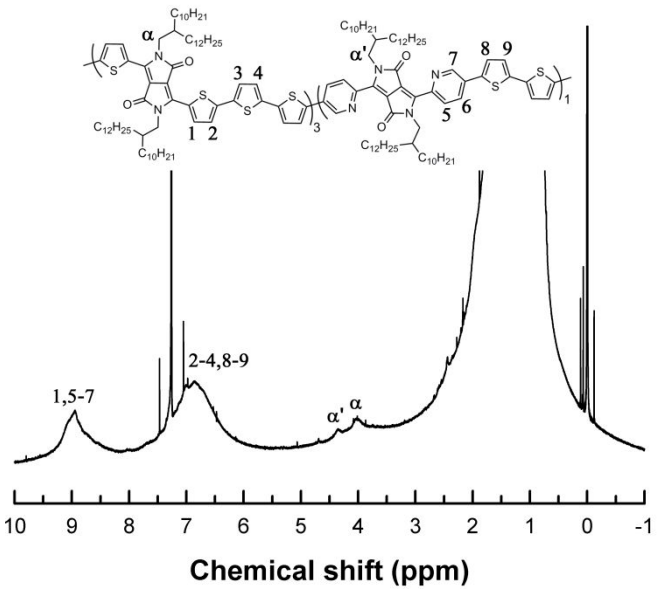

Figure 4.4. ^{1}H NMR spectrum of **PR2** in Scheme 4.2.

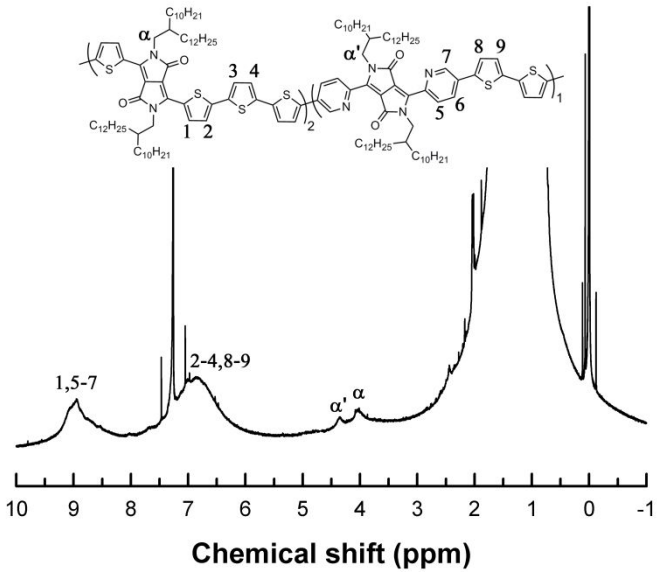

Figure 4.5. ^{1}H NMR spectrum of **PR3** in Scheme 4.2.

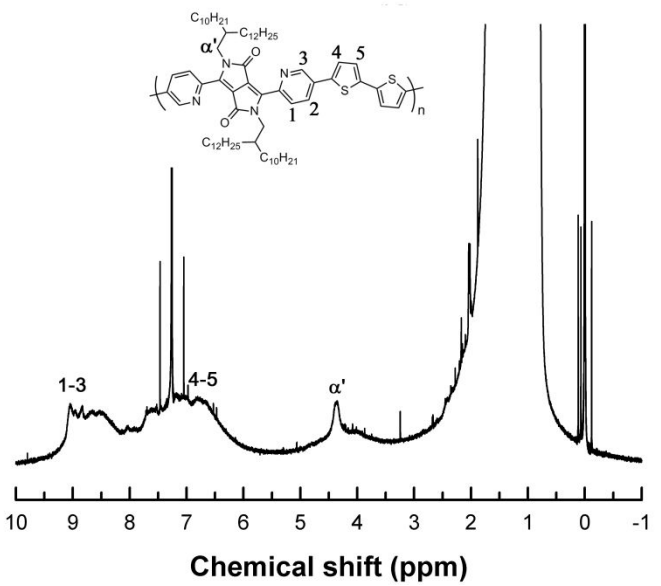

Figure 4.6. ^{1}H NMR spectrum of **PPyDPP2T** in Scheme 4.2.

acetone, ethyl acetate, hexane, dichloromethane and chloroform. The polymer was recovered from the chloroform fraction, and precipitated into methanol to yield the product of greenish solid (0.170 g, 70%).

Polymerization of PR2 and PR3: The PR2 and PR3 were synthesized by following the same procedure as the synthesis of PR1. The yield of PR2 and PR3 were 75% and 72%, respectively.

4.3 Results and discussion

The DPP-based polymers (PTDPP2T, PR1, PR2, PR3 and PPyDPP2T) were prepared by Stille coupling reaction. For Stille coupling, toluene/DMF co-solvent was used to obtain high molecular weight of polymer. To ensure good solubility of the polymers, we substituted 2-decyltetradecyl group on DPP unit. We synthesized two reference homopolymers (PTDPP2T and PPyDPP2T) and three random copolymers (PR1, PR2 and PR3) (Scheme 4.1) with different molar ratios of TDPP to PyDPP to investigate the effect of copolymer composition on photovoltaic properties. When we have tried to determine the compositions of TDPP and PyDPP in random copolymers from analysis of ^{1}H NMR spectra (Figure 4.2−4.6), we realize that it is not accurate to measure the intensity ratio of α-position protons in PTDPP2T to α'-position protons in PPyDPP2T because the intensities of α-and α'-position protons are too weak and broad to be accurately determined. Hence, we determined the compositions of TDPP and PyDPP using elemental analysis (Table 4.1), and

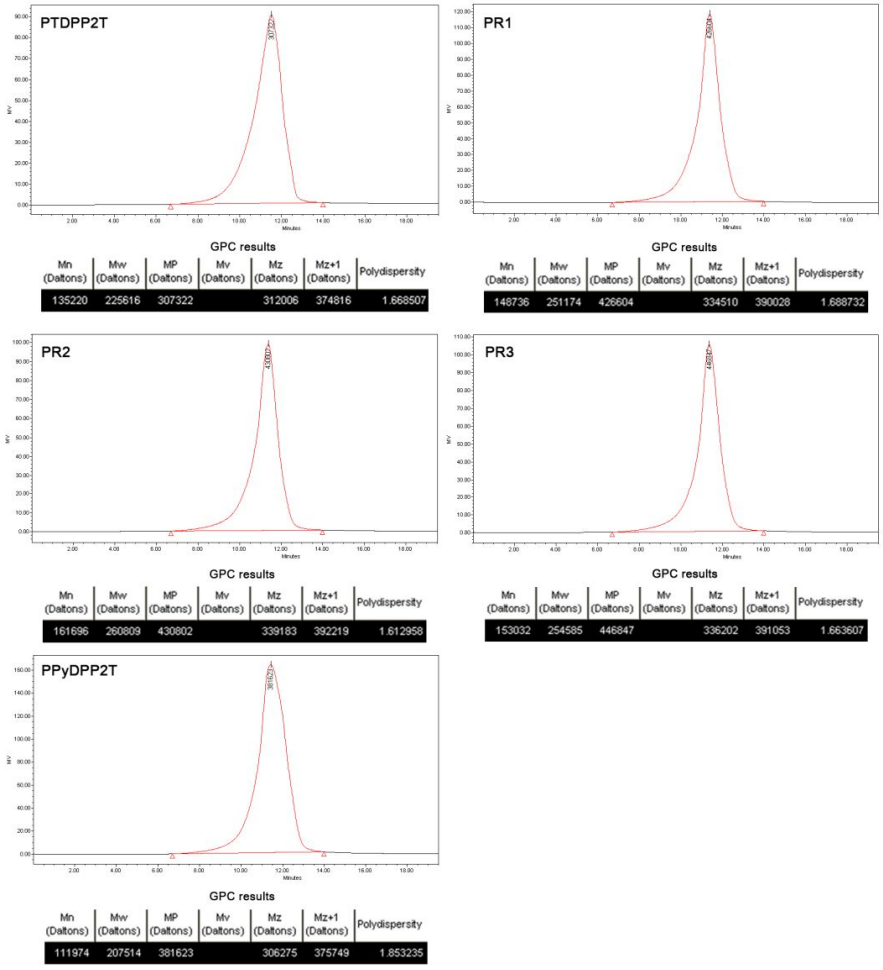

Figure 4.7. GPC traces of TDPP2T, PR1, PR2, PR3 and PPyDPP2T.

Table 4.1. Elemental analysis of random copolymers.

		C	H	N	S
PTDPP2T	Calcd.[a]	73.89	9.57	2.46	11.27
	Found	74.01	9.53	2.42	11.42
PR1	Calcd.[a]	74.52	9.48	2.97	10.20
	Found	74.59	9.43	2.93	10.31
PR2	Calcd.[a]	74.65	9.50	3.10	9.93
	Found	74.70	9.47	3.08	9.99
PR3	Calcd.[a]	74.90	9.55	3.30	9.43
	Found	74.96	9.52	3.25	9.49
PR4	Calcd.[a]	76.68	9.83	4.97	5.69
	Found	76.69	9.81	4.93	5.75

[a]The calculated values assume that the composition of comonomer is equal to the feed ratio.

have found that the compositions are nearly equal to the molar feed ratio of TDPP/PyDPP, indicating that the reactivities of two monomers are equal. When the number of molecular weights (M_n) and polydispersity index of polymers were measured by gel permeation chromatography using chloroform as eluent at 50 °C, all the polymers have high M_n exceeding 100 k (Figure 4.7, Table 4.2), and therefore the molecular weight dependence of photovoltaic performance may not be considered. All of synthesized polymers are soluble in common solvents such as chloroform, chlorobenzene and *o*-dichlorobenzene at 50 °C.

The absorption spectra of five conjugated copolymers show two absorption bands (Figure 4.8 (a)): one at 400–500 nm due to π–π* transition, and another broad band at 550–900 nm due to the ICT between electron deficient unit (TDPP or PyDPP) and electron donating unit (2T). It is noted here that 1D/2A-type conjugated copolymers extend their absorption range to long wavelength region through appearance of new ICT band.[159] When the UV–vis spectra of two reference homopolymers are compared, PTDPP2T absorbs the light in the range of 670–840 nm, while PPyDPP2T absorbs shorter wavelength of light (600–720 nm) than PTDPP2T due to weak push-pull electron transfer between pyridine and DPP core. Note here that the electron donating power of pyridine is much weaker than thiophene. The absorption range of random polymer can effectively be tuned by varying the copolymer composition. When we calculated the full-width half-maxima (FWHM) of absorption spectra to quantitatively compare the absorption ranges of random copolymers, the FWHMs of PR1, PR2 and PR3 are 202 nm,

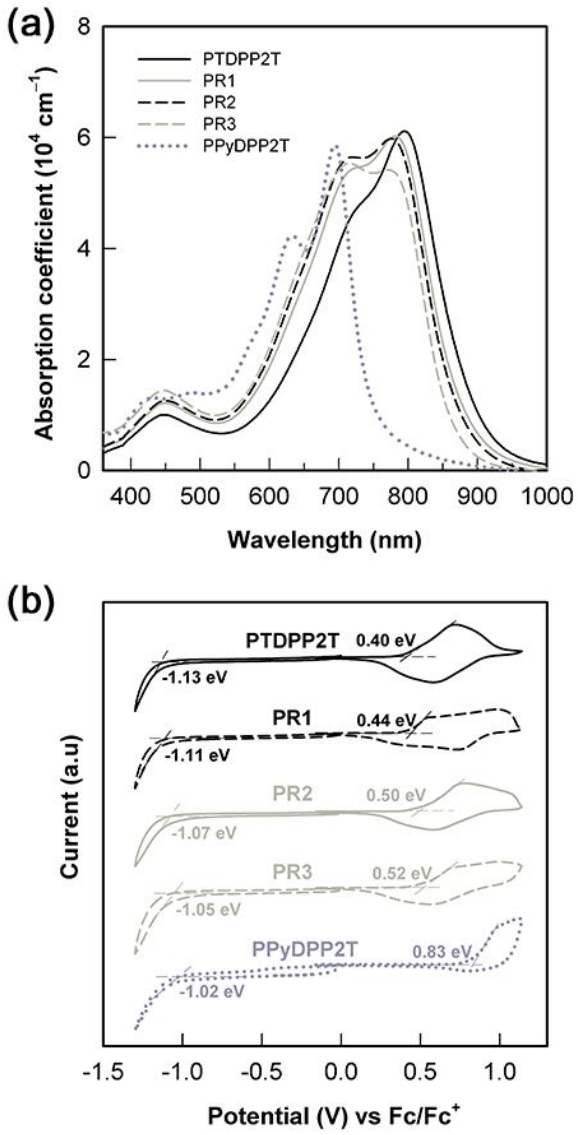

Figure 4.8. UV–vis absorption spectra (a) and cyclic voltammograms (b) of PTDPP2T, PR1, PR2, PR3 and PPyDPP2T in solid state.

Table 4.2. Characteristics of PTDPP2T, PR1, PR2, PR3 and PPyDPP2T.

Polymer	M_n (kg/mol)	PDI	E_g^{opt} (eV)[a]	FWHM (nm)	HOMO (eV)	LUMO (eV)[b]
PTDPP2T	135	1.66	1.32	171	–5.20	–3.88
PR1	149	1.68	1.35	202	–5.24	–3.89
PR2	162	1.61	1.37	205	–5.30	–3.93
PR3	153	1.66	1.40	211	–5.32	–3.92
PPyDPPP2T	112	1.85	1.60	126	–5.63	–4.03

[a]Determined from the onset of UV–vis absorption spectra.

[b]Calculated from LUMO=HOMO+E_g^{opt}

205 nm and 211 nm, respectively (Table 4.2), which are 30–80 nm broader than those of the two homopolymers. However, total absorption areas of PR1 and PR2 are larger than PR3 (Figure 4.8 (a)).

When the optical band gaps of polymers are determined by the onset of light absorption, the bandgap increases from 1.32 eV to 1.60 eV as the PyDPP composition in random copolymer is increased from 0 to 100% (Table 4.2). The HOMO energy level, as measured by the onset of oxidation potential of cyclic voltammogram, increases from –5.20 eV to –5.63 eV as the PyDPP content increases from 0 to 100% (Figure 4.8 (b), Table 4.2), indicating that the increase of pyridine content in the random copolymer lowers the HOMO energy level, because pyridine is more electron deficient than thiophene, which makes PyDPP stronger electron accepting unit than TDPP. This demonstrates that we can systematically tune the HOMO/LUMO energy levels of random polymer by varying the copolymer composition.

For measurement of the photovoltaic performances of the random copolymers, we fabricated PSC devices with conventional architecture (ITO/PEDOT:PSS/active layer/Ca/Al), where the active layer was composed of polymer and $PC_{71}BM$. We found that the optimum blend ratio of polymer to $PC_{71}BM$ was 1 to 2 (Figure 4.9 and Table 4.3). For further optimization of device performance, we fabricated various devices using mixed solvents with different mixing ratios. The current density–voltage (*J*–*V*) curves of the PSC device are shown in Figure 4.10, and the corresponding photovoltaic parameters are summarized in Table 4.4. The best PCEs of PR1, PR2 and PR3 are 7.59%, 8.11% and 6.29%, respectively, while the best PSCs of two

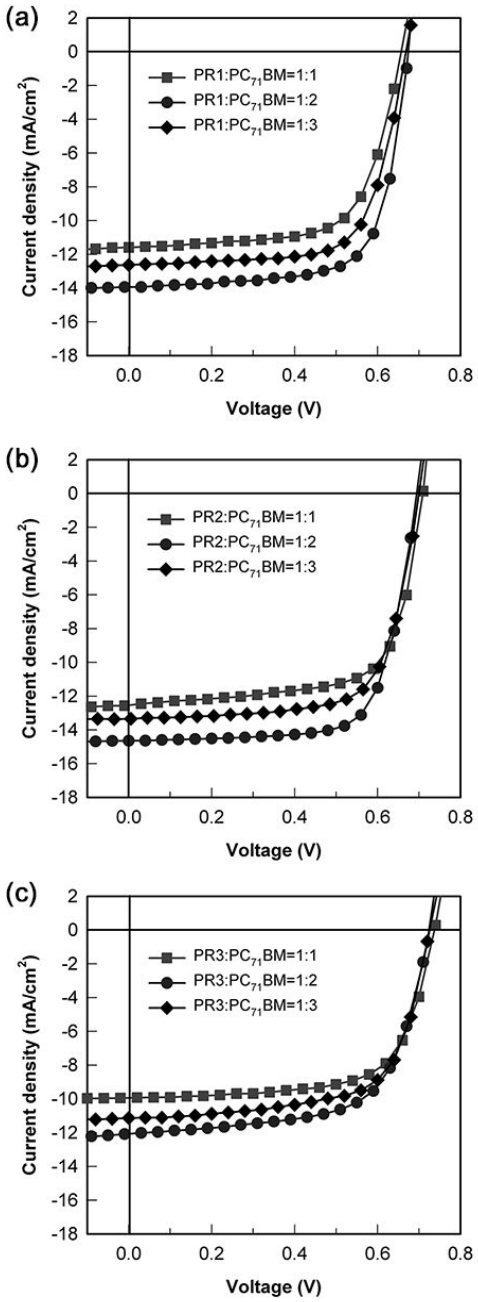

Figure 4.9. *J–V* curves of random copolymer:$PC_{71}BM$ BHJ solar cells under AM 1.5G, 100 mW/cm^2 cast from DCB with 2 vol% DIO.

Table 4.3. Photovoltaic properties of random copolymers under standard AM 1.5G illumination cast from DCB with 2 vol% DIO.

	Polymer:$PC_{71}BM$ (w/w)	J_{SC} (mA/cm^2)	V_{OC} (V)	FF	PCE (%)
PR1	1:1	11.63	0.66	0.68	5.33
	1:2	13.92	0.67	0.69	6.66
	1:3	12.63	0.67	0.68	5.96
PR2	1:1	12.54	0.70	0.68	5.99
	1:2	14.67	0.69	0.70	7.14
	1:3	13.38	0.69	0.69	6.43
PR3	1:1	9.86	0.73	0.66	4.77
	1:2	12.10	0.72	0.65	5.73
	1:3	11.16	0.72	0.64	5.20

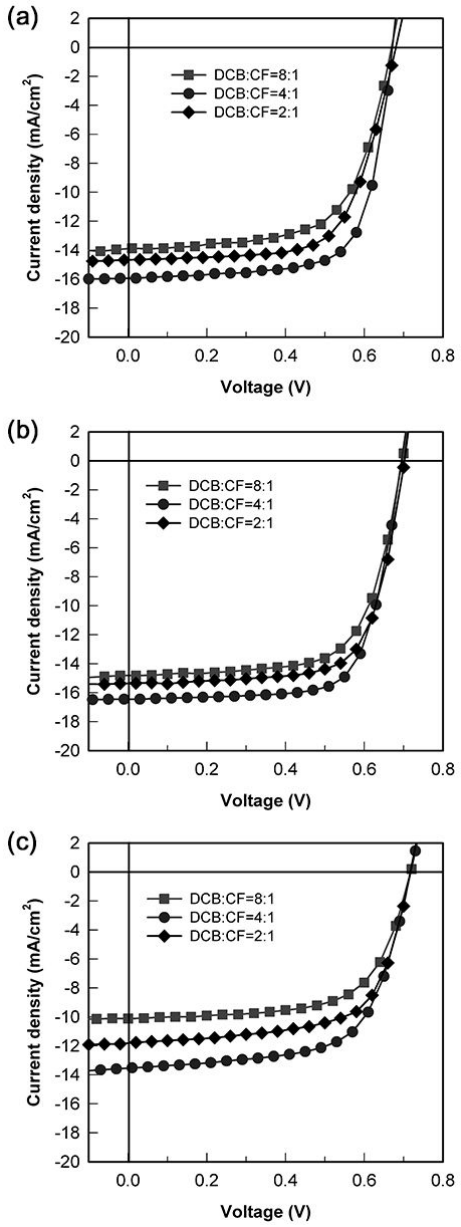

Figure 4.10. *J–V* curves of random copolymer:$PC_{71}BM$ BHJ solar cells under AM 1.5G, 100 mW/cm^2 cast from mixed solvent of DCB/CF with 2 vol% DIO.

Table 4.4. Photovoltaic properties of random copolymers under standard AM 1.5G illumination cast from mixed solvent of DCB/CF with 2 vol% DIO.

	DCB:CF (w/w)	J_{SC} (mA/cm^2)	V_{OC} (V)	FF	PCE (%)
PR1	8:1	13.88	0.67	0.65	6.18
	4:1	15.91	0.67	0.70	7.59
	2:1	14.66	0.68	0.68	6.72
PR2	8:1	14.80	0.70	0.69	7.16
	4:1	16.44	0.69	0.71	8.11
	2:1	16.28	0.70	0.70	8.03
PR3	8:1	10.22	0.73	0.67	4.93
	4:1	13.53	0.73	0.64	6.29
	2:1	11.83	0.73	0.63	5.51

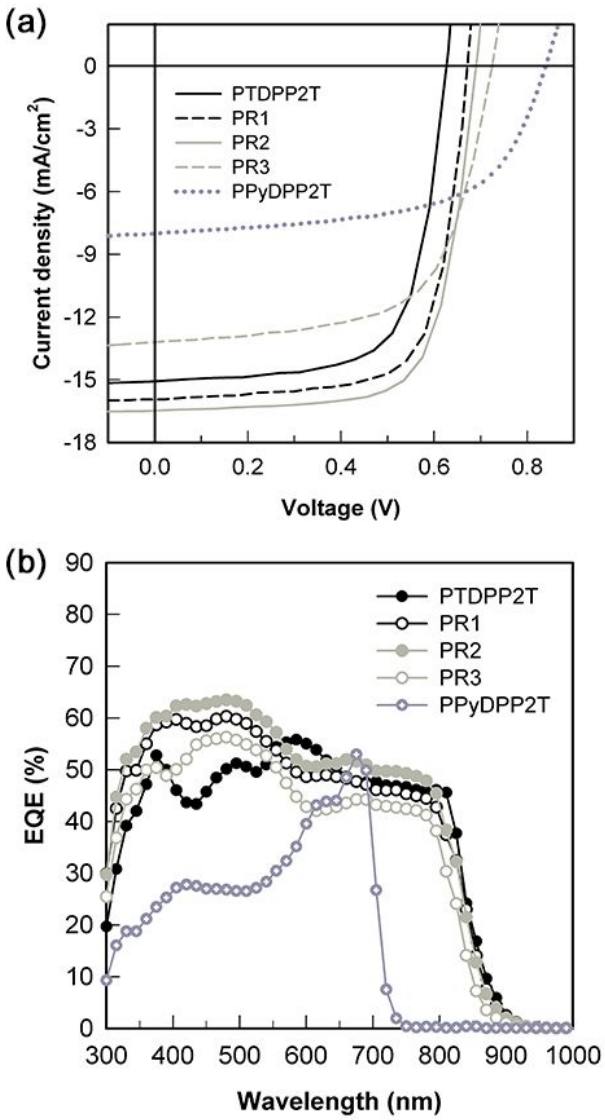

Figure 4.11. *J–V* curves of random polymer/$PC_{71}BM$ BHJ solar cells (a) and external quantum efficiency spectra of polymer/$PC_{71}BM$ solar cells (b) under optimum condition.

Table 4.5. Photovoltaic properties of PTDPP2T, PR1, PR2, PR3 and PPyDPP2T under the standard AM 1.5G illumination and charge carrier mobilities under dark condition.

Polymers	Thickness (nm)	J_{SC} (mA/cm^2)	V_{OC} (V)	FF	μ_h (cm^2/V s)[b]	PCE$_{max(ave)}$ (%)
PTDPP2T	120±5	15.05 (14.74)[a]	0.63	0.70	7.76×10^{-3}	6.70 (6.44)
PR1	120±5	15.91 (15.76)[a]	0.67	0.71	1.91×10^{-2}	7.59 (7.32)
PR2	120±5	16.44 (16.38)[a]	0.69	0.71	2.72×10^{-2}	8.11 (7.81)
PR3	115±5	13.51 (13.65)[a]	0.72	0.64	3.29×10^{-2}	6.29 (5.83)
PPyDPP2T	90±5	8.38 (7.99)[a]	0.83	0.59	4.10×10^{-4}	4.14 (3.92)

[a]Integrated from EQE data.

[b]Hole mobility in the blend of polymer:$PC_{71}BM$ as measured by SCLC method.

reference polymers (PTDPP2T and PPyDPP2T) are 6.70% and 4.14%, respectively. Here, PTDPP2T- and PPyDPP2T-based devices were optimized by following the method reported in the literatures.[164,166]

When the V_{OC}s of reference polymers and random copolymers are compared, the magnitude of V_{OC} is in the order of PTDPP2T (0.63 V) < PR1 (0.67 V) < PR2 (0.69 V) < PR3 (0.72 V) < PPyDPP2T (0.83 V). We can easily explain a correlation between PyDPP content and V_{OC} by the dependence of HOMO energy level on copolymer composition. Since V_{OC} is proportional to the difference between HOMO energy level of donor polymer and LUMO energy level of $PC_{71}BM$, the polymer with deeper HOMO energy level exhibits higher V_{OC}.

To understand the reason why J_{SC}s of PR1 (15.91 mA cm^{-2}) and PR2 (16.44 mA cm^{-2}) are higher than that of PTDPP2T (15.05 mA cm^{-2}), we measured the hole mobility of the active layer by measuring the dark J–V curve of hole-only device using the SCLC model (Figure 4.12 (a), Table 4.5). The devices made of PR1 and PR2 exhibit higher SCLC hole mobilities than PTDPP2T- based device, leading to higher J_{SC} of PR1 and PR2 than PTDPP2T. However, the PR3-based device shows the lowest J_{SC} (13.51 mA cm^{-2}) among the random copolymers, although it exhibits the highest hole mobility (3.29×10^{-2} cm^2 V^{-1} s^{-1}).

To reveal the discrepancy between hole mobility and J_{SC}, we measured crystallinity and crystal orientation of polymers and their blends with $PC_{71}BM$ by GIWAXS (Figure 4.13 and Figure 4.14). The GIWAXS shows that all pristine polymers exhibit (h00) diffraction peaks due to interchain stacking

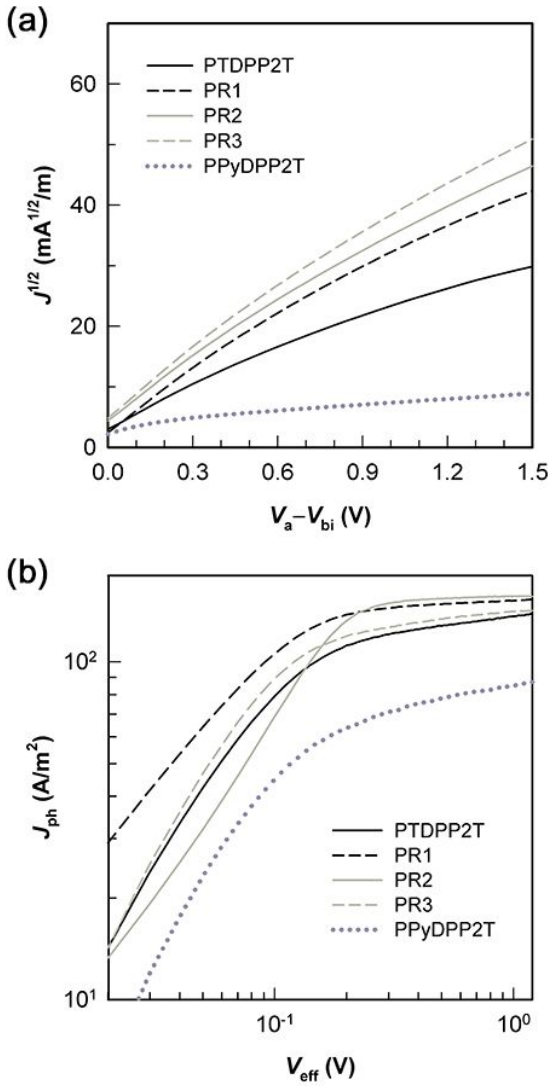

Figure 4.12. Dark *J–V* characteristics of random polymers/$PC_{71}BM$ blends with hole-only device (a) and photocurrent density (J_{ph}) plotted against effective voltage (V_{eff}) (b) under optimized condition.

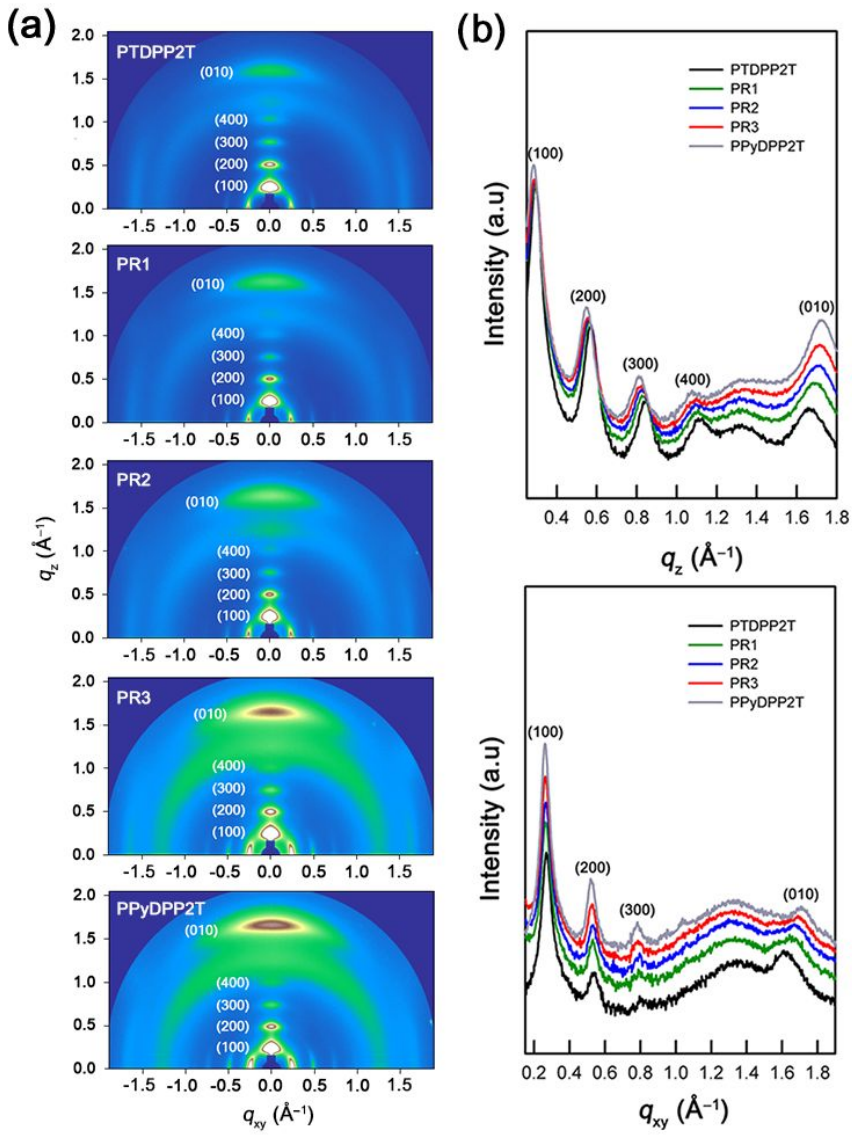

Figure 4.13. GIWAXS patterns of pristine random copolymers (a) and in-plane and out-of-plane line cuts of the corresponding GIWAXS images (b).

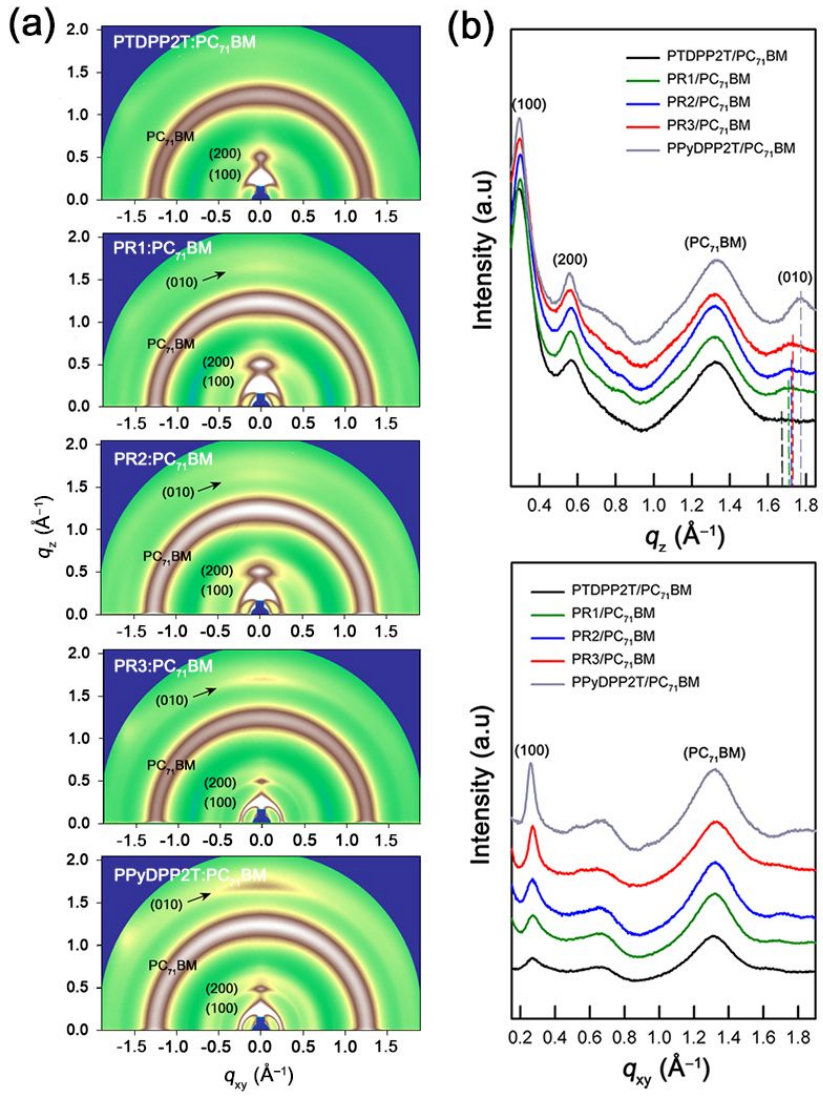

Figure 4.14. 2D-GIWAXS patterns of random copolymer/$PC_{71}BM$ blend films (a) and in-plane and out-of-plane line cuts of the corresponding GIWAXS images (b).

Table 4.6. π–π stacking parameters of pristine random copolymers and BHJ blend films in q_z direction of GIWAXS.

	Parameters	PTDPP2T	PR1	PR2	PR3	PPyDPP2T
Pristine polymer	q (Å^{-1})	1.662	1.688	1.707	1.720	1.726
	d-spacing (Å)	3.780	3.722	3.680	3.653	3.640
BHJ	q (Å^{-1})	1.663	1.702	1.719	1.730	1.778
	d-spacing (Å)	3.778	3.691	3.655	3.631	3.533

and an additional (010) diffraction peak due to π–π stacking in q_z direction (Figure 4.13). Since all pristine polymers show the (010) peak in both q_z and q_{xy} directions, all polymer crystals adopt mixed face-on and edge-on orientation on the substrate. Another important feature from GIWAXS pattern is that the intensity of (010) peak in q_z direction increases (Figure 4.13) while the π–π stacking distance decreases (Table 4.6), as the PyDPP content in random copolymer is increased.

The GIWAXS patterns of polymer:$PC_{71}BM$ blend films also show that the intensity of (010) diffraction peak increases (Figure 4) while the π–π stacking distance decreases (Table 4.14), as the PyDPP content in the copolymer is increased. The π–π stacking distances of copolymer blend films in q_z direction are shorter than those of the corresponding pristine copolymers while the distance of PTDPP2T blend film is nearly the same as that of pristine copolymer film (see Table 4.6). The shorter π–π stacking distance and preferential face-on orientation of random copolymers are the reasons why random copolymers show higher SCLC hole mobility than PTDPP2T. Particularly, the PPyDPP2T blend film shows the lowest SCLC hole mobility (4.10×10^{-4} cm^2 V^{-1} s^{-1}), although it has the strongest π–π stacking peak and the shortest π–π stacking distance (3.53 Å). This discrepancy will be explained in terms of active layer morphology as observed by transmission electron microscope (TEM).

To identify the reason for the highest J_{SC} of PR2, we calculated the G_{max} of blend films (Figure 4.12 (b)).[176] The G_{max} is estimated by plotting the photocurrent density (J_{ph}, defined as J_L–J_D, where J_L and J_D are the current

density under illumination and in the dark, respectively) as a function of effective voltage (V_{eff}, defined as V_0–V, where V_0 is the voltage where J_{Ph} is zero). Comparison of G_{max} values reveals that the G_{max} values of random copolymer-based devices (PR1=7.86×10^{27}, PR2=8.17×10^{27} and PR3=7.60×10^{27} m^{-3} s^{-1}) are higher than that of reference homopolymers (PTDPP2T=7.08×10^{27} and PPyDPP2T=5.97×10^{27} m^{-3} s^{-1}). Particularly, the PR2-based device shows the highest value. Therefore, we conclude that the highest J_{SC} of PR2 arises from the highest charge generation due to broad light absorption in range of 625–835 nm.

To explain the discrepancy between hole mobility and π–π stacking of PPyDPP2T blend, we observed the morphologies of blend films by TEM (Figure 4.15). Recently, Li *et al.*[146] have reported that the fibril width of DPP-based polymer is an important factor controlling the charge generation efficiency and that the fibril size smaller than 10 nm results in high EQE. All blend films show well-developed and interconnected network structure except for PPyDPP2T blend, while the fibril size of copolymer blend increases as the PyDPP content in copolymer is increased. Since large-sized phase separation in blends containing PR3 and PPyDPP2T may suppress the exciton dissociation at the polymer/$PC_{71}BM$ interface, the solar cell devices made of PR3 and PPyDPP2T show lower J_{SC} than the devices of PR1, PR2 and PTDPP2T. Especially, the PPyDPP2T blend shows the largest and disconnected polymer domains, and therefore the device exhibits the lowest SCLC hole mobility and thus the lowest J_{SC}, although the GIWAXS of PPyDPP2T shows the strongest π–π stacking peak and the shortest π–π

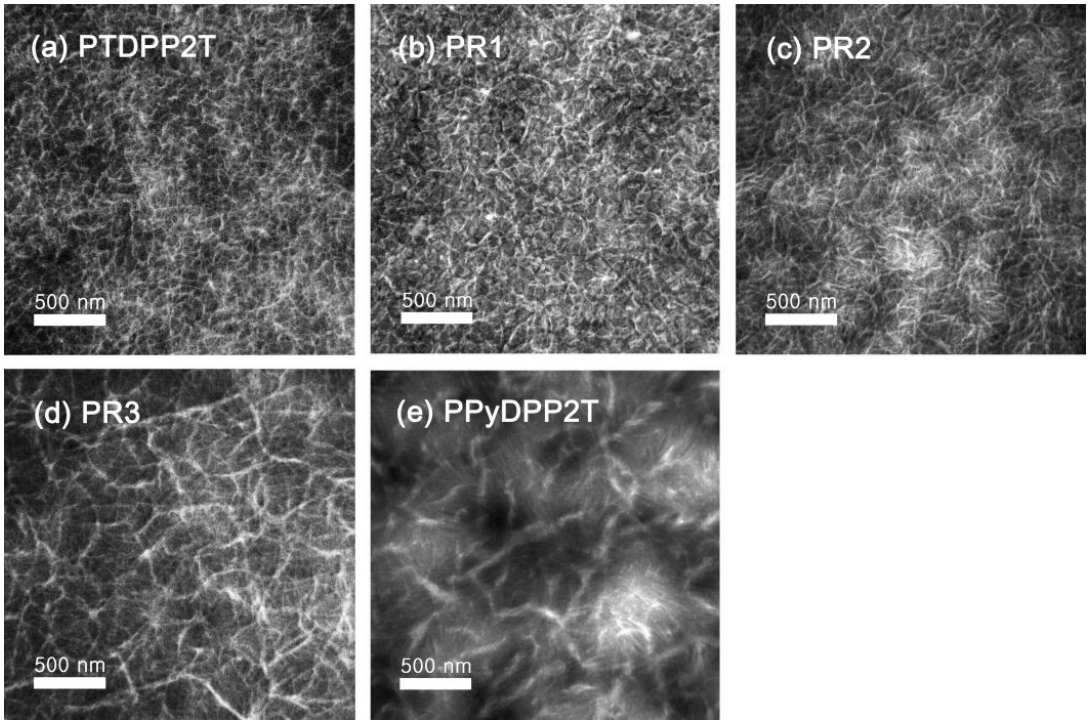

Figure 4.15. TEM images of random copolymer/$PC_{71}BM$ blend films under optimized condition.

stacking distance.[180]

4.4 Summary

Random copolymers composed of one electron donating unit and two electron accepting units have been recognized as a promising donor material in organic photovoltaics, because the two electron accepting units may show synergetic effect on the solar cell performance. TDPP and PyDPP have recently attracted great interest as an electron accepting unit for conjugated semi-conducting polymers: A low bandgap polymer (PTDPP2T) composed of TDPP and bithiophene (2T) shows high J_{SC} due to low bandgap, while the polymer composed of PyDPP and 2T exhibits V_{OC} due to its low-lying HOMO energy level. In this work, a new series of conjugated random copolymer was synthesized by copolymerization of 2T as an electron donating unit with TDPP and PyDPP as co-electron accepting unit. The V_{OC} of the random copolymer can systematically be controlled by varying the ratio of PyDPP to TDPP: The V_{OC} was increased with increasing the PyDPP content in the random copolymer was increased. Consequently, the solar cell device based on the random copolymer shows a promising power conversion efficiency of 8.11%, which is higher than that of the reference polymer, PTDPP2T (6.70%).

Chapter 5. Conclusions

During the last decade, significant progress has been made in improving the PCE of PSCs. These days a single junction BHJ PSC with a PCE over 10% is listed in the efficiency table of the Journal Progress in Photovoltaics. However, prior to commercialization with large scale and competition with state of the art inorganic PV technologies, further improvements especially in PCE are required. One of directions to enhance in PCE of PSCs is to improve the light absorption ability of the active layer through molecular design of polymers and introduction of third component such as ternary blends.

In this study, we tried to design and synthesize new conjugated polymer which shows efficient light absorption. We also investigated the photovoltaic properties of the synthesized polymers in terms of the absorption ability, molecular energy level and molecular orientation. First we synthesized a new electron-donating unit, BC, by introducing an oxygen atom into fluorene, for the purpose to reduce the bandgap of the conjugated polymer, since the fluorene-based polymers show relatively low J_{SC}s due to large bandgaps. The bandgaps of BC-based polymers, PBCDTBT (1.77 eV) and PBCDPP2T (1.64 eV), are lower than those of fluorene-based counterparts, PFDTBT (1.81 eV) and PFDPP2T (1.73 eV), respectively, by raising the HOMO energy level, due to the introduction of the electronegative oxygen atom into fluorene.

Secondly, ternary blends composed of two organic donors (PTDPP2T and $(TDPP)_2Ph$) and one acceptor ($PC_{71}BM$) was prepared for the active layer for

the purpose to enhance the J_{SC} without V_{OC} sacrifice. The device made of a ternary blend with 10 wt% $(TDPP)_2Ph$ exhibit an enhanced J_{SC} of 16.16 mA cm^{-2} relative to that of binary system of PTDPP2T:$PC_{71}BM$ (14.91 mA cm^{-2}). The enhancement of J_{SC} is mainly attributed to complementary absorption of two donors, considering that the absorption range of $(TDPP)_2Ph$ and PTDPP2T are 550–700 nm and 670–840 nm, respectively. However, the J_{SC} decreases when the amount of $(TDPP)_2Ph$ exceeds 10 wt% since high concentration of $(TDPP)_2Ph$ (>10 wt%) is phase-separated with large domain size.

Finally, for enhancing both J_{SC} and V_{OC} we synthesized random conjugated copolymers with two different accepting units (TDPP and PyDPP) to achieve panchromatic light absorption. Utilizing the random copolymer strategy, we successfully controlled the light absorption range, the frontier molecular orbital energy levels and the crystallinity of polymer by varying the copolymer composition. The random copolymer (PR2) shows broader absorption range (625–835 nm) and deeper HOMO energy level (–5.30 eV) than the corresponding homopolymer (PTDPP2T) (670–840 nm, –5.20 eV), which are beneficial to achieving high J_{SC} and high V_{OC}

In conclusion, electrochemical and photovoltaic properties of conjugated polymer are significantly influenced by chemical modification of the polymers. Especially, we can lower the bandgap of the polymer by introducing oxygen atom, which results in improvement of absorption ability. Also ternary blend is another promising approach to extend the absorption spectrum by third component. Here, we clearly demonstrate that the

morphology and compatibility of ternary blends as well as absorption ability are important factors to achieve high J_{SC}. Compared to D–A type alternating copolymers, from the random copolymer strategy, light absorption, HOMO/LUMO energy levels and crystallinity of the polymers can be controlled by the introduction of the third monomer, resulting in enhancement of both J_{SC} and V_{OC}. From these results, it can be concluded that design and synthesis of conjugated polymer with effective absorption plays a key role for high performance polymer solar cells.

Bibliography

(1) Tao, C. S.; Jiang, J.; Tao, M. *ECS Transactions.* **2011**, *33*, 3.

(2) U.S. Department of Energy, Basic Research Needs for Solar Energy Utilization **2005**

(3) Kazmerski, L. *Renew. Sust. Energ. Rev.* **1997**, *1*, 71.

(4) Alsema E. *Renew. Sust. Energ. Rev.* **1998**, *2*, 387.

(5) Chapin, D. M.; Fuller, C. S.; Pearson, G. L. *J. Appl. Phys.* **1954**, *25*, 676.

(6) Bergmann, R. B. *Appl. Phys. A,* **1999**, *69*, 187.

(7) Green, M. A. *Prog. Photovolt: Res. Appl.* **2009**, *17*, 183.

(8) Green, M. A.; Emery, K.; Hishikawa, Y.; Warta, W.; Dunlop, E. D. *Prog. Photovolt: Res. Appl.* **2015**, *23*, 805.

(9) Maennig, B.; Drechsel, J.; Gebeyehu, D.; Simon, P.; Kozlowski, F.; Werner, A.; Li, F.; Grundmann, S.; Sonntag, S.; Koch, M.; Leo, K.; Pfeiffer, M.; Hoppe, H.; Meissner, D.; Sariciftci, N. S.; Riedel, I.; Dyakonov, V.; Parisi. J. *Appl. Phys. A* **2004**, *79*, 1.

(10) Wang, J.-C.; Weng, W.-T.; Tsai, M.-Y.; Lee, M.-K.; Horng, S.-F.; Perng, T.-P.; Kei, C.-C.; Yuc, C.-C.; Meng, H.-F. *J. Mater. Chem.* **2010**, *20*, 862.

(11) Yin, Z.; Sun, S.; Salim, T.; Wu, S.; Huang, X.; He, Q.; Lam, Ming. Y.; Zhang, H. *ACS nano.* **2010**, *4*, 5263.

(12) Helgesen, M.; Søndergaard, R.; Krebs, F. C. *J. Mater. Chem.* **2010**, *20*, 36.

(13) da Silva, W. J.; Kim, H. P.; bin Mohd Yusoff, A. R.; Jang, J. *Nanoscale* **2013**, *5*, 9324.

(14) Søndergaard, R. R.; Hösel, M.; Krebs, F. C. *J. Polym. Sci. Part B: Polym. Phys.* **2013**, *51*, 16.

(15) Yim, J. H.; Joe, S.-y.; Pang, C.; Lee, K. M.; Jeong, H.; Park, J.-Y.; Ahn, Y. H.; de Mello, J. C. Lee, S. *ACS nano.* **2014**, *8*, 2857.

(16) Espinosa, N.; Hösel, M.; Jørgensen, M.; Krebs, F. C. *Energy Environ. Sci.* **2014**, *7*, 855.

(17) Zhao, B.; He, Z.; Cheng, X.; Qin, D.; Yun, M.; Wang, M.; Xiaodong, H.; Wu, J.; Wu, H.; Cao, Y. *J. Mater. Chem. C* **2014**, *2*, 5077.

(18) Helgesen, M.; Carlé, J. E.; dos Reis Benatto, G. A.; Søndergaard, R. R.; Jørgensen, M.; Bundgaard, E.; Krebs, F. C. *Adv. Energy Mater.* **2015***,* DOI: 10.1002/aenm.201401996.

(19) Angmo, D.; Andersen, T. R.; Bentzen, J. J.; Helgesen, M.; Søndergaard, R. R.; Jørgensen, M.; Carlé, J. E.; Bundgaard, E.; Krebs, F. C. *Adv. Funct. Mater.* **2015**, *25*, 4539.

(20) Kim, T.; Kim, J.-H.; Kang, T. E.; Lee, C.; Kang, H.; Shin, M.; Wang, C.; Ma, B.; Jeong, U.; Kim, T.-S.; Kim, B.J. *Nat. Commun.* **2015***, 6*, 8547.

(21) Peumans, P.; Forrest, S. R. *Chem. Phys. Lett.* **2004**, *398*, 27.

(22) Veenstra, S. C.; Loos, J.; Kroon, J. M. *Prog. Photovolt: Res. Appl.* **2007**, *15*, 727.

(23) Tang, C. W. *Appl. Phys. Lett.* **1986**, *48*, 183.

(24) Antohe, S.; Tugulea, L. *phys. stat. sol. (a)* **1991**, *128*, 253.

(25) Sariciftci, N. D.; Braun, D.; Zhang, C.; Srdanov, V. I.; Heeger, A. J.; Stucky, G.; Wudl, F. *Appl. Phys. Lett.* **1993**, *62*, 585.

(26) Halls, J. M.; Pichler, K.; Friend, R. H.; Moratti, S. C.; Holmes, A. B. *Appl. Phys. Lett.* **1996**, *68*, 3120.

(27) Peumans, P.; Yakimov, A.; Forrest, S. R. *J. Appl. Phys.* **2003**, *93*, 3693.

(28) Yu, G.; Gao, J.; Hummelen, J. C.; Wudl, F.; Heeger, A. J. *Science* **1995**, *270*, 1789.

(29) Halls, J. J. M.; Walsh, C. A.; Greenham, N. C.; Marseglia, E. A.; Friend, R. H.; Moratti, S. C.; Holmes, A. B. *Nature* **1995**, *376*, 498.

(30) Granström, M.; Petritsch, K.; Arias, A. C.; Lux, A.; Andersson, M. R.; Friend, R. H. *Nature* **1998**, *395*, 257.

(31) Nguyen, T. L.; Choi, H.; Ko, S.-J.; Uddin, M. A.; Walker, B.; Yum, S.; Jeong, J.-E.; Yun, M. H.; Shin, T. J.; Hwang, S.; Kim, J. Y.; Woo, H. Y. *Energy Environ. Sci.* **2014**, *7*, 3040.

(32) Liu, Y.; Zhao, J.; Li, Z.; Mu, C.; Ma, W.; Hu, H.; Jiang, K.; Lin, H.; Ade, H.; Yan, H. *Nat. Commun.* **2014**, *5*, 5293.

(33) Zhang, M.; Guo, X.; Ma, W.; Ade, H.; Hou, J. *Adv. Mater.* **2015**, 27, 4655.

(34) Liu, C.; Yi, C.; Wang, K.; Yang, Y.; Bhatta, R. S.; Tsige, M.; Xiao, S.; Gong, X. *ACS Appl. Mater. Interfaces* **2015**, *7*, 4928.

(35) Subbiah, J.; Purushothaman, B.; Chen, M.; Qin, T.; Gao, M.; Vak, D.; Scholes, F. H.; Chen, X.; Watkins, S. E.; Wilson, G. J.; Holmes, A. B.; Wong, W. W. H.; Jones, D. J. *Adv. Mater.* **2015**, *27*, 702.

(36) Huo, L.; Liu, T.; Sun, X.; Cai, Y.; Heeger, A. J.; Sun, Y. *Adv. Mater.* **2015**, 27, 2938.

(37) Chen, J.-D.; Cui, C.; Li, Y.-Q.; Zhou, L.; Ou, Q.-D.; Li, C.; Li, Y.; Tang, J.-X. *Adv. Mater.* **2015**, 27, 1035.

(38) Kim, J.-H.; Park, J. B.; Jung, I. H.; Grimsdale, A. C.; Yoon, S. C.; Yang, H.; Hwang, D.-H. *Energy Environ. Sci.* **2015**, *8*, 2352.

(39) Jo, J. W.; Jung, J. W.; Jung, E. H.; Ahn, H.; Shin, T. J.; Jo, W. H. *Energy Environ. Sci.* **2015**, *8*, 2427.

(40) Vohra, V.; Kawashima, K.; Kakara, T.; Koganezawa, T.; Osaka, I.; Takimiya, K.; Murata, H. *Nat. Photonics* **2015**, *9*, 403

(41) Zhang, S.; Ye, L.; Zhao, W.; Yang, B.; Wang, Q.; Hou, J. *Sci. China Chem.* **2015**, *58*, 248.

(42) Brabec, C. J.; Sariciftci, N. S.; . Hummelen, J. C. *Adv. Funct. Mater.* **2001**, 11, 15.

(43) Savenije, T. J.; Warman J. M.; Goossens, A. *Chem. Phys. Lett*. **1998**, 287, 148.

(44) Haugeneder, A.; Neges, M.; Kallinger, C.; Spirkl, W.; Lemmer, U.; Feldmann, J. *Pys. Rev. B*. **1999**, 59, 15346.

(45) Theander, M.; Yartsev, A.; Zigmantas, D.; Sundström, V.; Mammo, W.; Andersson, M. R.; Inganäs, O. *Pys. Rev. B*. **2000**, 61, 12957.

(46) Spanggaard, H.; Krebs, F. C. *Sol. Energy Mater. Sol. Cells* **2004**, *83*, 125.

(47) Nalwa, H. S. Handbook of organic conductive molecules and polymers **1997**, Wiley, New York.

(48) Skotheim, T. A.; Reynolds, J. R. *Handbook of conjugated polymers* **1998**, Taylor & Francis group, Abingdon.

(49) Brabec, C. J.; Shaheen, S. E.; Winder, C.; Sariiftci, N. S.; Denk, P. *Appl. Phys. Lett.* **2002**, *80*, 1288.

(50) Kim, J. Y.; Kim, S. H.; Lee, H.-H.; Lee, K.; Ma, W.; Gong, X.; Heeger, A. J.; *Adv. Mater.* **2006**, *18*, 572.

(51) Rostalski, J.; Meissner, D. *Sol. Energy Mater. Sol. Cells* **2000**, *61*, 87.

(52) Nicholson, P. G.; Castro, F. A. *Nanotechnology* **2010**, *21*, 492001.

(53) Shaheen, S. E.; Brabec, C. J.; Sariciftci, N. S.; Padinger, F.;Fromherz, T.; Hummelen, J. C. *Appl. Phys. Lett.* **2001**, *78*, 841.

(54) Wienk, M. M.; Kroon, J. M.; Verhees, W. J. H.; Knol, J.; Hummelen, J. C.; van Hal, P. A.; Janssen R. A. J. *Angew. Chem. Int. Ed.* **2003**, *42*, 3371.

(55) Padinger, F.; Rittberger, R. S.; Sariciftci, N. S. *Adv. Fucnt. Mater.* **2003**, *13*, 85.

(56) Roncali, J. *Macromol. Rapid Commun.* **2007**, *28*, 1761.

(57) Kim, J. Y.; Kim, S. H.; Lee, H.-H.; Lee, K.; Ma, W.; Gong, X.; Heeger, A. J. *Adv. Mater.* **2006**, 1*8*, 572.

(58) Ma. W.; Yang, C.; Gong, X.; Lee, K.; Heeger, A. J. *Adv. Fucnt. Mater.* **2005**, *15*, 1617.

(59) Kim, Y.; Cook, S.; Tuladhar, S. M.; Choulis, S. A.; Nelson, J.; Durrant, J. R.; Bradley, D. D. C.; Giles, M.; Mcculloch, I.; Ha, C.-S.; Ree, M. *Nat. Mater.* **2006**, *5*, 197.

(60) Svensson, M.; Zhang, F.; Veenstra, S. C.; Verhees, W. J. H.;

Hummelen, J. C.; Kroon, J. M.; Inganäs, O.; Andersson, M. R. *Adv. Mater.* **2003**, *15*, 988.

(61) Yamaguchi, J.; Yaginuma, S.; Haemori, M.; Itaka, K.; Koinuma, H. *Jpn. J. Appl. Phys.* **2005**, *44*, 3757.

(62) Anthopoulos, T. D.; Singh, B.; Marjanovic, N.; Sariciftci, N. S.; Ramil, A. M.; Sitter, H.; Cölle, M.; de Leeuw, D. M. *Appl. Phys. Lett.* **2006**, *89*, 213504.

(63) Zhang, X.-H.; Domercq, B.; Kippelen, B. *Appl. Phys. Lett.* **2007**, *91*, 092114.

(64) Kitamura, M.; Kuzumoto, Y.; Kamura, M.; Aomori, S.; Arakawa, Y. *Appl. Phys. Lett.* **2007**, *91*, 183514.

(65) Johnson, R. D.; Meijer, G.; Bethune, D. S. *J. Am.Chem. Soc.* **1990**, *112*, 8983.

(66) Johnson, R. D.; Bethune, D. S.; Yannoni, C. S. *Acc. Chem. Res.* **1992**, *25*, 169.

(67) He, Y.; Li, Y. *Phys. Chem. Chem. Phys.* **2011**, *13*, 1970.

(68) Zhao, G.; He, Y.; Li, Y. *Adv. Mater.* **2010**, *22*, 4355.

(69) Guo, X, Cui, C.; Zhang, M.; Huo, L.; Huang, Y.; Hou, J.; Li, Y. *Energy Environ. Sci.* **2012**, *5*, 7943.

(70) Günes, S.; Neugebauer, H.; Sariciftci, N. S. *Chem.Rev.* **2007**, *107*, 1324.

(71) Chochos, C. L.; Choulis, S. A. *Prog. Photovolt: Res. Appl.* **2011**, *36*, 1326.

(72) Uy, R. L.; Price, S. C.; You, W. *Macromol. Rapid Commun.* **2012**,

33, 1162.

(73) Maurano, A.; Hamilton, R.; Shuttle, C. G.; Ballantyne, A. M.; Nelson, J.; O'Regan, B.; Zhang, W.; McCulloch, I.; Azimi, H.; Morana, M.; Brabec, C. J.; Durrant, J. R. *Adv. Mater.* **2010**, *22,* 4987.

(74) Li, Y. *Acc. Chem. Res.* **2012**, *45,* 723.

(75) Faist, M. A.; Kirchartz, T.; Gong, W.; Ashraf, R. S.; McCulloch, I.; de Mello, J. C.; Ekins-Daukes, N. J.; Bradley, D. D. C.; Nelson, J. *J. Am.Chem. Soc.* **2012**, *134*, 685.

(76) Bundgaard, E.; Krebs, F. C. *Sol. Energy Mater. Sol. Cells* **2007**, *91*, 954.

(77) Blog.Sunspotter.org.

(78) Shoaee, S.; Clarke, T. M.; Huang, C.; Barlow, S.; Marder, S. R.; Heeney, M.; McCulloch, I.; Durrant, J. R. *J. Am. Chem. Soc.* **2012**, *132*, 12919.

(79) Lee, Y. and Jo, W. H. *J. Phys. Chem. C* **2012**, *116*, 8379.

(80) Veldman, D.; Meskers, S. C. J.; Janssen, R. A. J. *Adv. Fucnt. Mater.* **2009**, *19*, 1939.

(81) Dennler, G.; Scharber, M.; Brabec, C. J. *Adv. Fucnt. Mater.* **2009**, *21*, 1323.

(82) Jen, K.-Yue.; Maxfield, M.; Shacklette, L. W.; Elsenbaumer, R. L. *Chem. Soc., Chem. Commun.* **1987**, *28*, 309.

(83) Roncali, J.; Thobie-Gautier, C. *Adv. Mater.* **1994**, *6*, 846.

(84) Zheng, Q.; Jung, B. J.; Sun, J.; Katz, H. E. *J. Am. Chem. Soc.* **2010**, *132*, 5394.

(85) Cheng, Y.-J.; Chen, C.-H.; Lin, Y.-S.; Chang, C.-Y.; Hsu, C.-S. *J. Chem. Mater.* **2011**, *23*, 5068.

(86) Zhang, M.; Guo, X.; Ma, W.; Ade, H.; Hou, J. *Adv. Mater.* **2014**, *26*, 5880.

(87) Aoyama, Y.; Yamanari, T.; Murakami, T. N.; Nagamori, T.; Marumoto, K.; Tachikawa, H.; Mizukado, J.; Suda, H.; Yoshida, Y. *Polym. J.* **2015**, *47*, 26.

(88) Bijleveld, J. C., Zoombelt, A. P.; Mathijssen, S. G. J.; Wienk, M. M.; Turbiez, M.; de Leeuw, D. M.; Janssen, R. A. J. *J. Am. Chem. Soc.* **2009**, *131*, 16616.

(89) Wang, E.; Ma, Z.; Zhang, Z.; Henriksson, P.; Inganäs, O, Zhang, F.; Andersson, M. R. *Chem. Commun.* **2011**, *47*, 4908.

(90) Bijleveld, J. C.; Verstrijden, R. A. M.; Wienk, M. M.; Janssen, R. A. *J. Mater. Chem.* **2011**, *21*, 9224.

(91) Pearson, A. J.; Watters, D. C.; Hunan Yi, Sarjadi, M. S.; Reynolds, L. X.; Marchisio, P. P.; Kingsley, J.; Haque, S. A.; Iraqi, A.; Lidzey, D. G. *RSC Adv.* **2014**, *4*, 43142.

(92) Bijleveld, J. C.; Gevaerts, V. S.; Nuzzo, D. D.; Turbiez, M.; Mathijssen, S. G. J.; de Leeuw, D. M.; Wienk, M. M.; Janssen, R. A. J. *J. Am. Chem. Soc.* **2010**, *22*, E242.

(93) Li, W.; Furlan, A.; Roelofs, W. S. C.; Hendriks, K. H.; van Pruissen, G. W. P.; Wienk, M. M.; Janssen, R. A. J. *Chem. Commun.* **2014**, *50*, 679.

(94) Sonar, P.; Singh, S. P.; Li, Y.; Ooi, Z.-E.; Ha, T., Wong, I.; Soh, M.

S.; Dodabalapur, A. *Energy Environ. Sci.* **2011**, *4*, 2288.

(95) Watters, D. C.; Yi, H.; Pearson, A. J.; Kingsley, J.; Iraqi, A.; Lidzey, D. *Macromol. Rapid Commun.* **2013**, *34*, 1157.

(96) Jo, J. W.; Kim, S. S.; Jo, W. H. *Org. Electron.* **2012**, *13*, 1322.

(97) Lee, Y.; Nam, Y. M.; Jo, W. H. *J. Mater. Chem.* **2011**, *21*, 8583.

(98) Zhang, Y.; Zou, J.; Cheuh, C.-C.; Yip, H.-L.; Jen, A. K.-Y. *Macromolecules.* **2012**, *45*, 5427.

(99) Li, Y.; Zou, J.; Yip, H.-L.; Li, C.-Z.; Zhang, Y.; Chueh, C.-C.; Intemann J.; Xu, Y.; Liang, P.-W.; Chen, Y.; Jen, A. K.-Y. *Macromolecules.* **2013**, *46*, 5497.

(100) Liang, Y.; Feng, D.; Wu, Y.; Tsai, S.-T.; Li, G.; Ray, C.; Yu, L. *J. Am. Chem. Soc.* **2009**, *131*, 7792.

(101) Huo, L.; Hou, J. *Pol. Chem.* **2011**, *2*, 2453.

(102) Ye, L.; Zhang, S.; Huo, L.; Zhang, M.; Hou, J. *Acc. Chem. Res.* **2014**, *47*, 1595.

(103) Chen, K.-S.; Zhang, Y.; Yip, H.-L.; Sun, Y.; Davies, J. A.; Ting, C.; Chen, C.-P.; Jen, A. K.-Y. *Org. Electron.* **2011**, *12*, 794.

(104) Zhang, Y.; Zou, J.; Yip, H.-L.; Chen, K.-S.; Zeigler, D. F.; Sun, Y.; Jen, A. K.-Y. *Chem. Mater.* **2011**, *23*, 2289.

(105) Mcculloch, I.; Ashraf, R. S.; Biniek, L.; Bronstein, H.; Combe, C.; Donaghey, J. E.; James, D. I.; Nielsen, C. B.; Schroeder, B. C.; Zhang, W. *Acc. Chem. Res.* **2012**, *45*, 714.

(106) Liang, Y.; Xu, Z.; Xia, J.; Tsai, S.-T.; Wu, Y.; Li, G.; Ray, C.; Yu, L. *Adv. Mater.* **2010**, *22*, E135.

(107) Son, H. J.; Lu, L.; Chen, W.; Xu, T.; Zheng, T.; Carsten, B.; Strzalka, J.; Darling, S. B.; Chen, L. X.; Yu, L. *Adv. Mater*. **2013**, *25*, 838.

(108) Zhang, M.; Guo, X.; Zhang, S.; Hou, J. *Adv. Mater.* **2014**, *26*, 1118.

(109) Yingping, Z.; Najari, A.; Berrouard, P.; Beaupré, S.; Aïch, B. R.; Tao, Y.; Leclerc, M. *J. Am. Chem. Soc.* **2010**, *132*, 5330.

(110) Su, M.-S.; Kuo, C.-Y.; Yuan, M.-C.; Jeng, U.-S.; Su, C.-J.; Wei, K.-H. *Adv. Mater*. **2011**, *23*, 3315.

(111) Small, C. E.; Chen, S.; Subbiah, J.; Amb, C. M.; Tsang, S.-W.; Lai, T.-H.; Reynolds, J. R.; So, F. *Nat. Photonics* **2012**, *6*, 115.

(112) Wang, E.; Ma, Z.; Zhang, Z.; Vandewal, K.; Henriksson, P.; Inganäs, O.; Zhang, F.; Andersson, M. R. *J. Am. Chem. Soc.* **2011**, *133*, 14244.

(113) Deng, Y.; Liu, J.; Wang, J.; Liu, L.; Li, W.; Tian, H.; Zhang, X.; Xie, Z.; Geng, Y.; Wang, F. *Adv. Mater*. **2014**, *26*, 471.

(114) Ho, C.-C.; Chen, C.-A.; Chang, C.-Y.; Darling, S. B.; Su, W.-F. *J. Mater. Chem. A* **2014**, *2*, 8026.

(115) Kitazawa, D.; Watanabe, N.; Yamamoto, S.; Tsukamoto, J. *Appl. Phys. Lett.* **2009**, *95*, 053701.

(116) Kim, Y.; Yeom, H. R.; Kim, J. Y.; Yang, C. *Energy Environ. Sci.* **2013**, *6*, 1909.

(117) Reichenbächer, K.; Süss, H. I.; Hulliger, J. *Chem. Soc. Rev.* **2005**, *34*, 22.

(118) Wang, Y.; Parkin, S. R.; Gierschner, J.; Watson, M. D *Org. Lett.* **2008**, *10*, 3307.

(119) Jo, J. W.; Bae, S.; Liu, F.; Russell, T. P.; Jo, W. H. *Adv. Funct.*

Mater. **2015**, *25*, 120.

(120) Dou, L.; Chen, C.-C.; Yoshimura, K.; Ohya, K.; Chang, W.-H.; Gao, J.; Liu, Y.; Richard, E.; Yang, Y. *Macromolecules.* **2013**, *46*, 3384.

(121) Ameri, T.; Li, N.; Brabec, C. J. *Energy Environ. Sci.* **2013**, *6*, 2390.

(122) Li, W.; Furlan, A.; Hendriks, K. H.; Wienk, M. M.; Janssen, R. A. J. *J. Am. Chem. Soc.* **2013**, *135*, 5529.

(123) bin Mohd Yusoff, A. R.; Kim, D.; Kim, H. P.; Shneider, F. K.; da Silva, W. J.; Jang, J. *Energy Environ. Sci*. **2015**, *8*, 303.

(124) Chen, C.-C.; Chang, W.-H.; Yoshimura, K.; Ohya, K.; You, J.; Gao, J.; Hong, Z.; Yang, Y. *Adv. Mater.* **2014**, *26*, 5670.

(125) Ameri, T.; Khoram, P.; Min, J.; Brabec, C. J. *Adv. Mater.* **2013**, *25*, 4245.

(126) Huang, J.-S.; Goh, T.; Li, X.; Sfeir, M. Y.; Bielinski, E. A.; Tomasulo, S.; Lee, M. L.; Hazari, N.; Taylor, A. *Nat. Photonics* **2013**, *7*, 479.

(127) An, Q.; Zhang, F.; Li, L.; Wang, J.; Zhang, J.; Zhou, L.; Tang, W. *ACS Appl. Mater. Interfaces* **2014**, *6*, 6537.

(128) Kokil, A.; Poe, A. M.; Bae, Y.; Della Pelle, A. M.; Homnick, P. J.; Lahti, P. M.; Kumar, J.; Thayumanavan, S. *ACS Appl. Mater. Interfaces* **2014**, *6*, 9920.

(129) An, Q.; Zhang, F.; Li, L.; Wang, J.; Sun, Q.; Zhang, J.; Tang, W.; Deng, Z. *ACS Appl. Mater. Interfaces* **2015**, *7*, 3691.

(130) Koppe, M.; Egelhaaf, H.-J.; Dennler, G.; Scharber, M. C.; Brabec, C. J.; Schilinsky, P.; Hoth, C. N. *Adv. Funct. Mater.* **2010**, *20*, 338.

(131) Kang, H.; Kim, K.-H.; Kang, T. E.; Cho, C.-H.; Park, S.; Yoon, S. C.; Kim, B. J. *ACS Appl. Mater. Interfaces* **2013**, *5*, 4401.

(132) Khlyabich, P. P.; Burkhart, B.; Thompson, B. C. *J. Am. Chem. Soc.* **2011**, *133*, 14534.

(133) Yang, L.; Zhou, H.; Price, S. C.; You, W. *J. Am. Chem. Soc.* **2012**, *134*, 5432.

(134) Lu, L.; Xu, T.; Chen, W.; Landry, E. S.; Yu, L. *Nat. Photonics* **2014**, *8*, 716.

(135) Zhang, Y.; Deng, D.; Lu, K.; Zhang, J.; Xia, B.; Zhao, Y.; Fang, J.; Wei, Z. *Adv. Mater.* **2015**, *27*, 1071.

(136) Lu, L.; Chen, W.; Xu, T.; Yu, L. *Nat. Commun.* **2015**, *6*, 7327.

(137) Yang, Y.; Chen, W.; Dou, L.; Chang, W.-H.; Duan, H.-S.; Bob, B.; Li, G.; Yang, Y. *Nat. Photonics* **2015**, *9*, 190.

(138) Yao, K.; Xu, Y.-X.; Li, F.; Wang, X.; Zhou, L. *Adv. Optical Mater.* **2015**, *3*, 321.

(139) Liu, S.; You, P.; Li, J.; Li, J.; Lee, C.-S.; Ong, B. S.; Surya, C.; Yan, F. *Energy Environ. Sci.* **2015**, *8*, 1463.

(140) Zhang, J.; Zhang, Y.; Fang, J.; Lu, K.; Wang, Z.; Ma, W.; Wei, Z. *J. Am. Chem. Soc.* **2015**, *137*, 8176.

(141) An, Q.; Zhang, F.; Zhang, J.; Tang, W.; Deng, Z.; Hu, B. *Energy Environ. Sci.* **2015**, DOI: 10.1039/C5EE02641E.

(142) Jung, J. W.; Liu, F.; Russell, T. P.; Jo, W. H. *Energy Environ. Sci.* **2013**, *6*, 3301.

(143) Jiang, J.-M.; Chen, H.-C.; Lin, H.-K.; Yu, C.-M.; Lan, S.-C.; Liu, C.-

M.; Wei, K.-H. *Polym. Chem.* **2013**, *4*, 5321.

(144) Zhang, M.; Wu, F.; Cao, Z.; Shen, T.; Chen, H.; Li, X.; Tan, S. *Polym. Chem.* **2014**, *5*, 4054.

(145) Chao, Y.-H.; Jheng, J.-F.; Wu, J.-S.; Wu, K.-Y.; Peng, H.-H.; Tsai, M.-C.; Wang, C.-L.; Hsiao, Y.-N.; Wang, C.-L.; Lin, C.-Y.; Hsu, C.-S. *Adv. Mater.* **2014**, *26*, 5205.

(146) Shen, P.; Bin, H.; Xiao, L.; Li, Y. *Macromolecules* **2013**, *46*, 9575.

(147) Hou, R.; Zhao, B.; Wu, F.; Wang, G.; Shen, T.; Guo, H.; Zhang, J.; Chen, H.; Tan, S. *Org. Electron.* **2015**, *20*, 142.

(148) Wang, L.; Shi, S.; Ma, D.; Chen, S.; Gao, C.; Wang, M.; Shi, K.; Li, Y.; Li, X.; Wang, H. *Macromolecules* **2015**, *48*, 287.

(149) Fan, Q.; Liu, Y.; Xiao, M.; Su, W.; Gao, H.; Chen, J.; Tan, H.; Wang, Y.; Yang, R.; Zhu, W. *J. Mater. Chem. C* **2015**, *3*, 6240.

(150) Tamilavan, V.; Roh, K. H.; Agneeswari, R.; Lee, D. Y.; Cho, S.; Jin, Y.; Park, S. H.; Hyun, M. H. *J. Mater. Chem. A* **2014**, *2*, 20126.

(151) Kuznetsov, I. E.; Akkuratow, A. V.; Susarova, D. K.; Anokhin, D. V.; Moskvin, Y. L.; Kluyev, M. V.; Peregudov, A. S.; Troshin, P. A. *Chem. Commun.* **2015**, *51*, 7562.

(152) Li, H.; Liu, F.; Wang, X.; Gu, C.; Wang, P.; Fu, H. *Macromolecules* **2013**, *46*, 9211.

(153) Kim, K.-H.; Park, S.; Yu, H.; Kang, H.; Song, I.; Oh, J. H.; Kim, B. J. *Chem. Mater.* **2014**, *26*, 6963.

(154) Kim, J.-H.; Kim, H. U.; Kang, I.-N.; Lee, S. K.; Moon, S.-J.; Shin, W. S.; Hwang, D.-H. *Macromolecules* **2012**, *45*, 8628.

(155) Dang, D.; Chen, W.; Yang, R.; Zhu, W.; Mammo, W.; Wang, E. *Chem. Commun.* **2013**, *49*, 9335.

(156) Sun, W.; Ma, Z.; Dang, D.; Zhu, W.; Andersson, M. R.; Zhang, F.; Wang, E. *J. Mater. Chem. A* **2013**, *1*, 11141.

(157) Hendriks, K. H.; Heintges, G. H. L.; Wienk, M. M.; Janssen, R. A. J. *J. Mater. Chem. A* **2014**, *2*, 17899.

(158) Tao, Q.; Xia, Y.; Xu, X.; Hedström, S.; Bäcke, O.; James, D. I.; Persson, P.; Olsson, E.; Inganäs, O.; Hou, L.; Zhu, W.; Wang, E. *Macromolecules* **2015**, *48*, 1009.

(159) Kang, T. E.; Kim, K.-H.; Kim, B. J. *J. Mater. Chem. A* **2014**, *2*, 15252.

(160) Park, J. H.; Jung, E. H.; Jung, J. W.; Jo, W. H. *Adv. Mater.* **2013**, *25*, 2583.

(161) Jung, I. H.; Kim, J.-H.; Nam, S. Y.; Lee, C.; Hwang, D.-H.; Yoon, S. C. *Macromolecules* **2015**, *48*, 5213.

(162) Jung, J. W.; Jo, W. H. *Pol. Chem.* **2015**, *6*, 4013.

(163) Um, H. A.; Lee, D. H.; Heo, D. U.; Yang, D. S.; Shin, J.; Baik, H.; Cho, M. J.; Choi, D. H. *ACS Nano* **2015**, *9*, 5264.

(164) Li, W.; Hendriks, K. H.; Furlan, A.; Roelofs, W. S. C.; Wienk, M. M.; Janssen, R. A. J. *J. Am. Chem. Soc.* **2013**, *135*, 18942.

(165) Lee, J. W.; Choi, Y. S.; Jo, W. H. *Org. Electron.* **2013**, *13*, 3060.

(166) Jung, J. W.; Liu, F.; Russell, T. P.; Jo, W. H. *Chem. Commun.* **2013**, *49*, 8495.

(167) Sun, B.; Hong, W.; Yan, Z.; Aziz, H.; Li, Y. *Adv. Mater.* **2014**, *26*,

2636.

(168) Zhang, X.; Xiao, C.; Zhang, A.; Yang, F.; Dong, H.; Wang, Z.; Zhan, X.; Li, W.; Hu, W. *Polym. Chem.* **2015**, *6*, 4775.

(169) Carsten, B.; Szarko, J. M.; Lu, L.; Son, H. J.; He, F.; Botros, Y. Y.; Chen, L. X.; Yu, L. *Macromolecules* **2012**, *45*, 6390.

(170) Stuart, A. C.; Tumbleston, J. R.; Zhou, H.; Li, W.; Liu, S.; Ade, H.; You W. *J. Am. Chem. Soc.* **2013**, *135*, 1806.

(171) Inganäs, O.; Svensson, M.; Zhang, F.; Gadisa, A.; Persson, N. K.; Wang, X.; Andersson, M.R. *Appl. Phys. Lett.* **2004**, *79*, 31.

(172) Chen, M.-H.; Hou, J.; Hong, Z.; Yang, G.; Sista, S.; Chen, L.-M.; Yang, Y. *Adv. Mater.* **2009**, *21*, 4238.

(173) Slooff, L. H.; Veenstra, S. C.; Kroon, J. M.; Moet, D. J.; Sweelssen, J. *Appl. Phys. Lett.* **2007**, *90*, 143506.

(174) Zoombelt, A. P.; Mathijssen, S. G. J.; Turbiez, M. G. R.; Wienka, M. M.; Janssen, R. A. J. *J. Mater. Chem.* **2010**, *20*, 2240.

(175) Müller, C.; Wang, E.; Andersson, L. M.; Tvingstedt, K.; Zhou, Y.; Andersson, M. R.; Inganäs, O. *Adv. Funct. Mater.* **2010**, *20*, 2124.

(176) Lu, L.; Luo, Z.; Xu, T.; Yu, L. *Nano Lett.* **2013**, *13*, 59.

(177) Liu, J.; Choi, H.; Kim, J. Y.; Bailey, C.; Durstock, M.; Dai, L. *Adv. Mater.* **2012**, *24*, 538.

(178) Cha, H.; Chung, D. S.; Bae, S. Y.; Lee, M.-J.; An, T. K.; Hwang, J.; Kim, K. H.; Kim, Y.-H.; Choi, D. H.; Park, C. E. *Adv. Funct. Mater.* **2013**, *23*, 1556.

(179) van Franeker, J. J.; Heintges, G. H. L.; Schaefer, C.; Portale, G.; Li,

W.; Wienk, M. M.; van der Schoot, P.; Janssen, R.A. J. *J. Am. Chem. Soc.* **2015**, *137*, 11783.

(180) Bartelt, J. A.; Beiley, Z. M.; Hoke, E. T.; Mateker, W. R.; Douglas, J. D.; Collins, B. A.; Tumbleston, J. R.; Graham, K. R.; Amassian, A.; Ade, H.; Fréchet, J. M. J.; Toney, M. F.; McGehee, M. D. *Adv. Energy Mater.* **2013**, *3*, 364.

초 록

반도체적 성질과 함께 투명성, 유연성을 갖는 전도성 고분자의 경우 스핀코팅, 잉크젯 프린팅 등 저가의 박막 및 대면적 소자제작에 응용 될 수 있기 때문에 유기태양전지 광활성층용 재료로 큰 관심을 받고 있다. 그 중에서도 전자주개-전자받개 구조를 갖는 고분자의 경우 낮은 밴드갭 특성을 보여 700–1000 nm의 장파장 영역의 빛 흡수를 가능하게 하고, 이와 더불어 적절한 전자주개 및 전자받개의 선택은 고분자의 HOMO 그리고 LUMO 에너지레벨을 조절 가능하게 한다. 따라서 이와 같이 광화학적 특성을 조절하여 유기태양전지의 단락전류와 개방전압을 증가시키는 연구들이 최근까지 활발하게 진행되고 있다.

유기태양전지에 쓰이는 고분자 중, dithienyl benzothiadiazole과 fluorene으로 구성된 PFDTBT 고분자의 경우 fluorene의 약한 전자주개 특성으로 인하여 HOMO 에너지 준위가 낮아 1 V가 넘는 높은 개방전압을 보이고 있다. 하지만 높은 밴드갭(1.8 eV) 특성 때문에 장파장 영역의 빛 흡수 제한으로 단락전류의 경우 다른 전도성 고분자에 비해 다소 낮은 편에 속한다. 이와 같은 특성은 PFDTBT 뿐만이 아니라 다른 fluorene 기반의 전자주개-전자받개 형태의 고분자에서도 전반적으로 나타난다. 따라서 fluorene의 전자주개 능력을 강화하여 밴드갭을 낮추고 그에 따라 단락전류를 향상시키고자 fluorene에 산소원자를 도입한 6*H*-benzo[*c*]chromene (BC)를 합성하였고, dithienyl benzothiadiazole과 dithienyl

diketopyrrolopyrrole과 공중합하여 태양전지 특성을 측정하였다. BC 기반의 고분자의 경우 fluorene기반의 고분자보다 HOMO 에너지 준위가 올라가서 밴드갭이 줄어들었고, 효과적인 엑시톤 분리와 함께 결정성이 향상되어 정공이동도가 증가하였다. 결과적으로 HOMO 에너지준위가 상승하였기 때문에 개방전압은 다소 줄어들었으나, 단락전류의 큰 증가로 인하여 BC 기반의 고분자들이 fluorene의 기반의 고분자들보다 더 높은 효율을 나타냈다.

다음으로 개방전압의 손실 없이 단락전류를 증가시키고자 thiophene-capped diketopyrrolopyrrole(TDPP)와 bithiophene(2T)로 구성된 PTDPP2T 고분자와, TDPP와 phenylene으로 구성된 $(TDPP)_2Ph$ 단분자를 포함하는 ternary 블렌딩 태양전지를 제작하였다. 여기에서 PTDPP2T 고분자(670–840 nm)와 $(TDPP)_2Ph$ 단분자(550–700 nm)는 서로 상보적인 빛의 흡수를 하기 때문에 PTDPP2T 고분자에 대비하여 $(TDPP)_2Ph$ 단분자 양이 증가할수록 광활성층의 단파장 영역 빛 흡수가 증가하였다. 하지만 10 wt% 이상의 $(TDPP)_2Ph$가 첨가되게 되면 더 이상 고분자와 단분자가 섞이지 않고 상분리가 발생하는 것을 엑스선 회절과 주사 현미경 분석을 통해 확인하였고, 이는 태양전지 효율을 저하시켰다. 결과적으로 10 wt%의 $(TDPP)_2Ph$가 첨가된 ternary blend 태양전지의 경우 기존의 binary blend 태양전지(6.60%) 보다 향상된 7.48%의 효율을 나타냈다.

마지막으로 빛의 흡수영역을 더 증가시키는 동시에 고분자의 HOMO 에너지 준위를 낮추어 개방전압을 높히고자 서로 다른 두 가지 전자받개를 포함하는 random 형태의 전자주개-전자받개 고분자를 설계하고 합성하였다. PTDPP2T의 경우 높은 단락전류를

보이는 반면, pyridine-capped diketopyrrolopyrrole(PyDPP)와 2T로 구성된 PPyDPP2T의 경우는 낮은 HOMO 에너지 준위로 인하여 높은 개방전압을 보인다. 또한 이 두 고분자는 서로 상보적인 빛 흡수를 하는 특성을 나타낸다. 따라서 본 연구에서는 서로 다른 두 개의 전자받개, TDPP와 PyDPP의 비율을 조절하고 2T와 공중합하여 고분자를 합성하였고, 태양전지 특성을 분석하였다. 고분자에서 PyDPP함량이 증가되게 됨에 따라서 HOMO 에너지 준위가 감소하여 그에 따라서 개방전압이 증가하였다. 고분자의 빛 흡수는 PyDPP 함량이 증가함에 따라 증가하였지만, 단락전류의 경우 PyDPP 함량이 25%일 때 가장 높은 16.44 mA cm^{-2} 값을 나타내었는데, 이는 PyDPP 함량이 25% 이상일 때는 고분자의 피브릴 크기가 수 nm 이상으로 증가하였기 때문이다. 결과적으로 25%의 PyDPP가 포함된 PR2 고분자가 기존의 PTDPP2T 고분자에 대비하여 단락전류와 개방전압이 모두 증가하여 8.11%의 가장 높은 고효율을 나타냈다. 이러한 결과들을 종합해 볼 때, 고분자의 화학적 구조 변화와 ternary 블렌딩을 통한 광활성층의 효율적인 빛 흡수가 고성능 고분자 태양전지를 위한 하나의 유용한 전략임을 확인 하였다.

주요어: 고분자 태양전지, 벌크 이종접합, 낮은 밴드갭, ternary 블렌드, random 고분자

학 번: 2011-22870

List of papers

1. Lee, J. W.; Choi, Y. S.; Jo, W. H. Diketopyrrolopyrrole-based small molecules with simple structure for high V_{OC} organic photovoltaics. *Org. Electron*. **2012**, *13*, 3060.
2. Kim, K. T.; Lee, J. W.; Jo, W. H. Charge-transport tuning of solution-processable graphene nanoribbons by substitutional nitrogen doping. *Macromol. Chem. Phys.* **2013**, *214*, 2768.
3. Lee, J. W.; Bae, S.; Jo, W. H. Synthesis of 6*H*-benzo[*c*]chromene as a new electron-rich building block of conjugated alternating copolymers and its application to polymer solar cells *J. Mater. Chem. A* **2014**, *2*, 14146.
4. Lee, J. W; Ahn, H.; Jo, W. H. Conjugated random copolymers consisting of pyridine- and thiophene-capped diketopyrrolopyrrole as co-electron accepting units to enhance both J_{SC} and V_{OC} of polymer solar cells. *Macromolecules* **2015**, *48*, 7836.
5. Lee, J. W.; Jo, W. H. Ternary blend composed of two organic donors and one acceptor for active layer of high performance organic solar cells. *ACS Appl. Mater. Interfaces* **2015**, submitted.